AD-A033 125 TRACOR INC AUSTIN TEX F/G 17/1
IN SITU PERFORMANCE PREDICTION.(U)
MAR 67 M N ANASTASI, S F FOWLER NOBSR-95149
UNCLASSIFIED TRACOR-67-262-C NL

1 OF 2
AD A033125

[redacted] MOST Project 3 FC

UNCLASSIFIED

Document Number
TRACOR 67-262-C
Contract Number NObsr-95149
Project Serial SS041-001
Task 8100, 10906, 8224
TRACOR Project No. 002-019-12

(1)

TECHNICAL MEMORANDUM

IN SITU PERFORMANCE PREDICTION (U)

by

M. N. Anastasi S. F. Fowler

Submitted to

Commander, Naval Ship Systems Command
Department of the Navy Code 1631
Washington, D. C., 20360

March 20, 1967

TRACOR

6500 Tracor Lane, Austin, Texas 78721, AC 512/926-2800

[redacted] UNCLASSIFIED

TRACOR, INC. 6500 TRACOR LANE, AUSTIN, TEXAS 78721

(16) SS041 (1)
(17) SS041001

(14) Document Number TRACOR-67-262-C
(15) Contract Number NObsr-95149
Project Serial SS041-001
Task 8100, 10906, 8224
TRACOR Project No. 002-019-12

(9) TECHNICAL MEMORANDUM

(6) IN SITU PERFORMANCE PREDICTION (U)

by

(10) M. N. Anastasi Stephen F. Fowler

Submitted to

Commander, Naval Ship Systems Command
Department of the Navy Code 1631
Washington, D. C., 20360

March 20, 1967

(11) 20 Mar 67
(12) 103 p.

Approved:

E. H. Batey
Program Manager

Submitted:

S. F. Fowler
Project Director

352100

[redacted] UNCLASSIFIED

TRACOR, INC. 6500 TRACOR LANE, AUSTIN, TEXAS 78721

ABSTRACT

This report discusses the parameters required for an in situ performance prediction, a method of obtaining estimates of these parameters from received reverberation levels, and a means of performance prediction based on these estimates. The problem is discussed in general and the solution is pursued for the particular case of the active bottom bounce modes of the AN/SQS-26. The ping-to-ping stability of AN/SQS-26 reverberation cycles is investigated and several sets of environmental parameters determined from an analysis of the reverberation data are included.

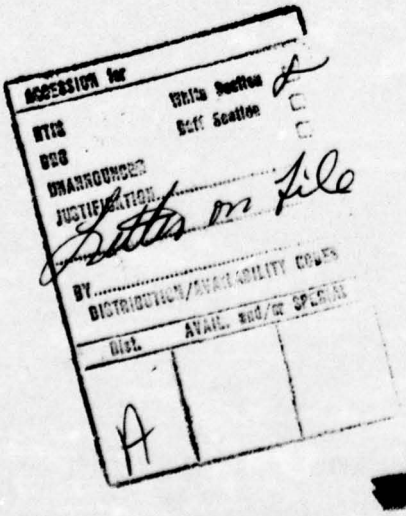

TRACOR, INC. 6500 TRACOR LANE, AUSTIN, TEXAS 78721

TABLE OF CONTENTS

TRACOR, INC. 6500 TRACOR LANE, AUSTIN, TEXAS 78721

LIST OF ILLUSTRATIONS

TRACOR, INC. 6500 TRACOR LANE, AUSTIN, TEXAS 78721

LIST OF ILLUSTRATIONS (Cont'd.)

TRACOR, INC. 6500 TRACOR LANE, AUSTIN, TEXAS 78721

LIST OF TABLES

TRACOR, INC. 6500 TRACOR LANE, AUSTIN, TEXAS 78721

IN SITU PERFORMANCE PREDICTION

1. INTRODUCTION

A number of fleet sonar systems already in existence or in various stages of development are capable of operation in several different modes. Mode selections may include, as broad categories, passive or active operation. Each of these may be further classified according to the particular type of propagation path to be used, such as bottom bounce, convergence zone, or surface channel, or according to certain system parameters, such as pulse type, keying rate, or beam depression angle.

The intelligent selection of the best operating mode for a given set of conditions has, of course, increased in difficulty along with this increase in system capability and complexity. In selecting a mode, account must be taken of factors such as own-ship mission and expected enemy mission, tactics, and capabilities. In addition to these considerations, which are properly investigated as parts of an overall problem in operations research, the mode selection must be influenced by the specific environment in which the sonar must operate.

Relative sonar performance among the possible modes is not fixed. A given set of environmental conditions will, in general, tend to enhance performance in some modes and degrade it in others. Such specific relationships cannot be anticipated by simple rules with a useful degree of accuracy, since environmental conditions vary greatly with both time and location. A means is thus needed to determine, in situ, estimates of the important local environmental parameters and to use these in a systematic prediction of sonar performance for each operating mode.

This report discusses the parameters required for an in situ performance prediction, a method of obtaining estimates of these parameters, and a means of performance prediction based

on these estimates. The problem is discussed in general and the solution is pursued for the particular case of the active bottom bounce modes of the AN/SQS-26.

TRACOR, INC. 6500 TRACOR LANE, AUSTIN, TEXAS 78721

2. PARAMETERS REQUIRED FOR SONAR PERFORMANCE PREDICTION

There are several recognized measures of sonar performance, such as maximum detection range, minimum detectable level, and sweep rate. Most of these may be derived from a curve representing the expected signal-to-noise ratio at the receiving beamformer output, displayed as a function of horizontal range to the target. A performance prediction necessarily depends on a knowledge of the sonar, target, and environmental parameters necessary for an estimate of the average power in both the signal and the total masking background (consisting of both noise and reverberation) as they would appear at the output of the receiving beamformer. The required parameters are summarized below:

A. Signal:
   1. Transmitting directivity pattern
   2. Receiving directivity pattern
   3. Sonar depth
   4. Source level
   5. Target location (depth and range)
   6. Target speed and course
   7. Target strength
   8. Target radiated noise spectrum (for passive prediction only)
   9. Bottom loss as a function of frequency and grazing angle
   10. Medium attenuation loss as a function of frequency
   11. Surface loss as a function of frequency, grazing angle, and wind speed (or sea state)
   12. Velocity profile
   13. Water depth

B. Masking Background:
   1. Ambient noise power spectrum and directional characteristics as a function of wind speed

2. Directivity index as a function of sonar operating frequency and mode
3. Sonar self noise as a function of ship speed
4. Reverberation intensity as a function of time, requiring a knowledge of:
   - Transmitting and receiving directivity patterns
   - Sonar depth
   - Pulse length
   - Keying rate
   - Velocity profile
   - Bottom depth
   - Scattering strengths for surface, bottom, and volume
   - Bottom loss as a function of grazing angle at the sonar frequency
   - Surface loss as a function of grazing angle and wind speed at the sonar frequency.

Values for the parameters characterizing the target -- such as target strength; target radiated noise spectrum (for passive operation); and target depth, speed, and course -- must, of course, be assumed. Guidelines for choosing these parameters include the type of target expected and its probable mission.

Values for some of the required sonar parameters, such as pulse length and source level, are easily obtained; however, it will be necessary to express other sonar parameters in terms of more fundamental characteristics of the sonar systems. Directivity patterns, for example, can be obtained from descriptions of the transmitting and receiving arrays and beam forming networks.

In sonar performance prediction carried out at shore-based installations (as, for example, in sonar design), the

environmental parameters are specified, the choice of values for these parameters being governed by a best estimate of typical or expected conditions. In an in situ performance prediction, these parameters must be measured.

Standard techniques already exist for the measurement of some of the required parameters, such as wind speed or wave height, bottom depth, and velocity profile. The medium attenuation coefficient is sufficiently insensitive to location so that an average value for this quantity may be used in place of a local measurement. The remaining parameters which would, in general, require in situ evaluation are:

$BL(\theta,f)$ = Bottom loss as a function of grazing angle, θ, within the frequency range of interest,

$N(\gamma,f)$ = average ambient noise power as a function of vertical angle, γ, and frequency,

$\mu_S(\theta,f)$ = surface scattering strength as a function of grazing angle and frequency,

$SL(\theta,f)$ = surface loss as a function of grazing angle, θ, within the frequency range of interest,

$\mu_B(\theta,\varphi)$ = bottom scattering strength as a function of grazing and scattering angles, θ and φ, and

$\mu_V(z,f)$ = volume scattering strength as a function of depth, z, and frequency.

TRACOR, INC. 6500 TRACOR LANE, AUSTIN, TEXAS 78721

3. PARAMETER DESCRIPTIONS

Sections 1 and 2 of this repcrt have listed the parameters involved in the general area of performance prediction. The remainder of this report pursues the performance prediction problem from the standpoint of an active sonar system, in particular, the AN/SQS-26. Many of the concepts which are discussed will, of course, apply to the general case.

As indicated in the previous section, the parameters for which estimates must be obtained for use in an in situ performance prediction for an active sonar are bottom and surface loss and the scattering strengths for volume, surface, and bottom. The noise field $N(\gamma,f)$ need not be specified since it is required only as an intermediate step in determining the noise power at the array output, a quantity which, in the case of in situ prediction, may be measured directly. The manner in which surface and bottom losses and the scattering strengths affect the total reverberation level are discussed in detail in a previous TRACOR report concerning reverberation[1]. Several sections from this report describing these effects and discussing the basic reverberation propagation paths for the AN/SQS-26 bottom bounce operation are included in Appendix A. A discussion of echo level prediction is presented in Appendix B.

The essential characteristics of the parameters listed in Section 2 are summarized in the following paragraphs. The equations used are given in a simplified form for convenience.

---

[1] Fowler, S. F., "Bottom Bounce Reverberation Modeling and Bottom Loss (U)", TRACOR Document Number 66-355-C, Contract NObsr-93140, November 16, 1966, Confidential.

3.1 BOTTOM LOSS

Bottom loss may vary widely from one ocean area to another, depending on the sediment structure of the bottom and the bottom topography. As used in sonar performance prediction it represents, essentially, the dB difference between the intensity of a signal specularly reflected from the bottom and the intensity of that signal if the bottom were replaced by a perfect reflector. As previously indicated, bottom loss depends on both the frequency and the bottom grazing angle. Some previous studies[2,3] of bottom loss for the particular operating frequency and signal processor of the AN/SQS-26 have indicated, however, little systematic dependence of bottom loss on grazing angle for grazing angles from 90^{o} (normal incidence) to approximately 15^{o}. This fact is illustrated in Figs. 1, 2, and 3 for a particular set of bottom loss data acquired in the Western North Atlantic[3]. The data shown were processed so that the bottom loss values were applicable to AN/SQS-26 performance prediction.

An in situ estimate of bottom loss requires an intensity measurement of sound energy which has undergone at least one specular bottom reflection. If the predicted intensity of the received bottom reflected signal is IR, then

$$IR = I_o h b^n ,$$

where

I_o = source level,

h = attenuation due to transmission loss (other than bottom loss),

b = attenuation due to bottom loss, and

n = number of bottom reflections.

---

[2]Collins, J. L., "Technical Memorandum: Interpretation of Explosive Source Data for Long Pulse Sonar (U)", TRACOR Document Number 65-105-C, Contract NObsr-91223, January 11, 1965, Confidential.

[3]Fowler, Op.Cit.

THIS DRAWING IS UNCLASSIFIED

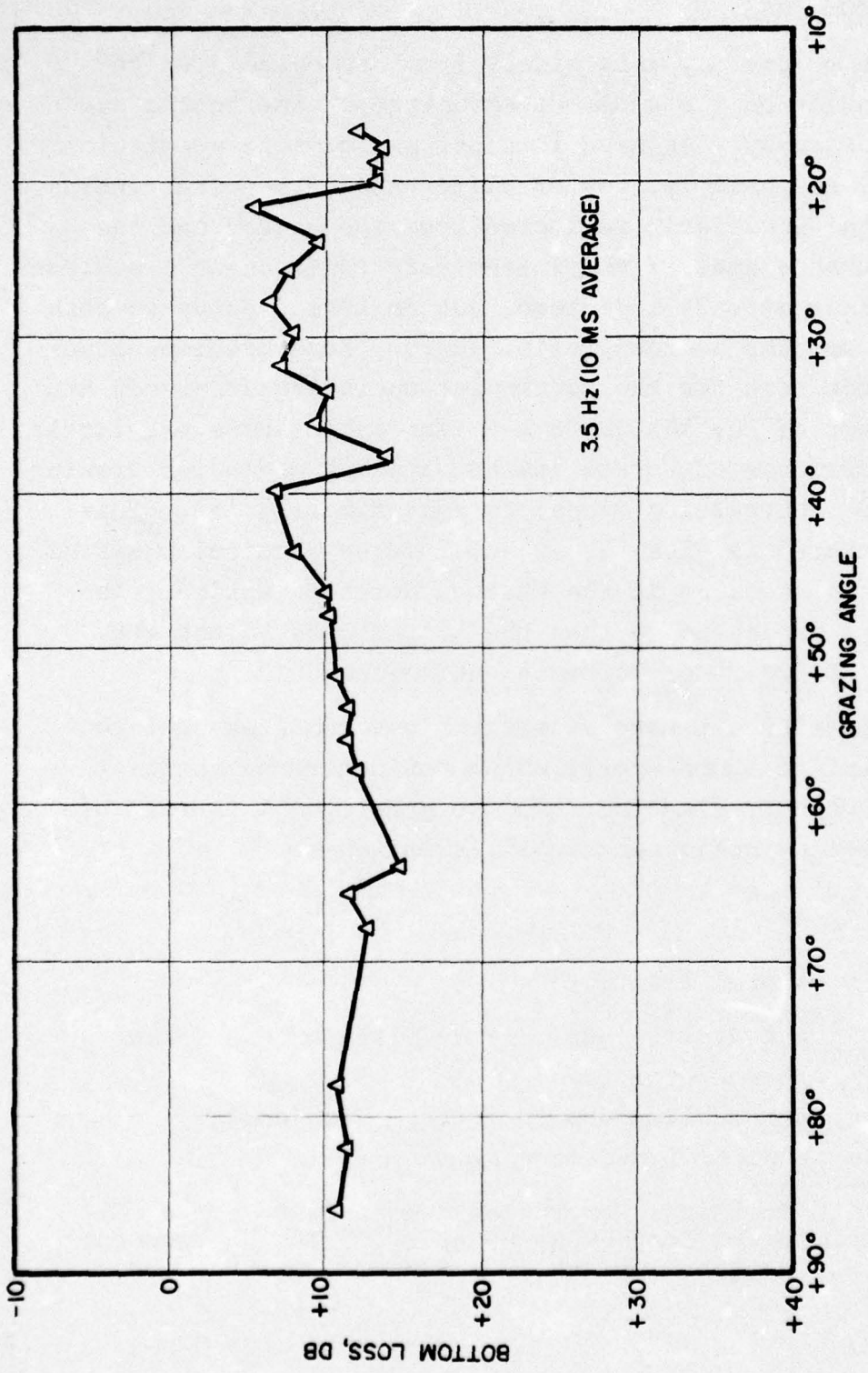

FIG. 1 – SMOOTH BOTTOM

TRACOR, INC. DWG. A6-55-42
AUSTIN, TEXAS 1·23·67 ANASTASI/SL

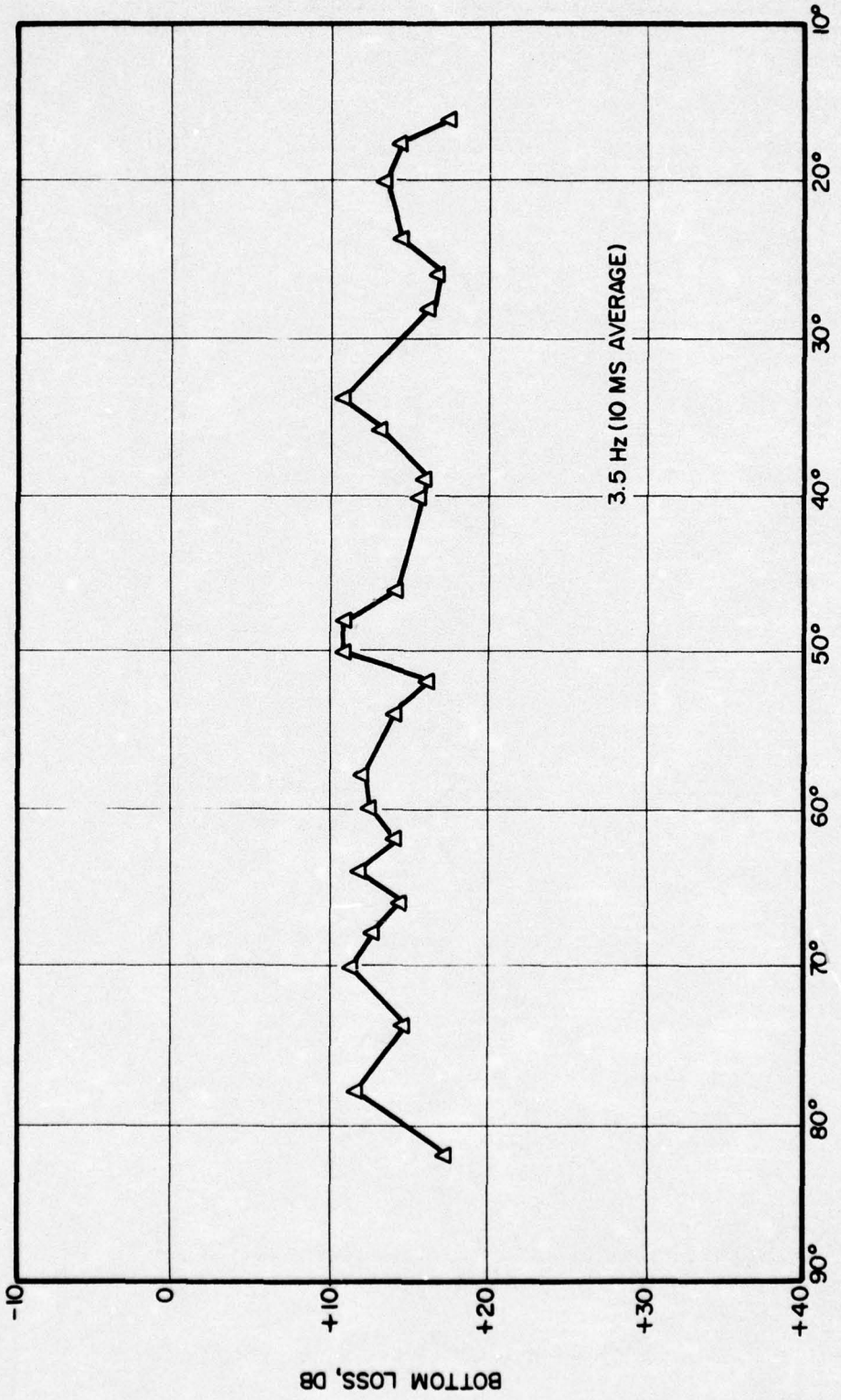

FIG.2 – MEDIUM ROUGH BOTTOM

TRACOR, INC. DWG. A6-55-41
AUSTIN, TEXAS 2-23-67 ANASTASI/SL

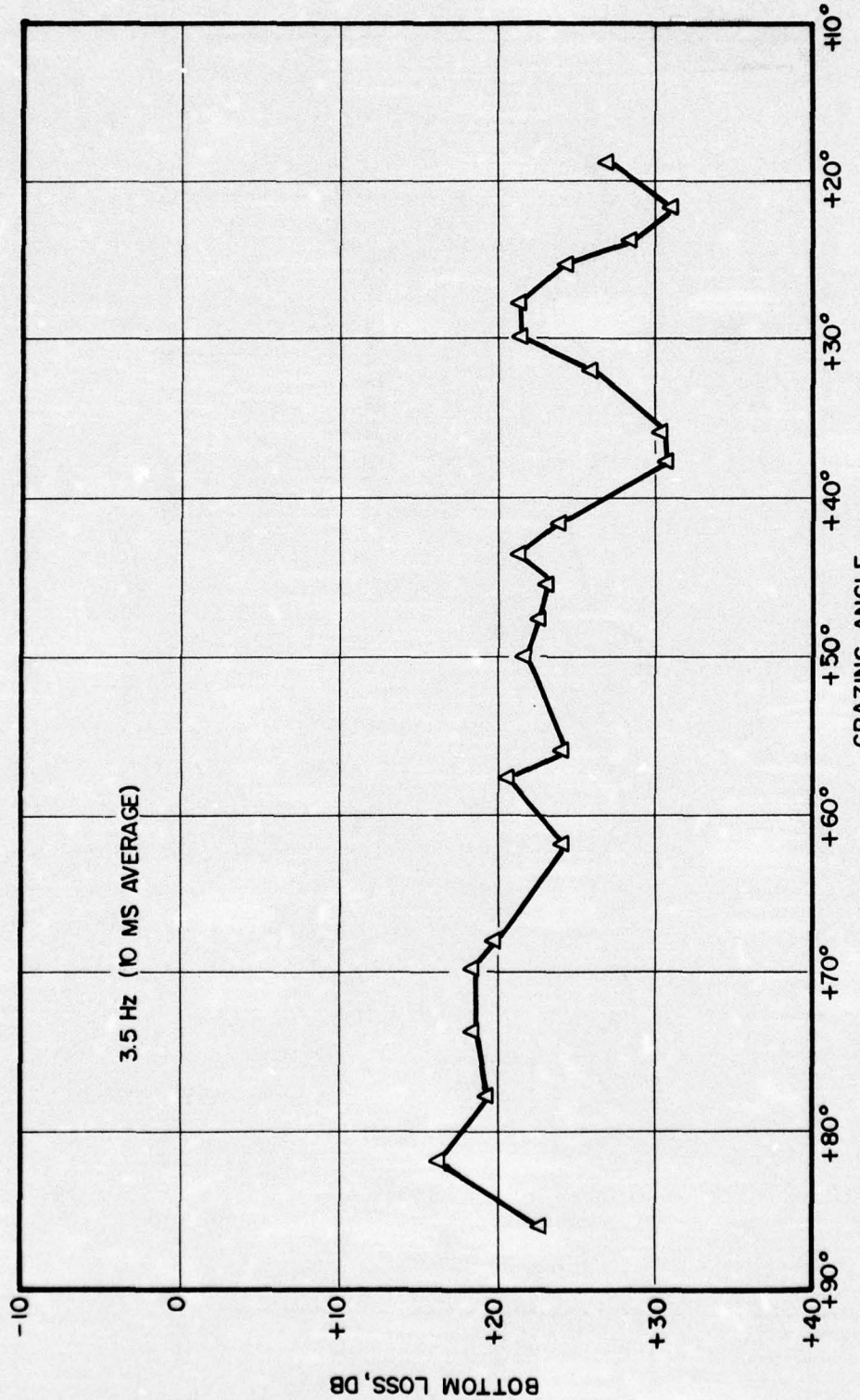

FIG. 3 – ROUGH BOTTOM

TRACOR, INC. DWG. A6-55-40
AUSTIN, TEXAS 2-23-67 ANASTASI/SL

If IRM is the measured intensity of a signal specularly reflected from the bottom, then

$$IRM = IR \ ,$$

from which

$$b = \left(\frac{IRM}{I_o h}\right)^{\frac{1}{n}} \ , \qquad (1)$$

and

$$\text{bottom loss (dB)} = BL = 10 \log b = \frac{1}{n} 10 \log \left(\frac{IRM}{I_o h}\right) \ .$$

When transmission loss and source level are known, Eq. (1) may be used to obtain estimates of bottom loss. Since this report concerns data which may be obtained with a single ASW ship, the bottom loss to be derived will be for a grazing angle of 90^o. This is not necessarily a theoretical restriction, since schemes involving distant sound sources or reflectors may provide bottom loss data for other grazing angles. Under operational conditions, however, a method which depends only on an on-board source and receiver of known characteristics will be far more practical. With source and receiver at the same location, then, bottom loss data will necessarily be associated with specular reflections in a bottom area directly beneath the ship. It would of course be desirable to have bottom loss estimates for each grazing angle from 90^o to 0^o. If, however, the bottom loss dependence on grazing angle is not pronounced within a certain range of grazing angles, as in Fig. 1, the value at normal incidence will be sufficient.

3.2 SURFACE LOSS

The definition of surface loss is patterned after that given for bottom loss in the previous section. Because of the sharp impedance discontinuity at the air-water interface, a smooth sea surface is a very good reflector for underwater sound. Surface loss is thus due primarily to surface roughness and may be related to measurements of wave height, sea state, wind speed, or more detailed surface characterizations such as wave spectra.

The principal significance of surface loss in AN/SQS-26 performance prediction is its contribution to total transmission loss in the surface channel operating modes, since the sound energy may be surface reflected several times in its round trip from sonar to target.

Theoretical formulas for surface loss have been developed, such as that given by Marsh[4], relating surface loss to wave spectra and signal frequency. Other investigators have obtained empirical or quasi-empirical relationships between surface loss, frequency, and sea state or wind speed[5]. In situ surface loss measurements for the grazing angles of interest (in this case, angles in the order of 1^{o}) generally require that sound source and receiver be separated by at least several hundred yards. It would not be feasible to measure surface loss on board an operating ASW ship; thus, an in situ estimate of this parameter must be obtained from a knowledge of local wind speed, sonar frequency, and a previously determined relationship between these quantities and surface loss.

---

[4]Marsh, H. W., "Sound Reflection and Scattering From the Sea Surface", J. Acoust. Soc. Am., Vol. 35, No. 2, 240-244, February, 1963.

[5]Garrison, G. R., S. R. Murphy, and D. S. Potter, "Measurements of the Backscattering of Underwater Sound from the Sea Surface", J. Acoust. Soc. Am., Vol. 32, No. 1, 104-111, January, 1960.

3.3 SCATTERING STRENGTHS

As indicated in Appendix A, reverberation is due to sound energy backscattered from the ocean bottom, from the ocean surface, and from volume scatterers within the body of the medium. The reverberation (one of the above types) received at some particular time following transmission is associated with a scattering area or scattering volume defined by the duration of the transmitted pulse and the propagation geometry. The intensity of the sound backscattered from this area or volume depends on the incident intensity, the size of the insonified area or volume (both of which may be determined by ray theory), and the scattering strength per unit area or volume. The scattering strength may be evaluated from reverberation measurements when all other parameters governing the reverberation level are known. The following three sections summarize some of the important characteristics of bottom, surface, and volume scattering strengths as they apply to AN/SQS-26 performance prediction.

3.3.1 Bottom Scattering Strength

The bottom reverberation received at t seconds after transmission is the result of sound energy backscattered from a bottom scattering area such as that shown in Fig. 4. The intensity, I_1, of the backscattered sound at a reference distance of one yard from the scattering area is given by

$$I_1 = I_i A \mu_B \ ,$$

where

I_i = intensity of sound incident on the scattering area,

A = total scattering area (total area of the annular ring shown in Fig. 4), and

μ_B = scattering strength/unit area of the bottom.

If h is the attenuation due to the one-way transmission loss from the source to the scattering area, then

$$I_i = I_o h \ ,$$

and

$$I_B = I_1 h \ ,$$

where I_o is the source intensity and I_B is the intensity of the received bottom reverberation. We may combine these expressions to obtain

$$I_B = I_o h^2 A \mu_B \ .$$

In the above discussion an omnidirectional source and receiver were assumed. If the source and receiver are directional, the net effect is a modification of the intensity contributions from different portions of the scattering area, as shown in Appendix A. We may indicate this dependence by writing

$$I_B = I_o h^2 A \mu_B \Delta BP \ , \qquad (2)$$

where ΔBP is obtained from the integral of the product of the transmitting and receiving beam patterns over the solid angle subtended at the receiver by the scattering area. With the exception of I_o, the factors on the right hand side of Eq. (2) change with time. For convenience, Eq. (2) may be written as

$$I_B = I_B\ (t) = \mu_B G_B(t) \ , \qquad (3)$$

where

$$G_B(t) = I_o h^2(t)\ A(t)\ \Delta BP(t) \ .$$

Equation (3) is the mathematical model used in predicting bottom reverberation. This same equation, used in survey work, forms the basis for the determination of bottom scattering strength. In a controlled experiment, values of G(t) may be obtained through

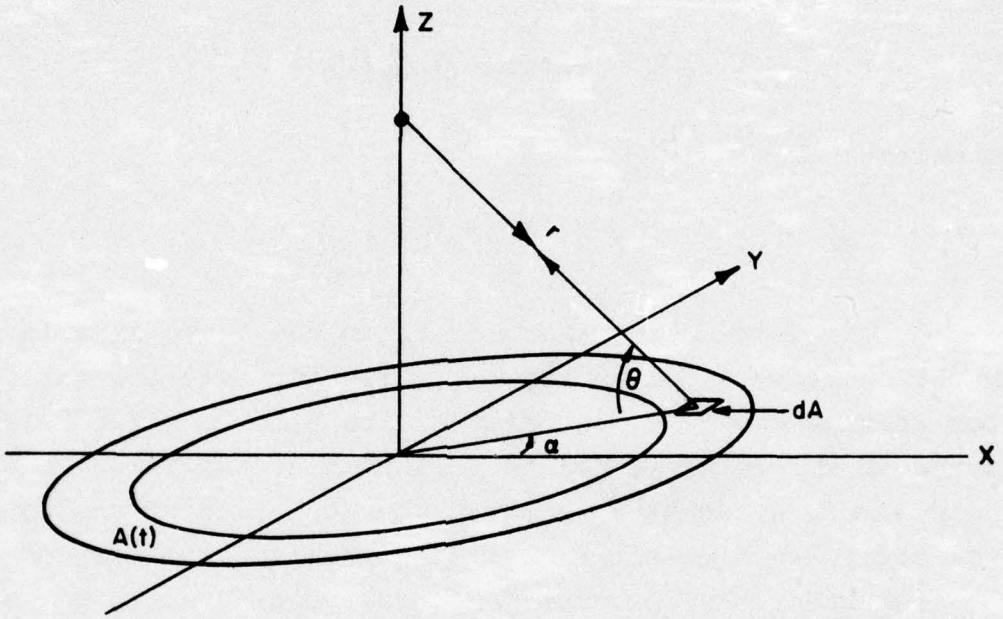

FIG. 4 –SCATTERING AREA FOR BOTTOM REVERBERATION RECEIVED AT TIME t

TRACOR, INC. AUSTIN, TEXAS | DWG 769-274 | 6/11/68 | BE/SL

the use of ray theory in conjunction with a knowledge of local propagation conditions and the sonar characteristics. If IMB is the measured average intensity of the bottom reverberation received at T seconds after transmission, the bottom scattering strength, μ_B, is the number such that

$$IMB = I_B(T) = \mu_B G_B(T) \ , \tag{4}$$

from which

$$\mu_B = IMB/G_B(T) \ . \tag{5}$$

The value determined for μ_B in the above example is, from the geometry shown in Fig. 4, valid for only the particular bottom grazing angle, θ, associated with time T. If IMB is measured at several time points following transmission, the values of μ_B determined can be associated with the grazing angles corresponding to each of the times. The grazing angle dependence of μ_B observed in such experiments has been found to be in reasonable agreement with the angular dependence predicted by Lambert's Law for diffuse scattering from a rough surface. That is,

$$\mu_B = \mu_B(\theta) = \mu_B' \sin^2 \theta \ , \tag{6}$$

where μ_B' is a constant. For certain types of bottom reverberation (see Fig. A-4, Appendix A) the scattered sound energy returns to the receiver by way of a path other than that followed by the incident energy. In this case the grazing and scattering angles, θ and ϖ, are not equal and Eq. (6) becomes

$$\mu_B = \mu_B(\theta,\varpi) = \mu_B' \sin \theta \sin \varpi \ . \tag{7}$$

The functional form of $\mu_B(\theta)$ given in Eqs. (6) and (7) will be assumed in the remainder of this report. The quantity which must be determined for in situ performance prediction is the constant factor μ_B'.

3.3.2 Surface Scattering Strength

Surface reverberation may be computed in the manner indicated for bottom reverberation in the previous section. That is, if I_S is the surface reverberation received at some particular time after transmission, then

$$I_S = I_o h^2 A \mu_S \, \Delta BP \ ,$$

or

$$I_S = I_S(t) = \mu_S G_S(t) \ , \tag{8}$$

where

$$G_S(t) = I_o h^2(t) \, A(t) \, \Delta BP(t) \ . \tag{9}$$

Surface scattering strength depends on grazing angle, sea state (or wind speed), and sonar frequency. Several investigators have proposed relationships between surface scattering strength and the above parameters[6]. The empirical equation given below was obtained by Chapman and Harris[7].

$$10 \log \mu_S = 33\beta \log \frac{\theta}{30} - 42.4 \log \beta + 2.6 \ , \tag{10}$$

[6]Shaffer, R. L., "Masking of Surface Reverberation by Volume Reverberation", J. Acoust. Soc. Am., Vol. 39, No. 2, 408-411 (L), (1966).

[7]Chapman, R. P. and J. H. Harris, "Surface Backscattering Strengths Measured with Explosive Sound Sources", J. Acoust. Soc. Am., Vol. 34, No. 10, 1592-1597, October, 1962.

where

$\beta = 158\ (vf^{1/3})^{-0.58}$,

v = wind speed in knots,

f = frequency in Hz, and

θ = grazing angle in degrees.

Although much more work is required in this area, the above expression gave good agreement with the Chapman-Harris data for a wide range of environmental conditions (frequencies and wind speeds).

3.3.3 Volume Scattering Strength

Volume reverberation, as it applies to the bottom bounce operation of the AN/SQS-26, is primarily governed by the volume scattering strength associated with the deep scattering layer. As shown in Appendix A, the reverberation from a scattering layer can be treated as reverberation from an equivalent scattering surface, whose scattering strength per unit area, μ_L, is independent of grazing angle and is given by

$$\mu_L = \int_{d_1}^{d_2} \mu_V(z)dz \ ,$$

where d_1 and d_2 define the upper and lower boundaries of the layer and $\mu_V(z)$ is the volume scattering strength per unit volume at the depth z for $d_1 \leq z \leq d_2$. Volume reverberation from volume scatterers within the deep scattering layer may thus be computed with an expression similiar to those used for bottom and surface reverberation, Eqs. (3) and (8). That is, if $I_V(t)$ is the intensity of the volume reverberation received at time t, then

$$I_V(t) = \mu_L G_V(t) \ , \qquad (11)$$

where $G_V(t)$ is the product of the time dependent quantities of transmission loss, scattering area, and beam pattern effects.

4. OBTAINING PARAMETER ESTIMATES WITH THE AN/SQS-26

We may conclude from the preceding sections that estimates of the boundary and volume scattering strengths may be obtained if identifiable reverberation of each type can be observed and measured, and if a means is available for evaluating G(t) in the general equation

$$\mu = IM/G(t).$$

The denominator G(t) in the above expression is equivalent to, and may be computed with the aid of, the equations given in Appendix A for the intensity of boundary and volume reverberation if the expression for scattering strength in each is set equal to unity. These equations have been programmed as a part of a larger scheme for in situ parameter estimation that will be subsequently discussed.

4.1 AN/SQS-26 BOTTOM BOUNCE REVERBERATION

Intensity predictions for the principal reverberation paths associated with bottom bounce operation of the AN/SQS-26 are discussed in Appendix A. A typical intensity vs. time plot for each of these paths is shown in Fig. 5a. In Fig. 5b, a corresponding curve of measured AN/SQS-26 reverberation is shown. The measured data represent the rectified and averaged output of the receiving beamformer. The figures indicate the time interval during which each type of reverberation is pre-

During about the first 5 seconds following transmission, the received sound energy is predominantly surface and volume reverberation. Surface and volume scatterers are reached by direct propagation paths during this period. The reverberation envelope (shown in Fig. 5b) for this interval is also affected

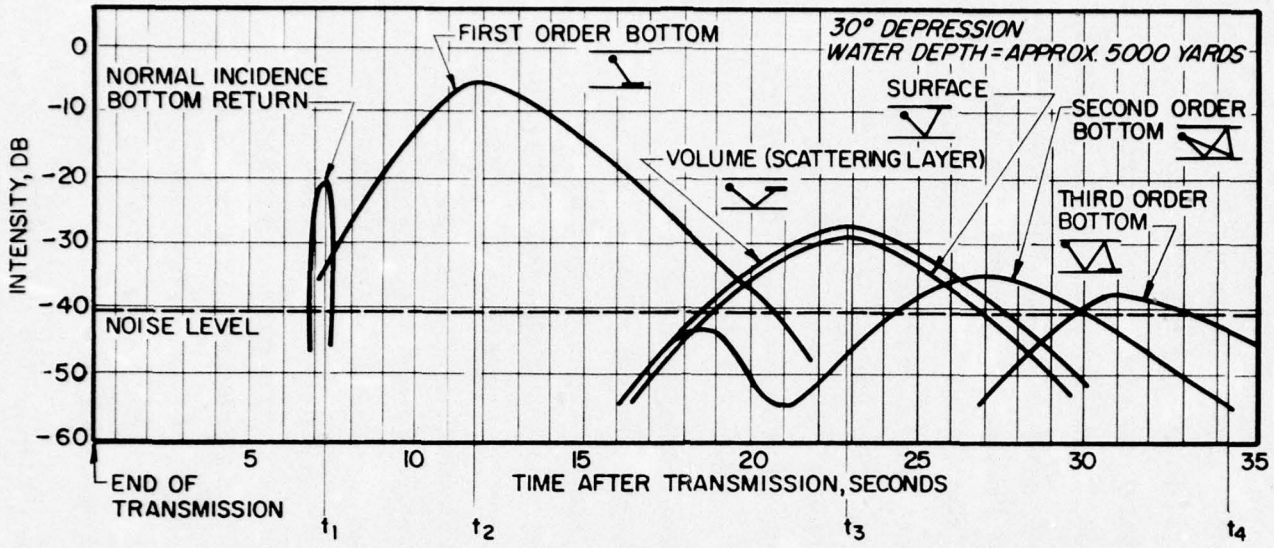

FIG. 5a – COMPUTED AN/SQS-26 BOTTOM REVERBERATION

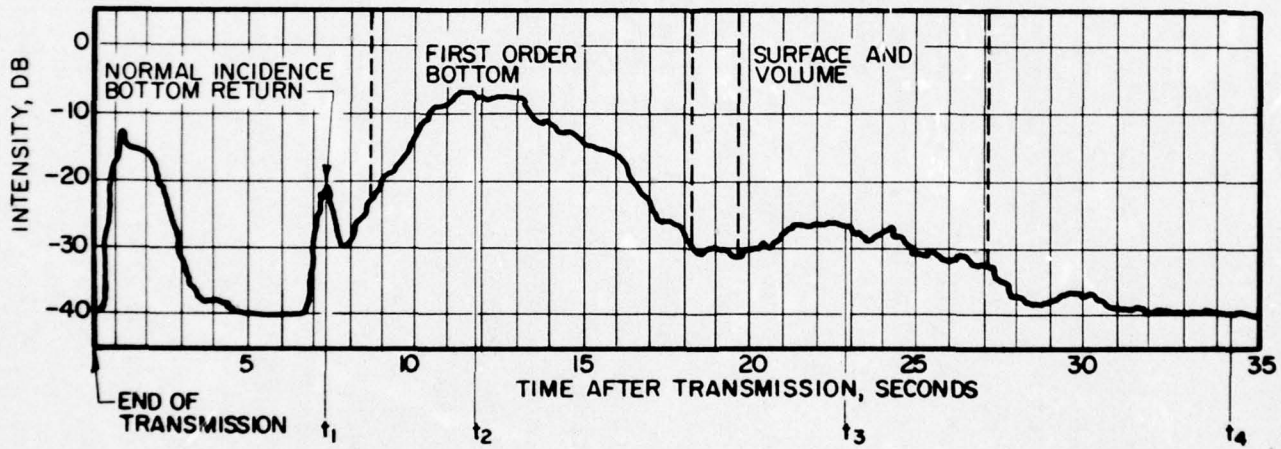

FIG. 5b – MEASURED AN/SQS-26 BOTTOM REVERBERATION

CONFIDENTIAL

TRACOR, INC.
AUSTIN, TEXAS
DWG A6-55-39
2-23-67 ANASTASI/SL

by the characteristics of the shipboard recording equipment since the transmission immediately following time zero exceeded the recorder's dynamic range.

At approximately 6 seconds following transmission, the sound energy which left the transducer from a lower side lobe of the transmitting beam pattern has had time to reach the bottom at a point directly beneath the ship, undergo specular reflection, and return to enter the array on a lower side lobe of the receiving beam pattern. This return, labeled "normal incidence bottom return" in Fig. 5(a and b), has a duration equal to that of the transmitted pulse. Sometimes loosely termed a "fathometer pulse," this return is generally observed on recorded AN/SQS-26 bottom bounce data, appearing as a distinct arrival on rectified and averaged Sanborn plots and at the output of the signal processor. Figure 6 shows in detail the propagation path for this return.

Immediately following the normal incidence bottom return is an interval (7-17 sec.) in which the reverberation is predominantly first order bottom. The small figure just below the label for this curve (Fig. 5a) shows the propagation path for this bottom scattered sound. In the next interval (17-25 sec.) surface and scattering layer reverberation appear along with second and third order bottom reverberation; the figures below the labels once again indicate the propagation path for each reverberation type. It is during this interval that target echoes would be expected. Figs. 7 through 9 are plots, similar to those in Fig. 5a, showing the intensity contributions of the various bottom bounce mode reverberation paths for other beam depression angles. In these graphs, all bottom scattered reverberation has been summed and plotted as one curve.

With AN/SQS-26 data following roughly the structure indicated in Figs. 5, 7, 8, and 9, sufficient information is available for computing estimates of bottom loss and the scattering strengths. From Eq. (1) it can be shown that the intensity of the normal incidence bottom return is given by

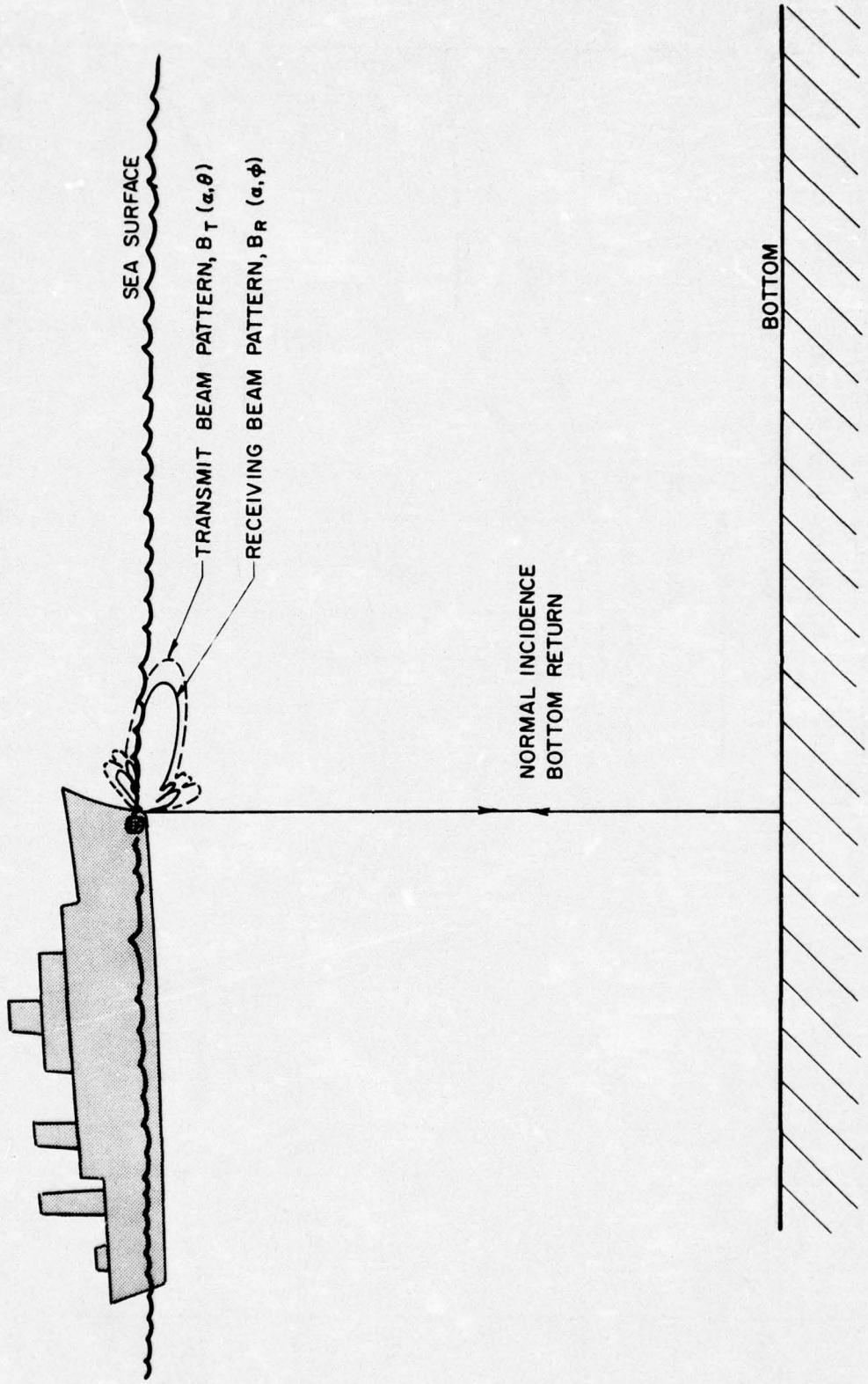

FIG. 6 – SPECULAR BOTTOM REFLECTION

TRACOR, INC. DWG. A6-55-6
AUSTIN, TEXAS 1-22-67 ANASTASI/SL

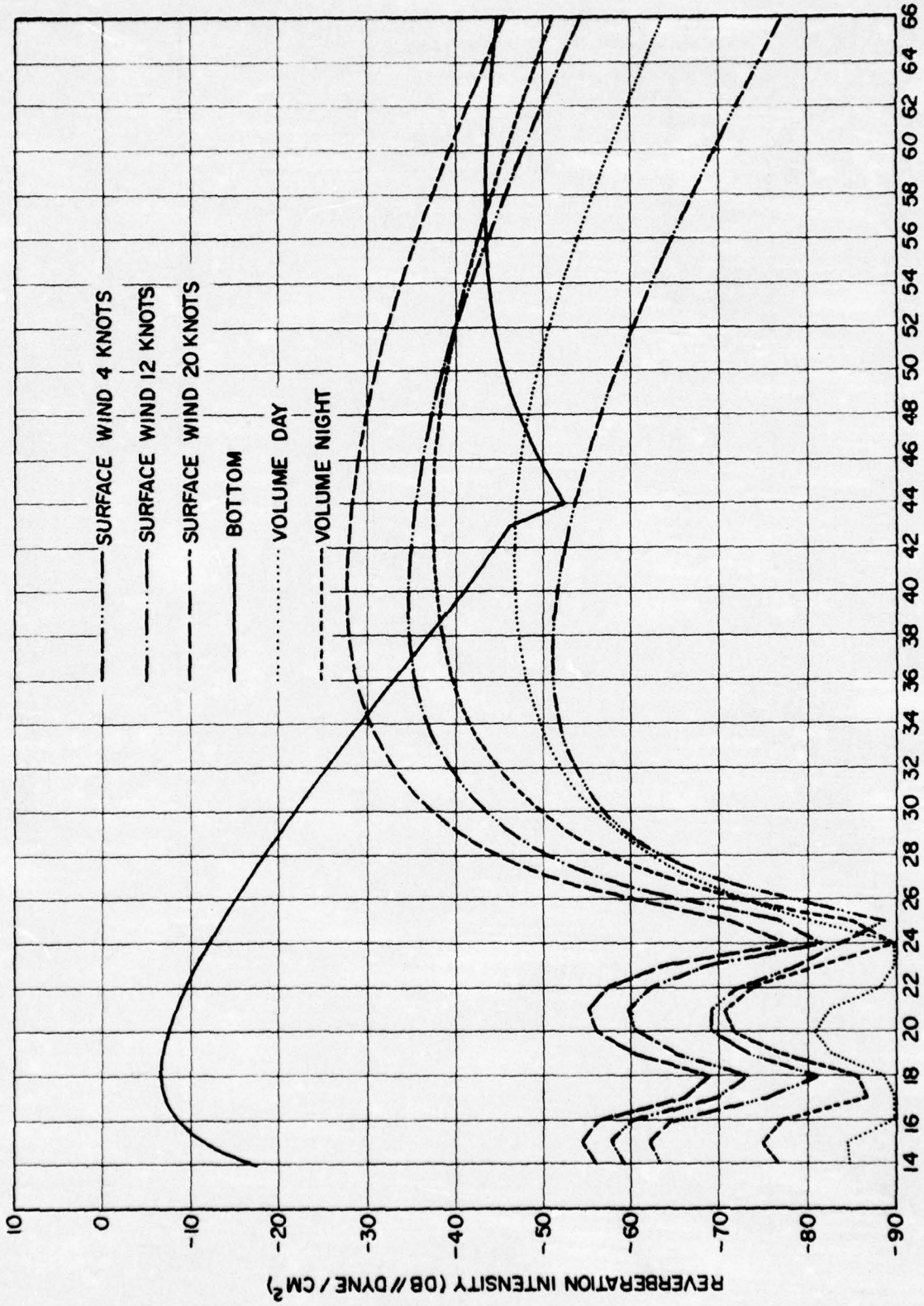

FIG. 7 - COMPUTED REVERBERATION FOR 15° BOTTOM BOUNCE SEARCH MODE

TRACOR, INC. DWG. A6-55-38
AUSTIN, TEXAS 2-23-67 ANASTASI/SL

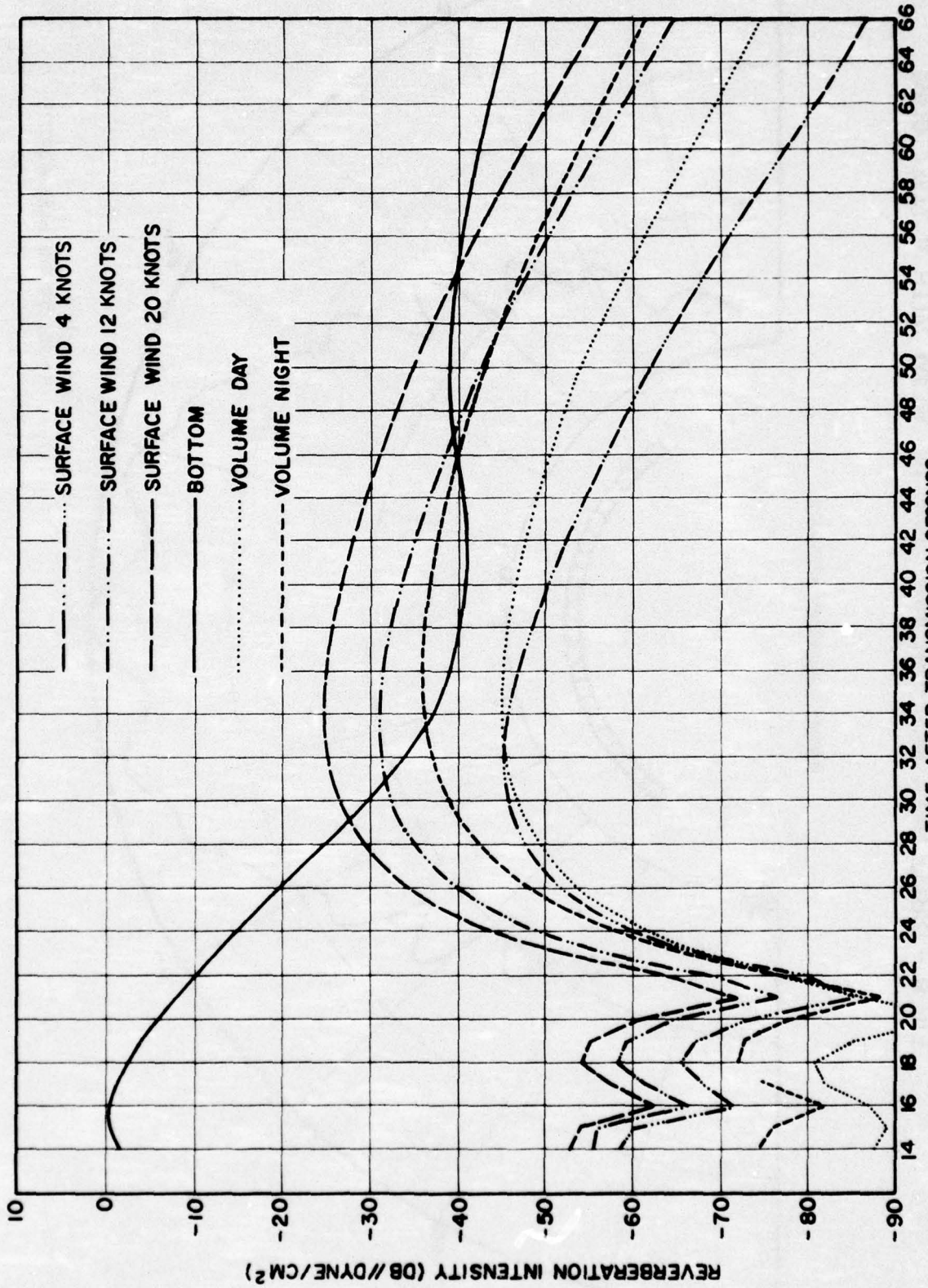

FIG. 8 – COMPUTED REVERBERATION FOR 20° BOTTOM BOUNCE SEARCH MODE

TRACOR, INC. AUSTIN, TEXAS DWG. A6-55-37 2-23-67 ANASTASI/SL

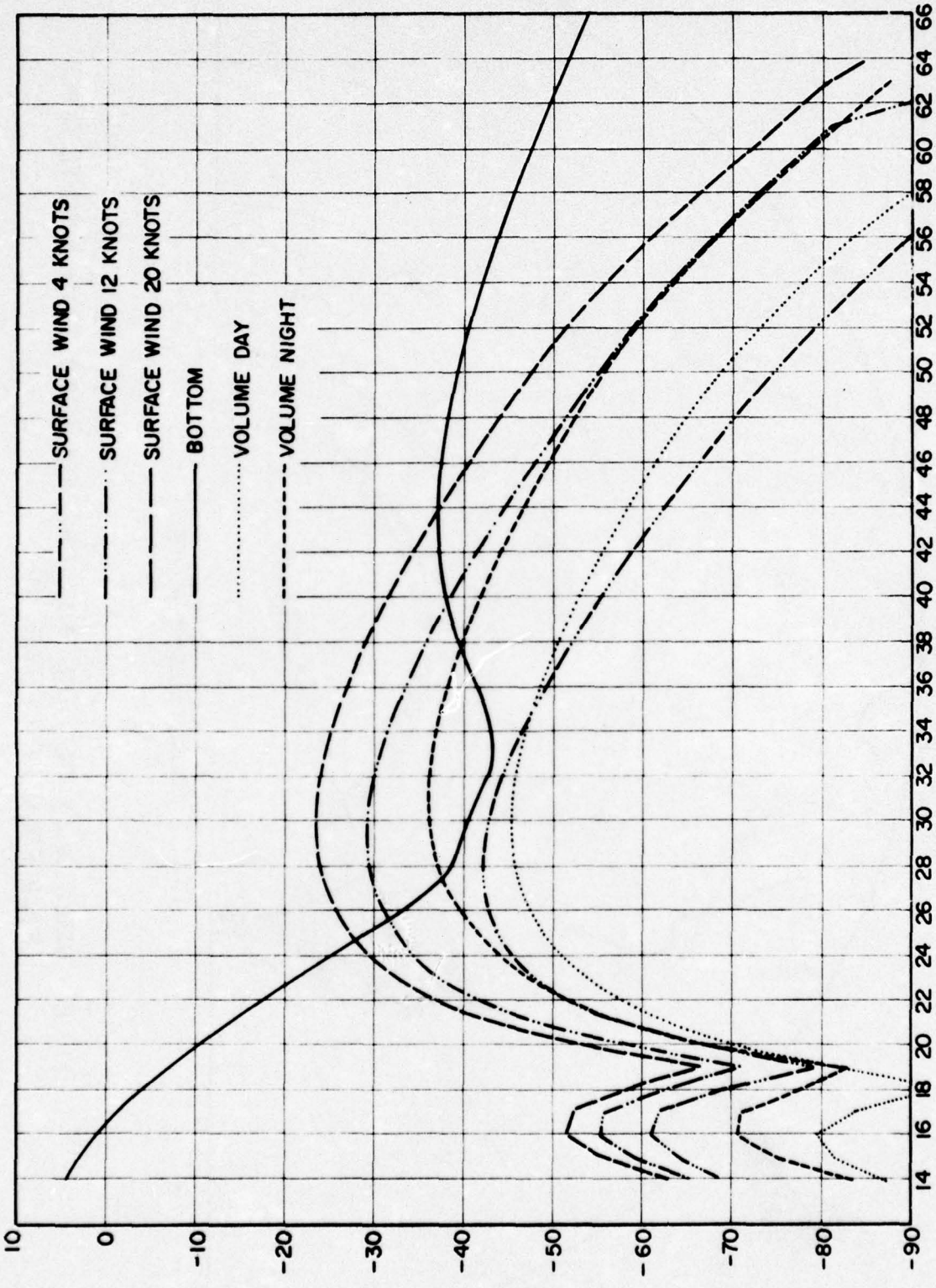

FIG. 9 – COMPUTED REVERBERATION FOR 25° BOTTOM BOUNCE SEARCH MODE

TRACOR, INC. DWG. A6-55-36
AUSTIN, TEXAS 2-23-67 ANASTASI/BL

$$I_F = \frac{I_o \Delta_T \Delta_R b}{(2d)^2} 10^{-\frac{k2d}{10}} ,$$

where Δ_T and Δ_R are signal attenuations due to the transmitting and receiving beams for a 90^o depressed ray,

I_o = on-axis source level,

b = attenuation due to bottom loss at normal incidence,

k = attenuation coefficient (dB/yd), and

d = water depth.

To obtain an estimate of the attenuation due to bottom loss, I_F is set equal to the measured intensity of the bottom return, which (from Fig. 5b) is $IM(t_1)$ minus the average noise power, NP. That is,

$$I_F = IM(t_1) - NP = \frac{I_o \Delta_T \Delta_R b}{(2d)^2} 10^{-\frac{k2d}{10}} ,$$

from which

$$b = \frac{4d^2[IM(t_1) - NP]}{I_o \Delta_T \Delta_R} 10^{\frac{k2d}{10}} .$$

The average noise power is given by a measurement of IM(t) at a time when the system is essentially noise limited, such as t_4 in Figs. 5a and b.

At t_2 seconds following transmission, IM is the intensity of the first order bottom reverberation. The bottom scattering strength, μ_B, from Eqs. (5) and (6), Section 3, is

$$\mu_B = \mu_B' \sin^2[\theta(t_2)] = IM_B(t_2)/G_B(t_2) \ , \qquad (12)$$

where $\theta(t_2)$ is the bottom grazing angle associated with time t_2, determined from a knowledge of the velocity profile and ray theory. Equation (12) is used to determine μ_B'; with an estimate of μ_B' the bottom scattering strength for any grazing angle may be obtained from Eq. (7).

Having determined bottom loss and bottom scattering strength, one may use the reverberation equations given in Appendix A to compute the intensity contributions of each of the bottom reverberation paths at each time point in the echo-ranging cycle. The total bottom reverberation intensity at time t, $I_B(t)$, is obtained by summing the contribution received from each of the bottom paths at time t. The solid curve in Fig. 10 represents $I_B(t)$, the total bottom reverberation, obtained by summing the first, second, and third order curves shown in Fig. 5a.

The volume and surface reverberation received during the interval 15 to 22 seconds comes from scatterers at and near the surface, as shown in Fig. 11. The scattering areas shown in Fig. 11 for volume and surface reverberation differ little in size, and the round trip transmission losses associated with each are approximately equal. This is of course an expected result as long as d_L, the average depth of the biological scattering layer, is small in comparison with the bottom depth. Fig. 12 shows several plots of this type of volume reverberation for values of d_L from zero to 300 yds. The water depth assumed in these computations was 5500 yds. The differences among the curves are slight, indicating that an exact estimate of layer depth is not essential for deep water prediction purposes. For convenience, the following discussion assumes a value of zero for d_L. This assumption is not critical, but allows the equations to be written in a less cumbersome form.

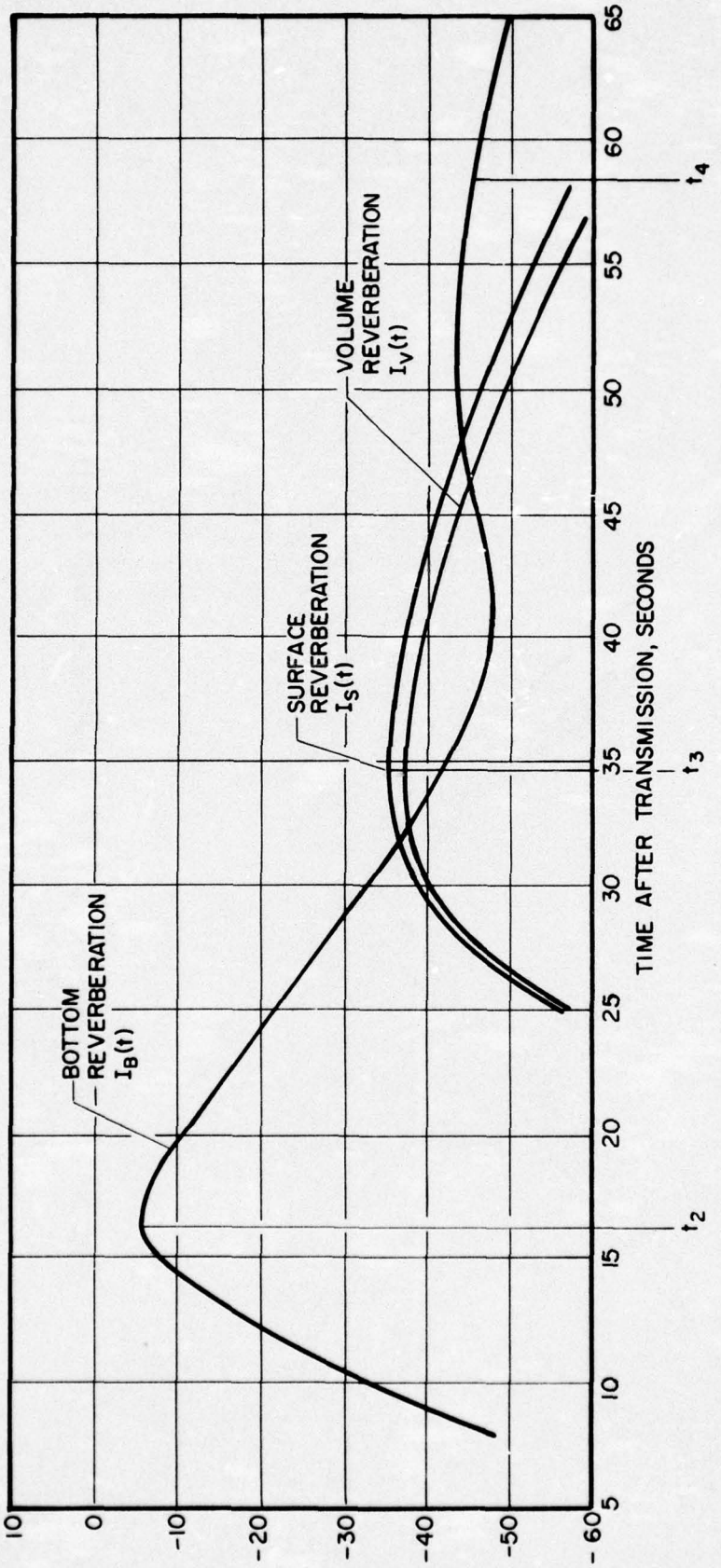

FIG. 10 – TOTAL BOTTOM REVERBERATION $I_B(t)$

TRACOR, INC. AUSTIN, TEXAS 3-8-67 DWG. A6-55-44 ANASTASI/SL

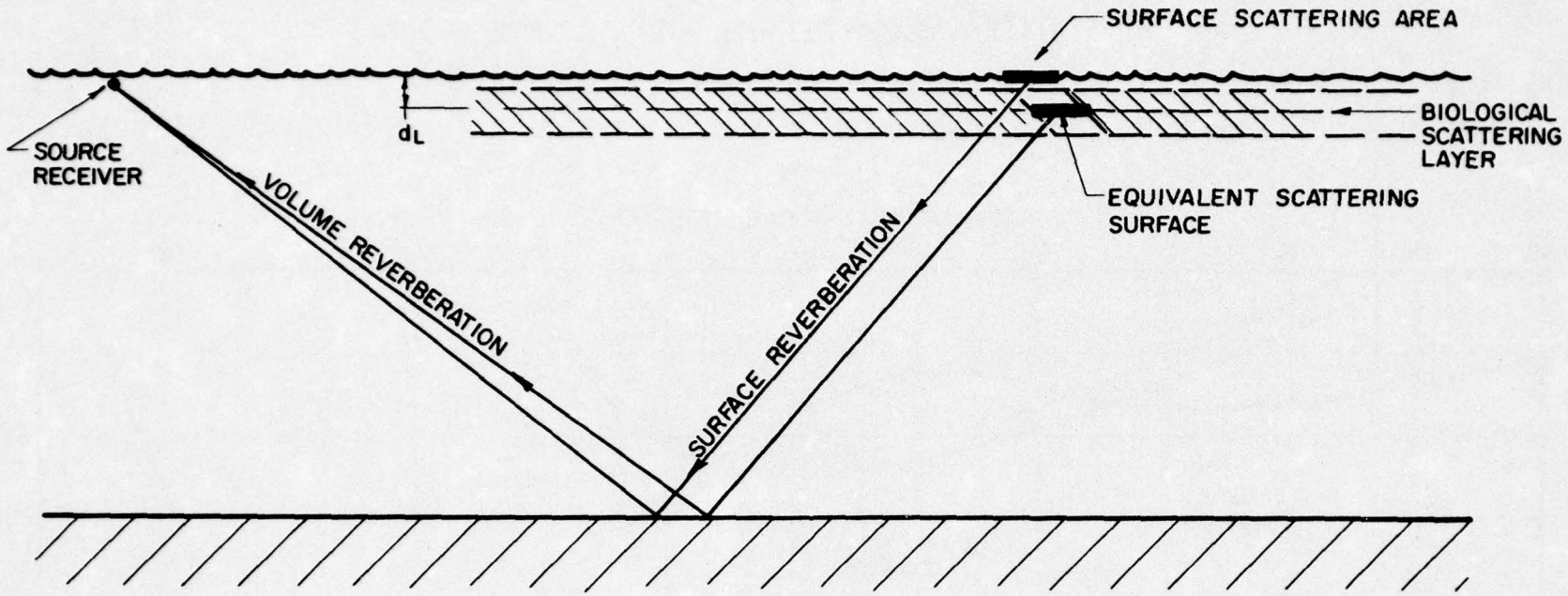

FIG. 11- SCATTERING AREAS FOR SURFACE AND VOLUME REVERBERATION

UNCLASSIFIED

TRACOR, INC. AUSTIN, TEXAS DWG. A6-55-5 1-22-67 ANASTASI/SL

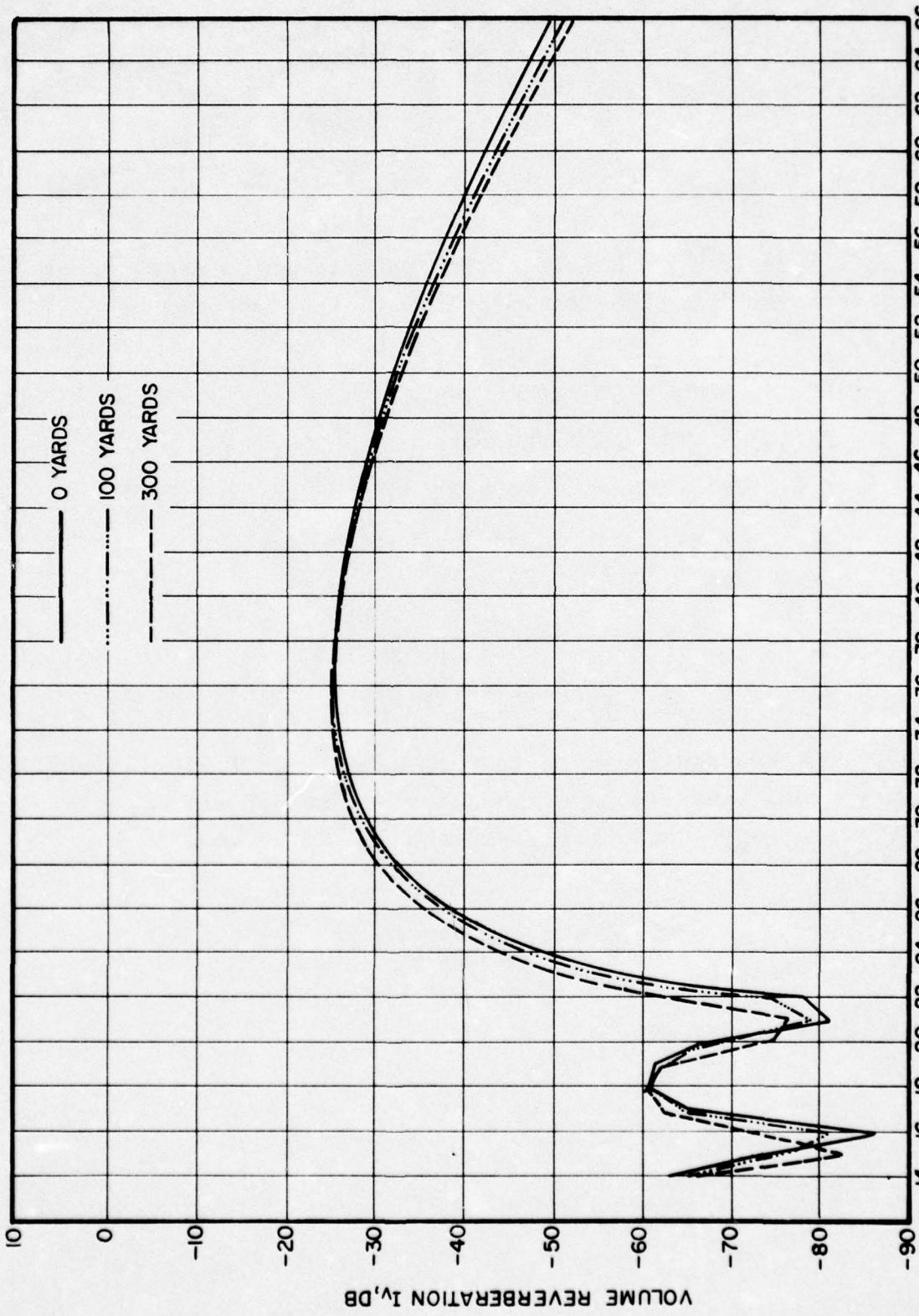

FIG. 12 – VOLUME REVERBERATION FOR SEVERAL LAYER DEPTHS

TRACOR, INC. DWG. A6-55-43
AUSTIN, TEXAS 2-23-67 ANASTASI/SL

From Fig. 5a, the measured intensity at time t_3, $IM(t_3)$, is the sum of the intensities of noise, volume, surface, and bottom reverberation. That is,

$$IM(t_3) = I_V(t_3) + I_S(t_3) + I_B(t_3) + NP, \qquad (13)$$

where $I_B(t_3)$ is the sum of all bottom reverberation received at t_3, a quantity which--from the previous discussion--may be computed,

NP = average noise power,

$I_V(t_3)$ = volume reverberation = $b^2 \mu_L G_V(t_3)$,

$I_S(t_3)$ = surface reverberation = $b^2 \mu_S(\theta_S)\, G_S(t_3)$,

b = attenuation due to bottom loss,

μ_L = volume scattering strength,

$\mu_S(\theta_S)$ = surface scattering strength, and

θ_S = the surface grazing angle giving rise to the surface reverberation received at time t_3.

Since d_L, the average depth of the biological scattering layer, was set to zero, the time functions for volume and surface reverberation, $G_V(t)$ and $G_S(t)$, are equal. If we let

$$G_R(t) = G_V(t) = G_S(t),$$

then Eq. (13) may be written as

$$IM(t_3) = b^2\mu_L G_R(t_3) + b^2\mu_S(\theta_S)\, G_R(t_3)$$

$$+ I_B(t_3) + NP$$

$$= b^2 G_R(t_3)\,[\mu_L + \mu_S(\theta_S)]$$

$$+ I_B(t_3) + NP,$$

from which

$$\mu_L + \mu_S(\theta_S) = \frac{IM(t_3) - I_B(t_3) - NP}{b^2 G_R(t_3)} . \qquad (14)$$

Since all quantities on the right hand side of Eq. (14) are known we have, at this point, one equation and two unknowns, μ_L and $\mu_S(\theta_S)$. To obtain estimates for both μ_L and $\mu_S(\theta_S)$ additional information is required. For example, a scheme may be developed for obtaining an independent measurement of μ_L, allowing Eq. (14) to be solved for $\mu_S(\theta_S)$. This approach has merit, but would probably require additional hardware onboard ship.

As an alternative, an estimate of $\mu_S(\theta_S)$ for the given frequency, wind speed, and grazing angle may be obtained from the result of previous oceanographic surveys. The value determined for $\mu_S(\theta_S)$ could, of course, then be used in Eq. (14) to obtain the volume scattering strength μ_L. With the existing onboard equipment this last approach seems the most promising. The equation given by Chapman and Harris[8] for $\mu_S(\theta_S)$ may prove

[8] Ibid.

sufficient for our purpose. It is expected that further refinement of this expression or, perhaps, the formulation of a similar function particularly suited to the specific frequency and bandwidth of the AN/SQS-26 can be determined from an analysis of AN/SQS-26 surface reverberation data obtained for various wind speeds and beam depression angles.

Given, then, a reliable expression for surface scattering strength, the methods outlined in the previous sections may be used in determining in situ estimates of all of the environmental parameters required for performance prediction. These parameters may then be used in the reverberation prediction equations of Appendix A to obtain the total masking background level at the receiver beamformer output for each possible depression angle of the bottom bounce mode. Using assumed values for target strength, target horizontal range and depth, and the in situ estimate of bottom loss, the equations of Appendix B may be used to obtain echo levels for each bottom bounce operating mode. The computation of the signal-to-noise ratio for each of the above operating modes follows directly.

4.2 STABILITY OF REVERBERATION LEVELS

An implicit assumption in the preceding discussion of in situ parameter estimation is that the effort is worthwhile; that is, that an in situ performance prediction based on a reverberation history will provide a good estimate of future results. This assumption requires a certain degree of temporal and spatial stability of the reverberation levels from which the parameter estimates are derived. As part of an initial investigation of this stability, an analysis was made of the variation of reverberation recorded on consecutive AN/SQS-26 echo-ranging cycles[9]. Ping-to-ping fluctuation in observed average reverberation

[9] Collins, J. L., "Technical Note on the Stability of AN/SQS-26 Echo Ranging Cycles (U)," TRACOR Doc. Number 65-206-C, Contract NObsr-93140, June 9, 1965, Confidential.

levels will, of course, be reflected in the derived parameter estimates and, thus, in the confidence which may be placed in the associated in situ performance prediction.

Figures 13 through 32 are Sanborn plots (in dB) of the ensemble average and standard deviation of varying numbers of consecutive AN/SQS-26 echo-ranging cycles. In the (b) part of each figure, a vertical line of length 2σ is plotted at time t, and centered on the ensemble average (for this time, t) computed over the reverberation envelopes obtained on pings 1 through n. σ is the standard deviation about the mean of this sample of size n (with the exception of ping 1). Thus, a curve through the center of the heavy line represents the ensemble average as a function of time for that ping and all previous pings, and the thickness of the heavy line is twice the time varying standard deviation. The data, representing the rectified and averaged output of the AN/SQS-26 receiving beamformer were recorded in the North Atlantic in Area Bravo. Since each ping cycle lasts approximately 30 seconds, a 20 ping history covers a time span of 10 minutes. For an assumed ship speed of 5 knots, this would correspond to a distance traveled of roughly one nautical mile. Data available for this study did not include more than 20 consecutive pings.

An inspection of Figs. 13 through 32 indicates that the average reverberation level and associated standard deviation are established in a relatively few echo ranging cycles. The final results shown in ping 20 differ little, for example, from the curves shown for the first few pings in the set.

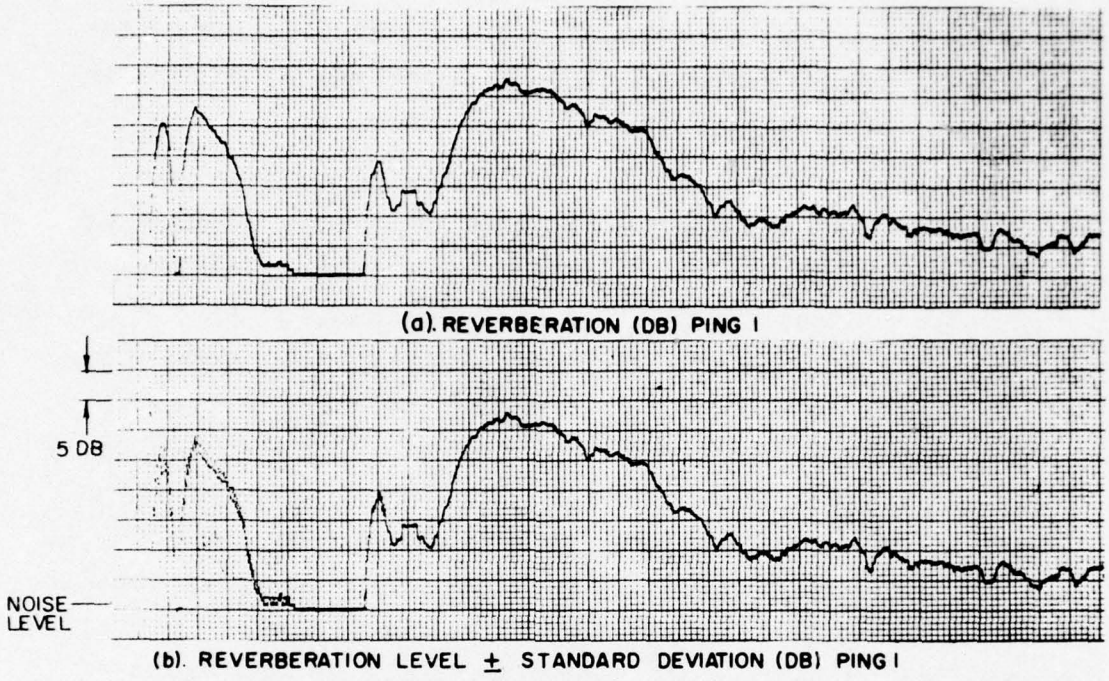

(a). REVERBERATION (DB) PING 1

(b). REVERBERATION LEVEL ± STANDARD DEVIATION (DB) PING 1

FIG. 13 – SANBORN PLOTS OF REVERBERATION AND ACCUMULATIVE DEVIATION FOR 30° DEPRESSED BOTTOM BOUNCE MODE IN AREA BRAVO

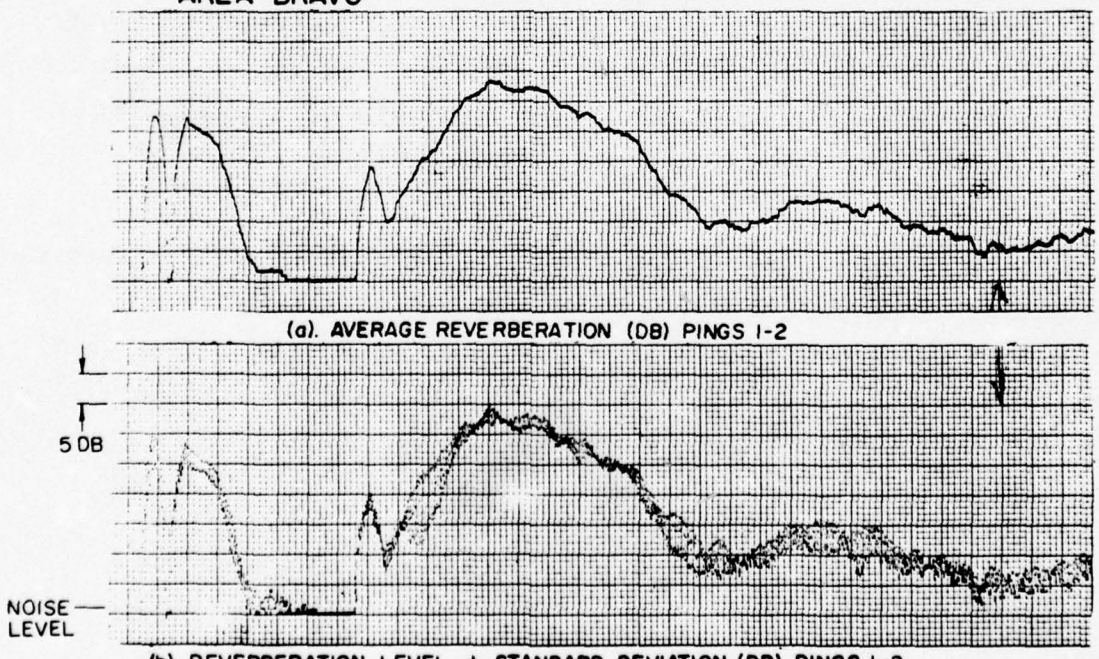

(a). AVERAGE REVERBERATION (DB) PINGS 1-2

(b) REVERBERATION LEVEL ± STANDARD DEVIATION (DB) PINGS 1-2

FIG. 14 – SANBORN PLOTS OF REVERBERATION AND ACCUMULATIVE DEVIATION FOR 30° DEPRESSED BOTTOM BOUNCE MODE IN AREA BRAVO

TRACOR, INC. DWG A6-55-8
AUSTIN, TEXAS 2-14-67 ANASTASI/SL

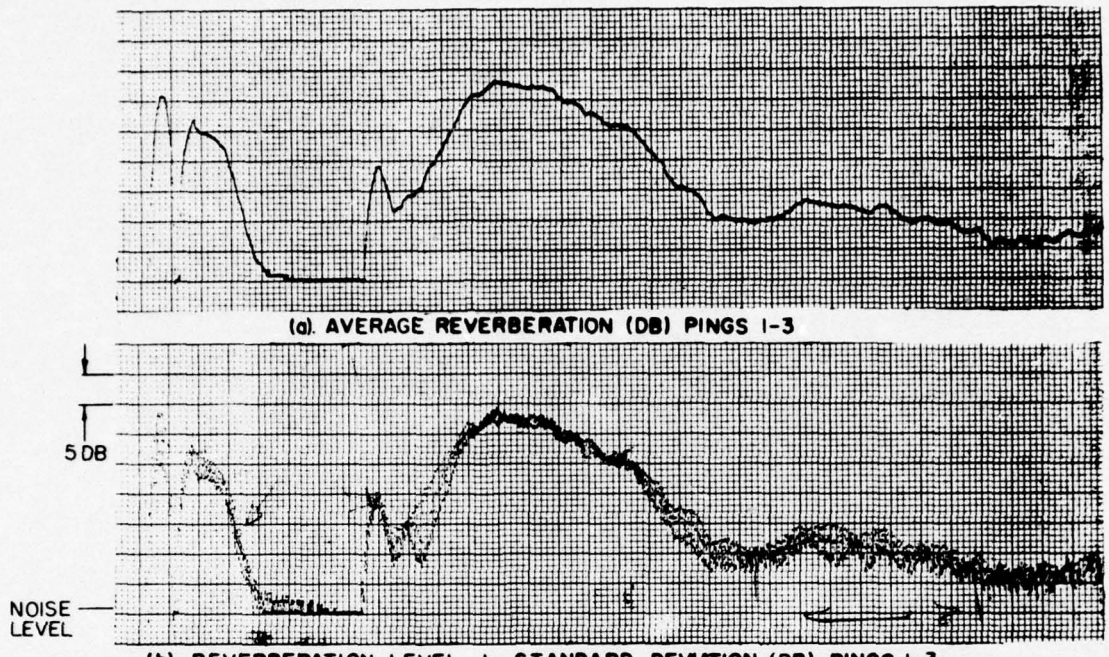

(a). AVERAGE REVERBERATION (DB) PINGS 1-3

(b). REVERBERATION LEVEL ± STANDARD DEVIATION (DB) PINGS 1-3

FIG. 15 – SANBORN PLOTS OF REVERBERATION AND ACCUMULATIVE DEVIATION FOR 30° DEPRESSED BOTTOM BOUNCE MODE IN AREA BRAVO

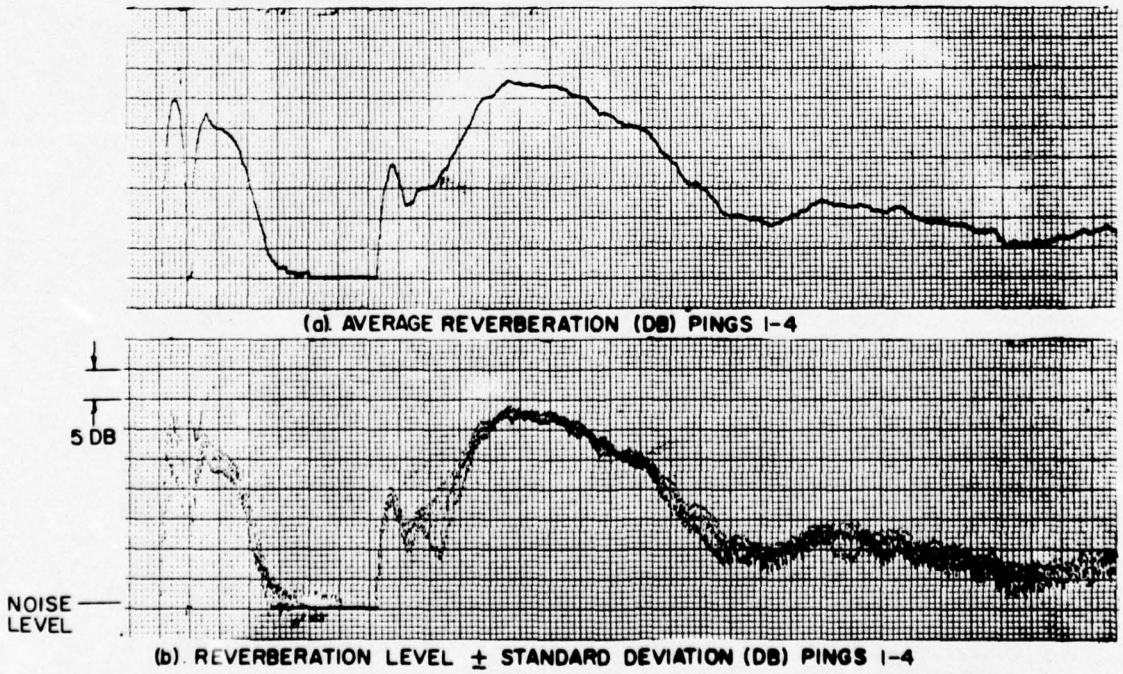

(a). AVERAGE REVERBERATION (DB) PINGS 1-4

(b). REVERBERATION LEVEL ± STANDARD DEVIATION (DB) PINGS 1-4

FIG. 16 – SANBORN PLOTS OF REVERBERATION AND ACCUMULATIVE DEVIATION FOR 30° DEPRESSED BOTTOM BOUNCE MODE IN AREA BRAVO

TRACOR, INC. AUSTIN, TEXAS — DWG. A8-35-9 — 8-14-67 — ANASTASI/BL

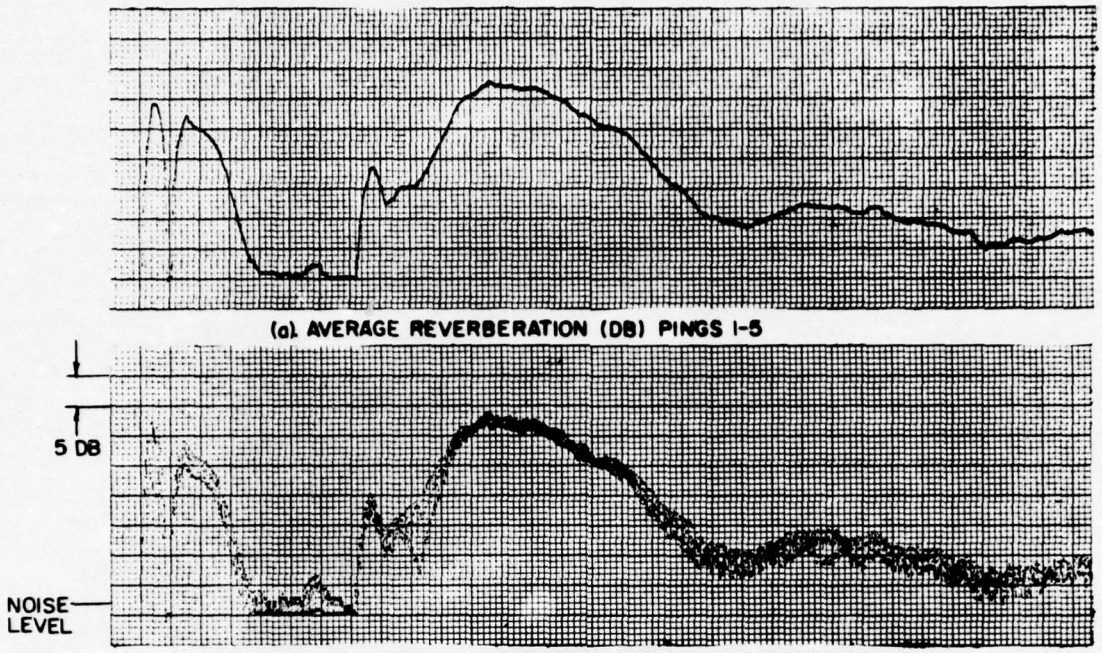

(a). AVERAGE REVERBERATION (DB) PINGS 1-5

(b). REVERBERATION LEVEL ± STANDARD DEVIATION (DB) PINGS 1-5

FIG. 17 – SANBORN PLOTS OF REVERBERATION AND ACCUMULATIVE DEVIATION FOR 30° DEPRESSED BOTTOM BOUNCE MODE IN AREA BRAVO

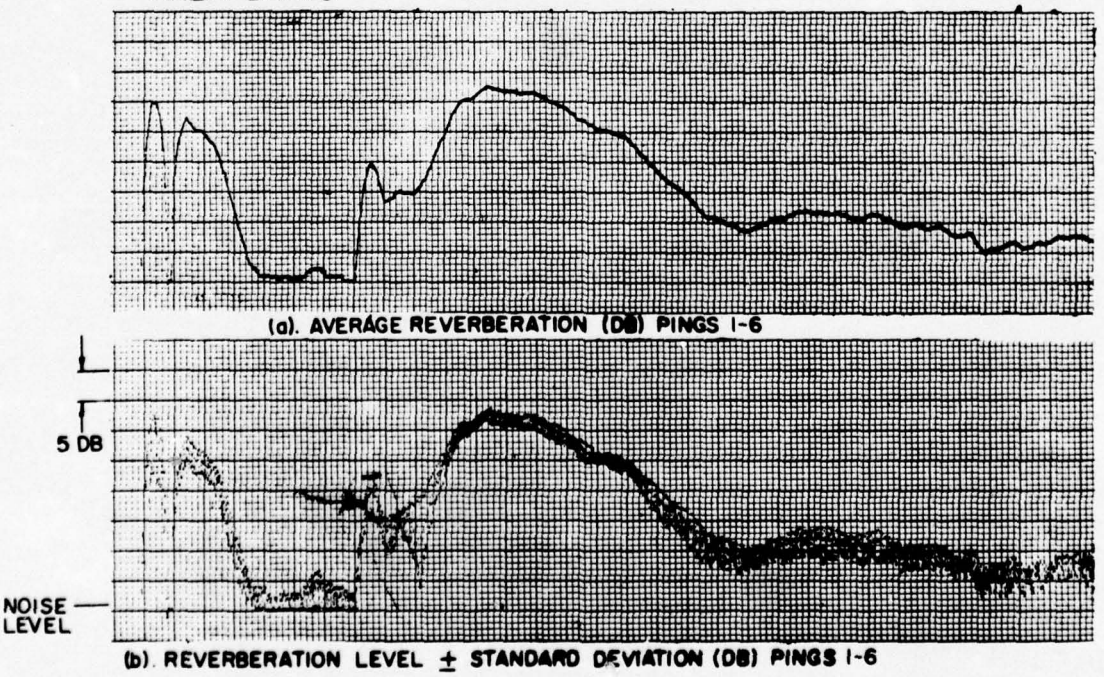

(a). AVERAGE REVERBERATION (DB) PINGS 1-6

(b). REVERBERATION LEVEL ± STANDARD DEVIATION (DB) PINGS 1-6

FIG. 18 – SANBORN PLOTS OF REVERBERATION AND ACCUMULATIVE DEVIATION FOR 30° DEPRESSED BOTTOM BOUNCE MODE IN AREA BRAVO

TRACOR, INC. AUSTIN, TEXAS DWG. A6-55-10 2-14-67 ANASTASI/SL

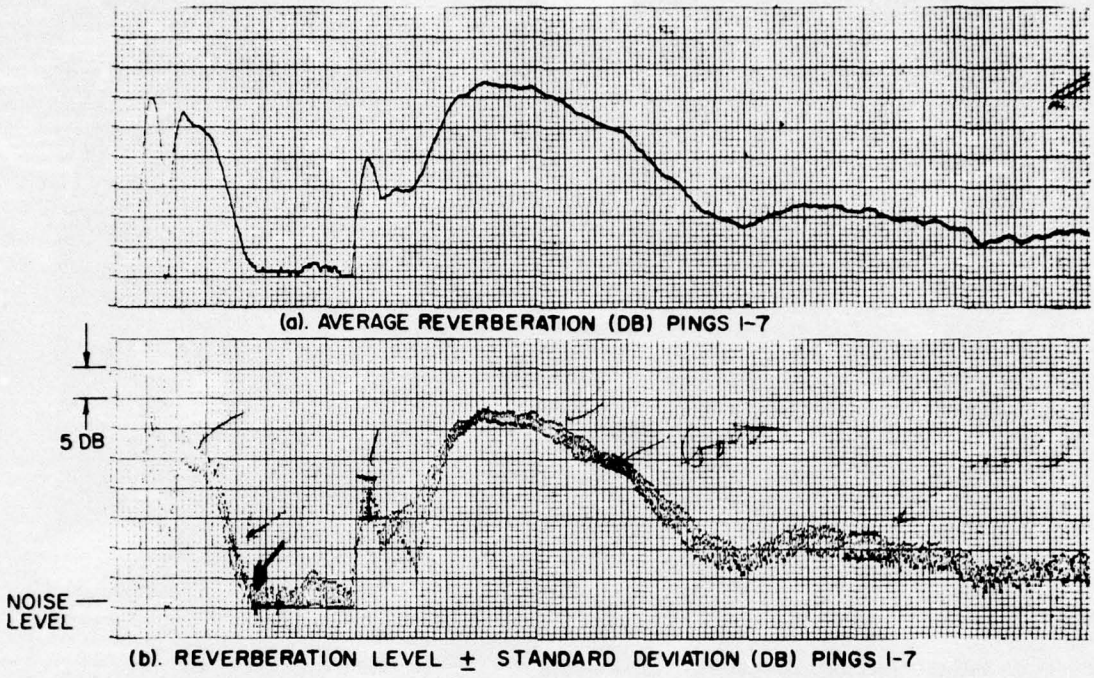

FIG.19 – SANBORN PLOTS OF REVERBERATION AND ACCUMULATIVE DEVIATION FOR 30° DEPRESSED BOTTOM BOUNCE MODE IN AREA BRAVO

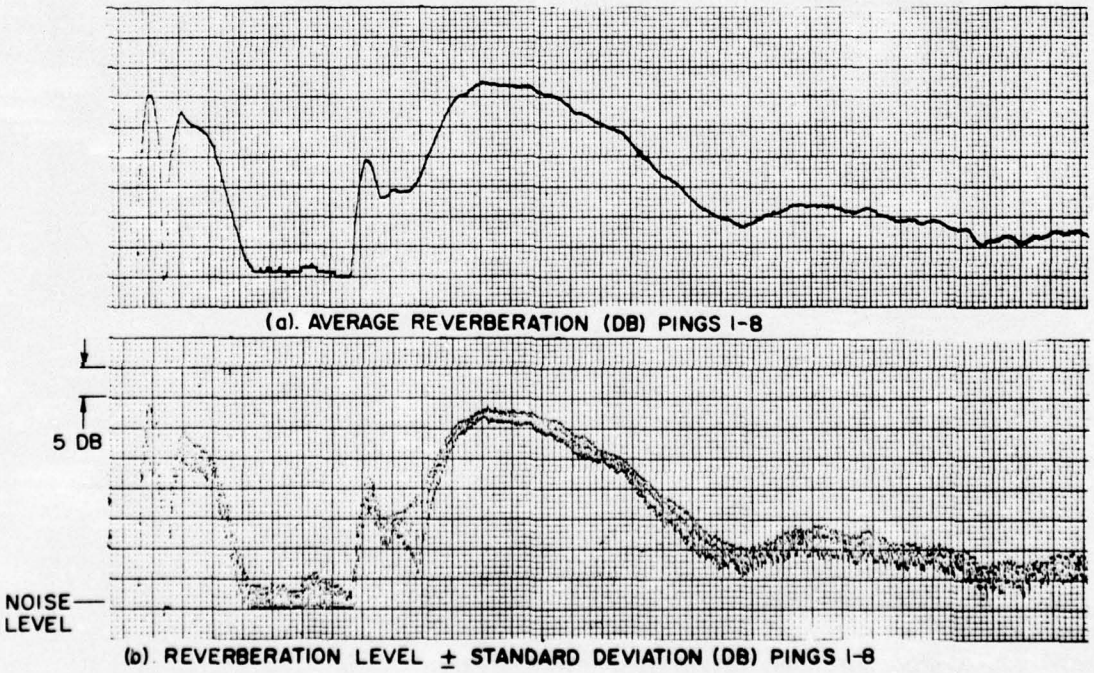

FIG.20 – SANBORN PLOTS OF REVERBERATION AND ACCUMULATIVE DEVIATION FOR 30° DEPRESSED BOTTOM BOUNCE MODE IN AREA BRAVO

TRACOR, INC. DWG. A6-55-11
AUSTIN, TEXAS 2-14-67 ANASTASI/BL

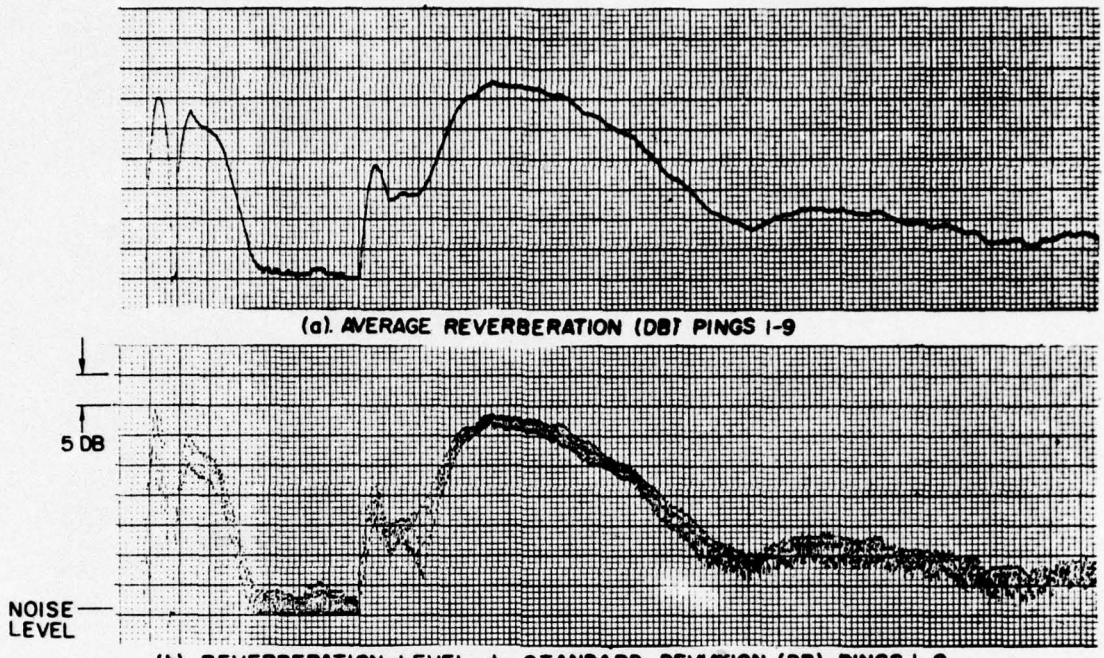

(a). AVERAGE REVERBERATION (DB) PINGS 1-9

(b). REVERBERATION LEVEL ± STANDARD DEVIATION (DB) PINGS 1-9

FIG.21 – SANBORN PLOTS OF REVERBERATION AND ACCUMULATIVE DEVIATION FOR 30° DEPRESSED BOTTOM BOUNCE MODE IN AREA BRAVO

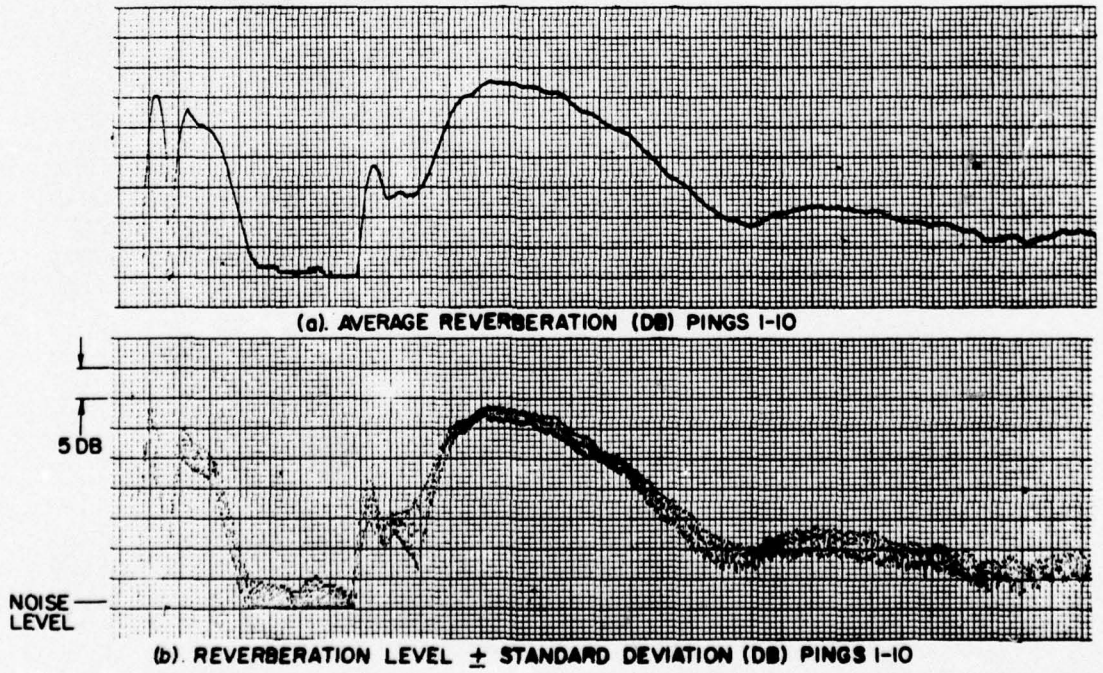

(a). AVERAGE REVERBERATION (DB) PINGS 1-10

(b). REVERBERATION LEVEL ± STANDARD DEVIATION (DB) PINGS 1-10

FIG.22 – SANBORN PLOTS OF REVERBERATION AND ACCUMULATIVE DEVIATION FOR 30° DEPRESSED BOTTOM BOUNCE MODE IN AREA BRAVO

TRACOR, INC. AUSTIN, TEXAS — DWG. A6-55-12 — 2-14-67 ANASTASI/SL

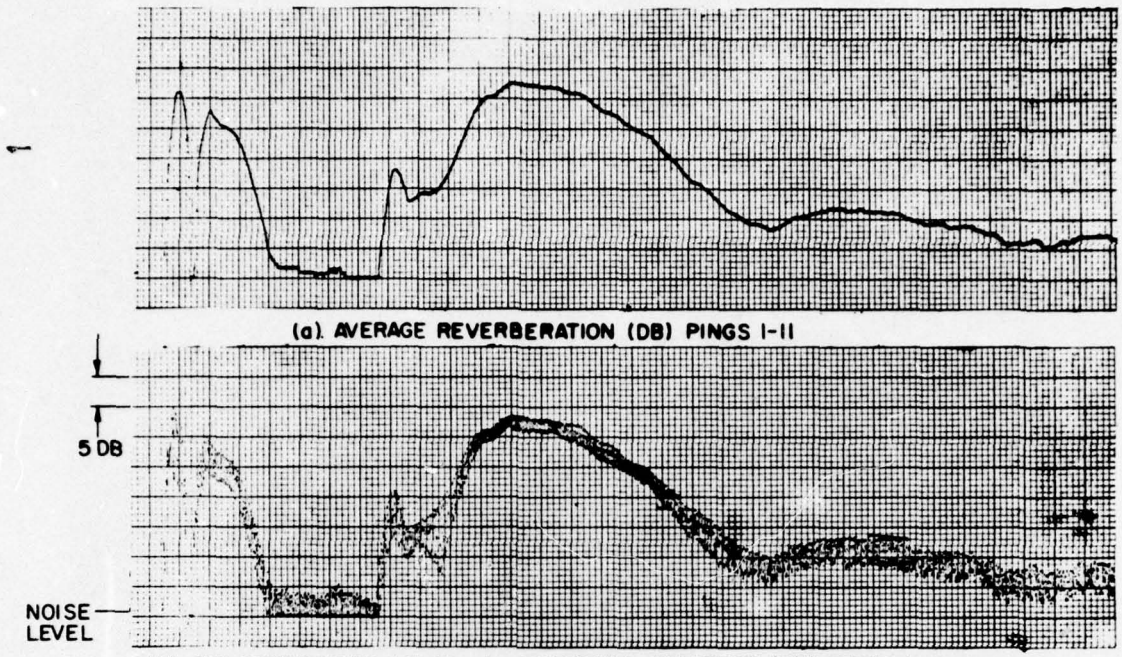

(a). AVERAGE REVERBERATION (DB) PINGS 1-11

(b). REVERBERATION LEVEL ± STANDARD DEVIATION (DB) PINGS 1-11

FIG. 23 – SANBORN PLOTS OF REVERBERATION AND ACCUMULATIVE DEVIATION FOR 30° DEPRESSED BOTTOM BOUNCE MODE IN AREA BRAVO

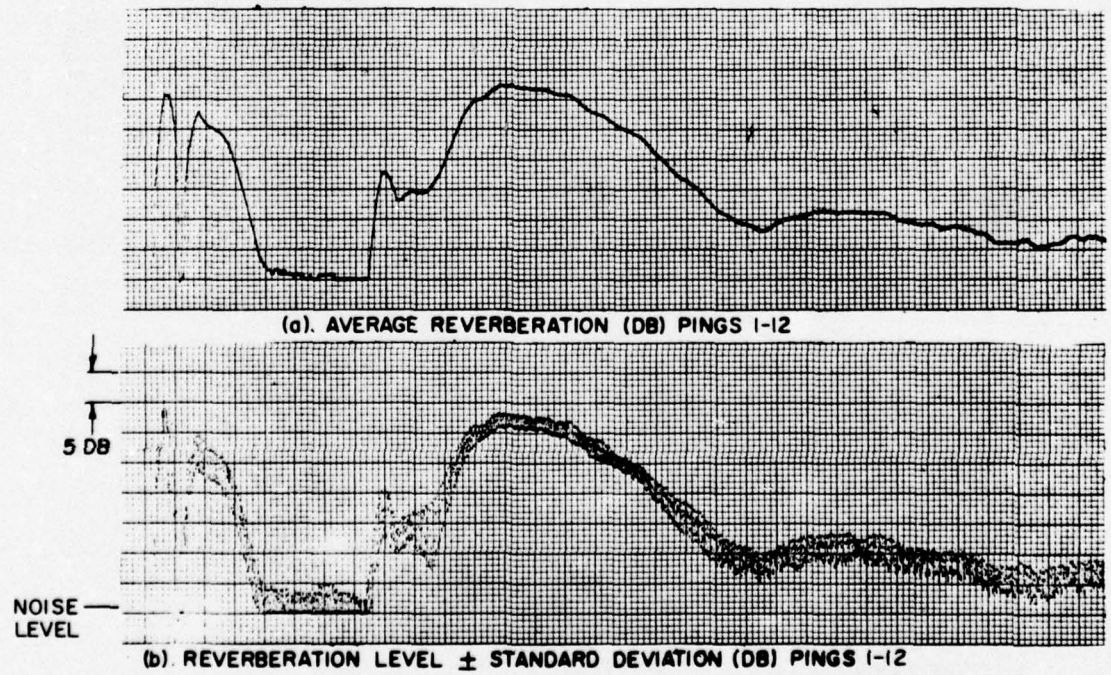

(a). AVERAGE REVERBERATION (DB) PINGS 1-12

(b). REVERBERATION LEVEL ± STANDARD DEVIATION (DB) PINGS 1-12

FIG. 24 – SANBORN PLOTS OF REVERBERATION AND ACCUMULATIVE DEVIATION FOR 30° DEPRESSED BOTTOM BOUNCE MODE IN AREA BRAVO

TRACOR, INC. DWG. A6-55-13
AUSTIN, TEXAS 2-14-67 ANASTASI/SL

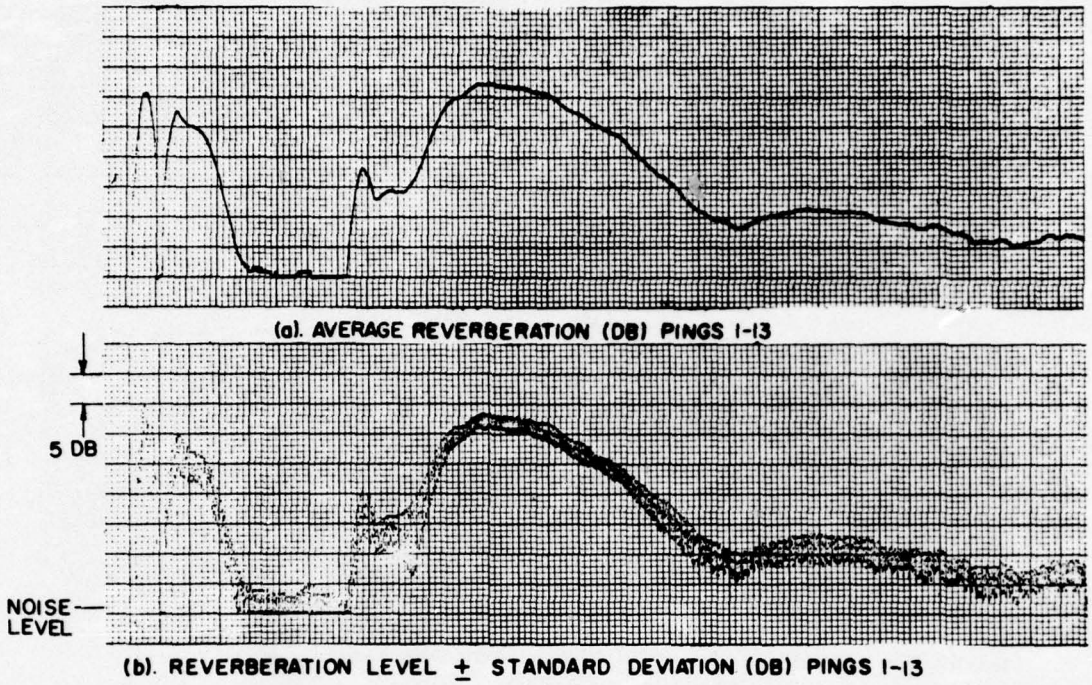

(a). AVERAGE REVERBERATION (DB) PINGS 1-13

(b). REVERBERATION LEVEL ± STANDARD DEVIATION (DB) PINGS 1-13

FIG. 25 – SANBORN PLOTS OF REVERBERATION AND ACCUMULATIVE DEVIATION FOR 30° DEPRESSED BOTTOM BOUNCE MODE IN AREA BRAVO

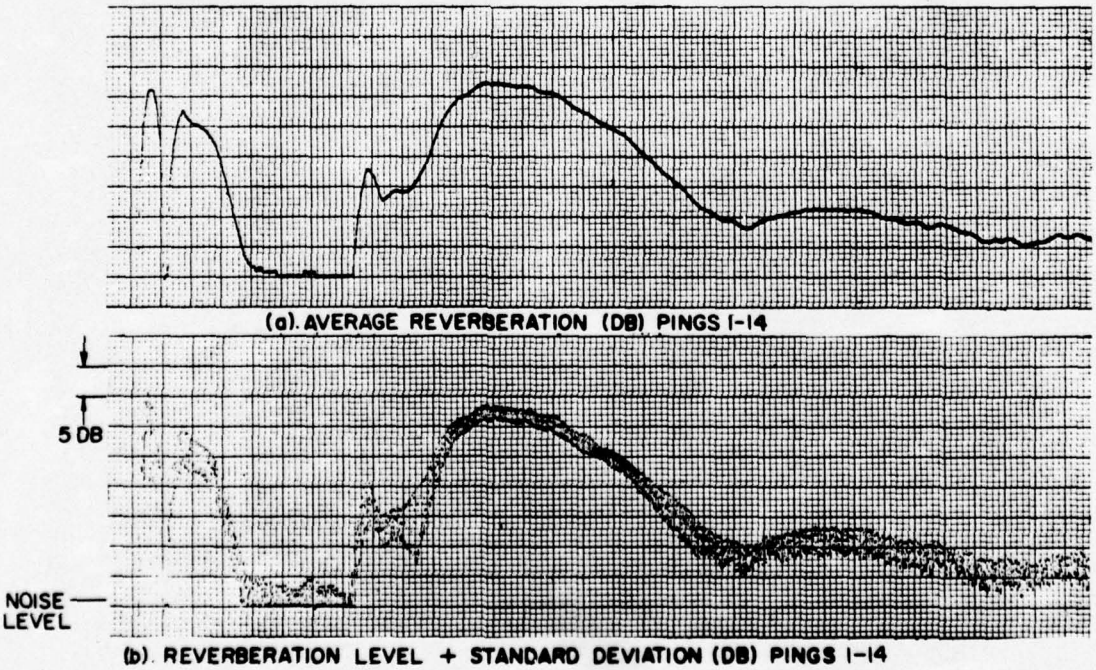

(a). AVERAGE REVERBERATION (DB) PINGS 1-14

(b). REVERBERATION LEVEL + STANDARD DEVIATION (DB) PINGS 1-14

FIG. 26 – SANBORN PLOTS OF REVERBERATION AND ACCUMULATIVE DEVIATION FOR 30° DEPRESSED BOTTOM BOUNCE MODE IN AREA BRAVO

TRACOR, INC. AUSTIN, TEXAS DWG. A6-55-14 2-14-67 ANAS7831/3L

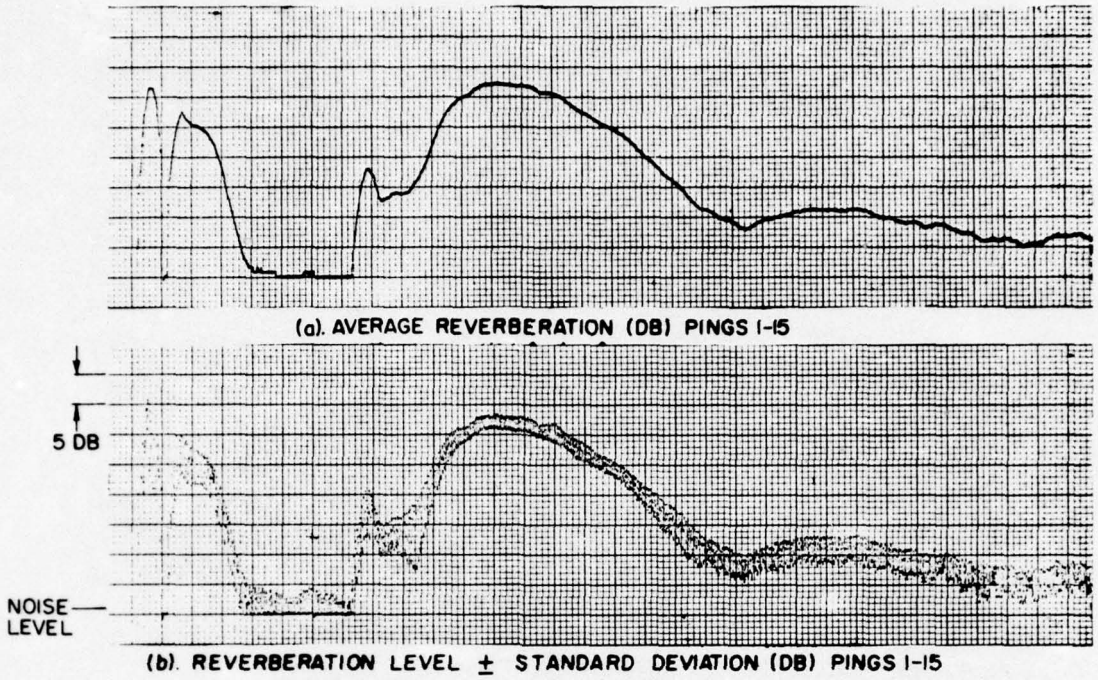

(a). AVERAGE REVERBERATION (DB) PINGS 1-15

(b). REVERBERATION LEVEL ± STANDARD DEVIATION (DB) PINGS 1-15

FIG. 27 – SANBORN PLOTS OF REVERBERATION AND ACCUMULATIVE DEVIATION FOR 30° DEPRESSED BOTTOM BOUNCE MODE IN AREA BRAVO

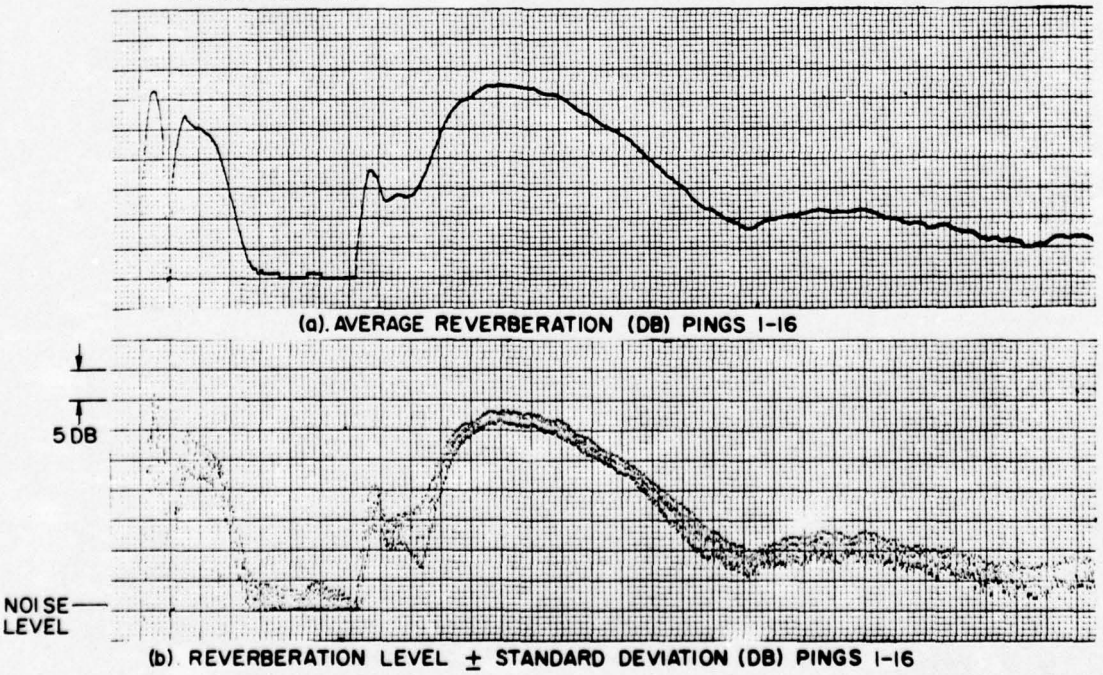

(a). AVERAGE REVERBERATION (DB) PINGS 1-16

(b). REVERBERATION LEVEL ± STANDARD DEVIATION (DB) PINGS 1-16

FIG. 28 – SANBORN PLOTS OF REVERBERATION AND ACCUMULATIVE DEVIATION FOR 30° DEPRESSED BOTTOM BOUNCE MODE IN AREA BRAVO

TRACOR, INC. DWG. A6-55-15
AUSTIN, TEXAS 2-14-67 ANASTASI/SL

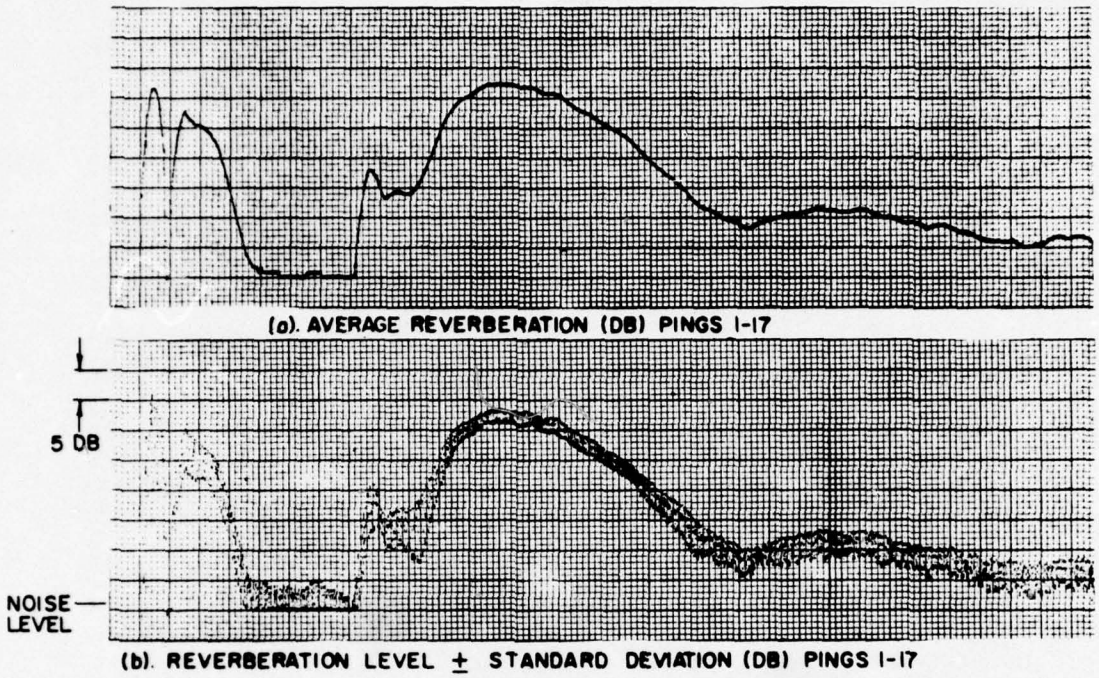

(a). AVERAGE REVERBERATION (DB) PINGS 1-17

(b). REVERBERATION LEVEL ± STANDARD DEVIATION (DB) PINGS 1-17

FIG. 29 – SANBORN PLOTS OF REVERBERATION AND ACCUMULATIVE DEVIATION FOR 30° DEPRESSED BOTTOM BOUNCE MODE IN AREA BRAVO

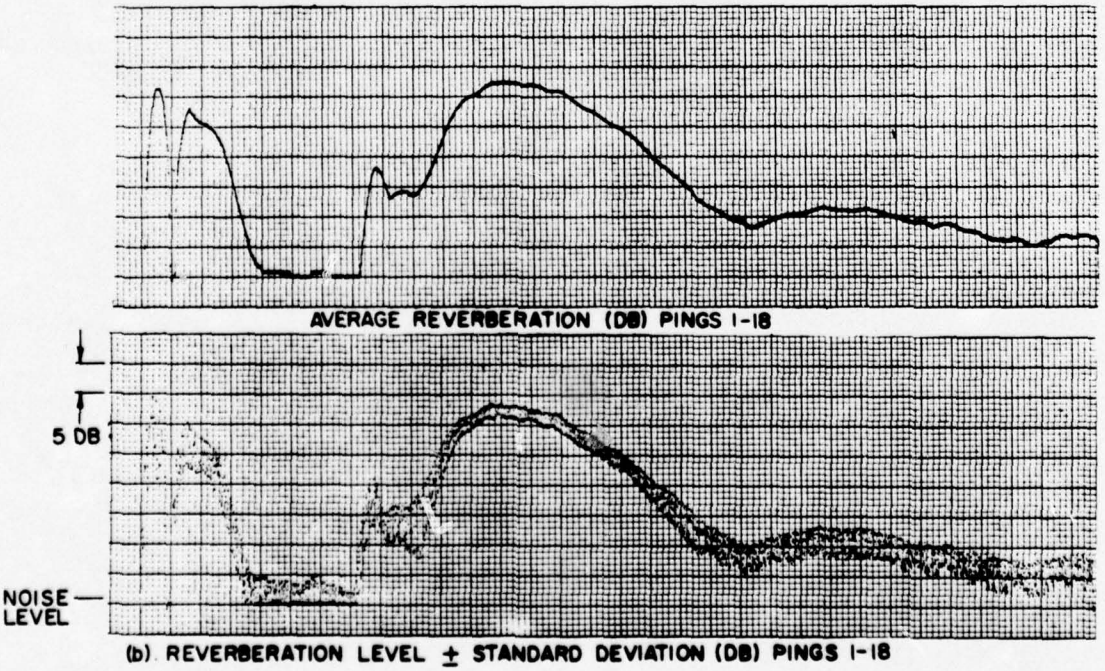

AVERAGE REVERBERATION (DB) PINGS 1-18

(b). REVERBERATION LEVEL ± STANDARD DEVIATION (DB) PINGS 1-18

FIG. 30 – SANBORN PLOTS OF REVERBERATION AND ACCUMULATIVE DEVIATION FOR 30° DEPRESSED BOTTOM BOUNCE MODE IN AREA BRAVO

TRACOR, INC. AUSTIN, TEXAS | DWG. A8-55-16 | 2-14-67 ANASTASI/SL

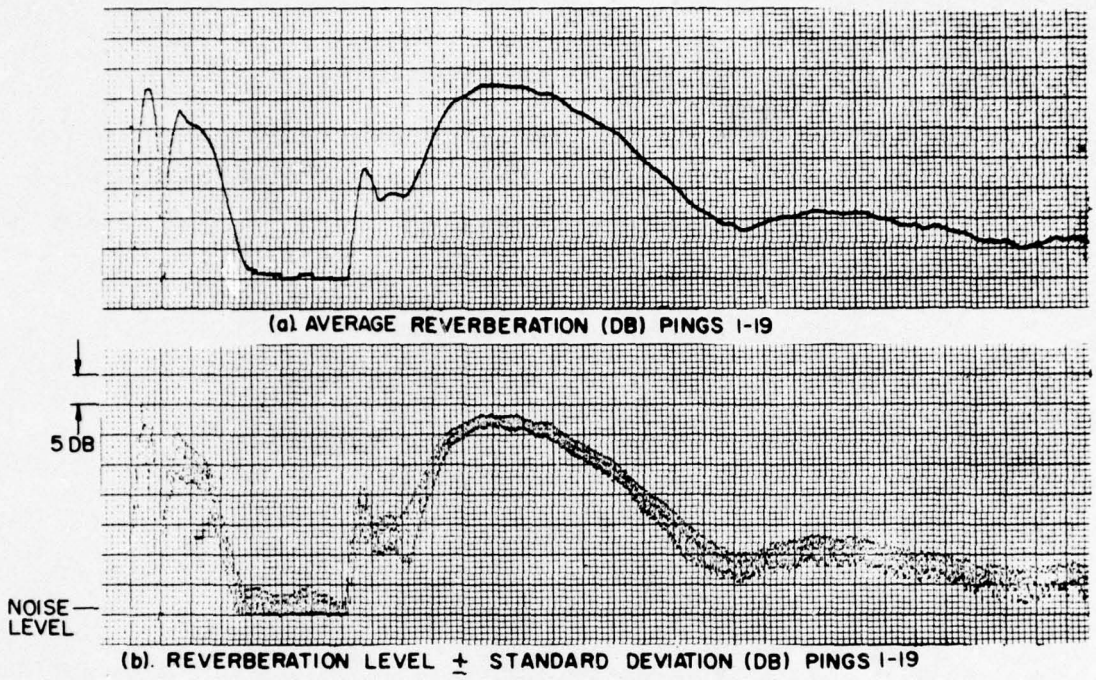

(a) AVERAGE REVERBERATION (DB) PINGS 1-19

(b). REVERBERATION LEVEL ± STANDARD DEVIATION (DB) PINGS 1-19

FIG. 31 – SANBORN PLOTS OF REVERBERATION AND ACCUMULATIVE DEVIATION FOR 30° DEPRESSED BOTTOM BOUNCE MODE IN AREA BRAVO

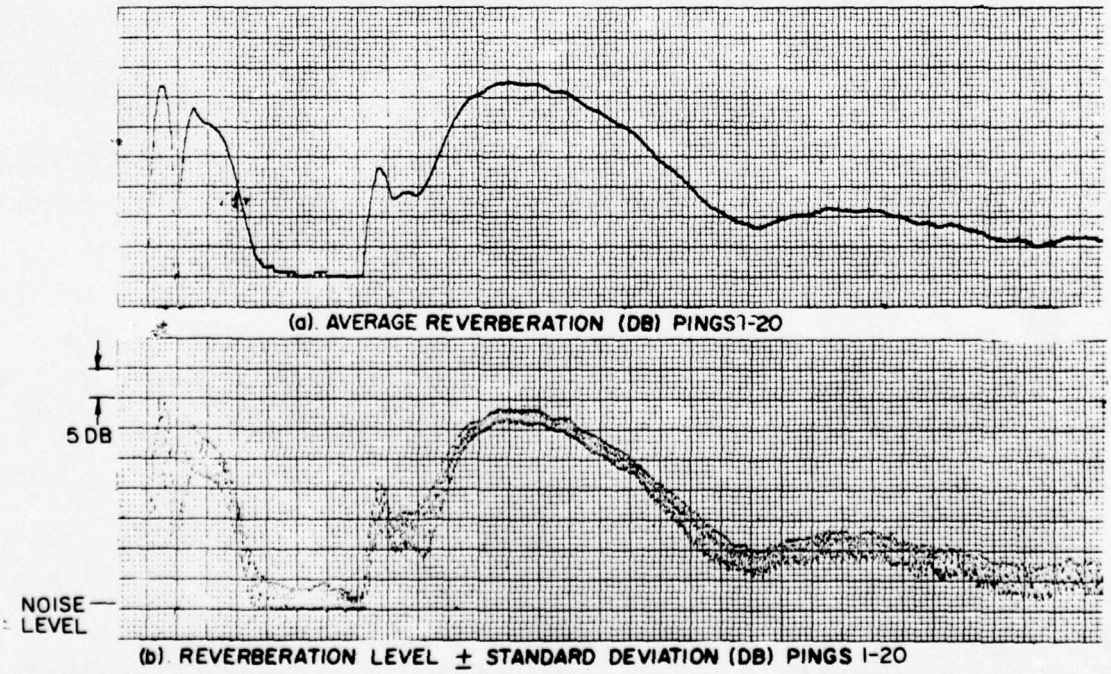

(a). AVERAGE REVERBERATION (DB) PINGS1-20

(b). REVERBERATION LEVEL ± STANDARD DEVIATION (DB) PINGS 1-20

FIG. 32 – SANBORN PLOTS OF REVERBERATION AND ACCUMULATIVE DEVIATION FOR 30° DEPRESSED BOTTOM BOUNCE MODE IN AREA BRAVO

TRACOR, INC. DWG. A6-55-17
AUSTIN, TEXAS 2-14-67 ANASTASI / SL

5. SAMPLE PARAMETER ESTIMATES

A method for obtaining in situ parameter estimates which incorporates the previously discussed equations and techniques has been developed and programmed for analysis of AN/SQS-26 data. The program inputs are:

1. Recorded AN/SQS-26 bottom bounce reverberation cycles (receiving beamformer output),
2. Description of bottom bounce operating mode in which the data were recorded,
3. Water depth,
4. Wind speed, and
5. Velocity profile data.

The program outputs are:

1. Bottom loss,
2. Bottom scattering strength, and
3. Volume (deep scattering layer) scattering strength.

The estimate of volume scattering strength as discussed in Section 4 depends on an independently determined value for surface scattering strength. This requires a relation within the program between surface scattering strength and wind speed. At present, surface scattering strength is being obtained from the Chapman-Harris equation (Eq. 10). This is a tentative arrangement subject to the analysis of additional AN/SQS-26 sea data.

Although the signal attenuations, $\wedge R$ and $\triangle T$, due to the transmitting and receiving beam patterns for a 90^{o} depressed ray are now being calculated theoretically from a knowledge of the array geometry and beamforming process, the accuracy of these computations is questionable. The beam pattern calculations neglect both radiation impedance and the surrounding dome and hull structure. It is expected that any significant effects on the pattern due to either of these would be pronounced for angles approaching

90°. In practice, measured values of both ΔR and ΔT should be used.

Tables I through III summarize the program output parameter estimates obtained for two 20 ping sets and one 19 ping set of recorded AN/SQS-26 reverberation. The data are similar to that shown in Figs. 13 through 32, and were taken in an area of the Western North Atlantic about 450 miles east of Newport, R. I., bounded by 38° and 39°50' N Latitude and 65°20' and 65°50' W Longitude. The operating mode was bottom bounce track at 30° depression; the water depth was approximately 5000 yards. Wind speed data were not taken, and as a result, the volume and surface scattering strengths could not be separated. Instead, the sum of these two parameters appears in the two right-hand columns of each table.

Some indication of the parameter variation is provided by the computed standard deviation listed below the columns in each table. From these quantities, a rough estimate can be made of the number of samples of each parameter required to obtain meaningful averages. If each of the parameters is assumed to have a Gaussian distribution about some true average, then the curves shown in Fig. 33 may be used to relate the number of samples, n, used in obtaining an average value for a parameter, the true standard deviation of the parameter, and the margin of error, that is, the difference between the computed average over n samples and the true average. For example, if the true standard deviation of a parameter (the abscissa in Fig. 33) is 1.5 dB, and it is necessary that the computed average differ by less than 1 dB from the true average, then the curve labeled d = 1 may be used to obtain the value of 10 as the required number of parameter samples (the ordinate in Fig. 33). The required number of samples drops rapidly as the margin of error is allowed to increase. If the margin of error were 2 dB in the above example only 3 to 4 parameter samples would be required.

TRACOR, INC. 6500 TRACOR LANE, AUSTIN, TEXAS 78721

Table I
ESTIMATED VALUES OF SCATTERING
STRENGTHS AND BOTTOM LOSS

Set 1

Ping i	μ_B' Bottom Scattering Strength (dB)	B_i = 10 log b Bottom Loss (dB)	$\mu_{SL}=\mu_S(\theta_S)+\mu_L$ Surface+Volume Scattering Strength (dB)-using B_i	$\mu_{SL20}=\mu_S(\theta_S)+\mu_L$ Surface+Volume Scattering Strength (dB)-using $\bar{B}_{20}$
1	-37.5	15.9	-31.6	-34.9
2	-38.2	16.6	-28.9	-33.6
3	-36.5	12.2	-37.6	-33.5
4	-36.3	15.8	-28.6	-31.6
5	-37.1	12.7	-35.0	-31.9
6	-37.8	13.8	-33.9	-33.1
7	-38.3	15.6	-30.3	-33.0
8	-35.7	15.8	-30.4	-33.5
9	-36.9	15.5	-30.9	-33.5
10	-36.1	16.5	-30.0	-34.5
11	-35.6	13.7	-34.2	-33.2
12	-36.1	14.9	-31.5	-32.9
13	-37.0	14.4	-31.7	-32.1
14	-36.8	12.9	-36.0	-33.5
15	-38.4	14.4	-34.1	-34.4
16	-37.3	16.6	-29.6	-34.2
17	-37.2	15.1	-33.1	-34.8
18	-37.6	11.3	-40.8	-34.8
19	-39.1	11.8	-38.0	-33.1
20	-36.4	15.7	-31.7	-34.7
Average	-36.3	14.6	-32.9	-33.5
Standard Deviation σ (dB)	1.2	1.6	3.2	1.0

TRACOR, INC. 6500 TRACOR LANE, AUSTIN, TEXAS 78721

Table II
ESTIMATED VALUES OF SCATTERING
STRENGTHS AND BOTTOM LOSS
Set 2

Ping i	μ'_B Bottom Scattering Strength (dB)	$B_i = 10 \log b$ Bottom Loss (dB)	$\mu_{SL} = \mu(\theta_S)$ Surface+Volume Scattering Strength (dB)-using B_i	$\mu_{SL20} = \mu_S(\theta_S) + \mu_L$ Surface+Volume Scattering Strength (dB)-using $\bar{B}_{20}$
1	-38.4	18.4	-30.9	-35.4
2	-39.5	17.1	-32.5	-35.4
3	-40.8	19.1	-31.7	-37.7
4	-41.2	18.7	-32.4	-37.6
5	-39.3	18.1	-33.8	-37.7
6	-39.4	15.4	-37.2	-35.7
7	-39.2	15.4	-38.4	-37.1
8	-40.7	11.6	-49.2	-40.1
9	-39.8	19.2	-29.8	-30.0
10	-41.2	17.3	-36.2	-38.5
11	-42.7	14.7	-41.1	-38.2
12	-39.4	17.7	-33.4	-36.6
13	-41.1	16.6	-35.6	-36.5
14	-39.1	16.7	-33.5	-34.7
15	-36.0	15.3	-35.2	-33.5
16	-40.1	16.9	-33.7	-35.3
17	-41.9	15.2	-38.5	-36.6
18	-37.3	14.8	-36.3	-33.7
19	-38.2	16.4	-35.5	-36.1
20	-39.8	15.9	-34.2	-33.8
Average	-39.8	16.5	-35.5	-36.3
Standard Deviation (dB)	1.4	1.8	3.6	1.7

TRACOR, INC. 6500 TRACOR LANE, AUSTIN, TEXAS 78721

Table III
ESTIMATED VALUES OF SCATTERING
STRENGTHS AND BOTTOM LOSS

Set 3

Ping i	μ'_B Bottom Scattering Strength (dB)	B_i = 10 log b Bottom Loss (dB)	$\mu_{SL}=\mu_S(\theta)+\mu_L$ Surface+Volume Scattering Strength (dB)-using B_i	$\mu_{SL20}=\mu_S(\theta_S)+\mu_L$ Surface+Volume Scattering Strength (dB)-using $\bar{B}_{20}$
1	-34.0	11.2	-44.0	-35.6
2	-33.1	16.5	-34.1	-36.2
3	-34.4	20.5	-27.9	-38.2
4	-34.7	19.1	-32.3	-39.7
5	-33.6	14.8	-38.7	-37.4
6	-33.8	17.1	-33.6	-37.0
7	-33.5	16.2	-37.4	-38.9
8	-34.7	18.5	-30.8	-37.0
9	-35.0	16.2	-36.4	-38.0
10	-34.4	9.3	-49.6	-37.3
11	-34.7	16.4	-33.1	-34.9
12	-35.0	13.2	-40.8	-36.3
13	-34.8	16.1	-35.1	-36.3
14	-35.1	15.9	-39.3	-40.3
15	-34.1	11.2	-46.3	-37.7
16	-34.7	11.3	-45.1	-36.8
17	-34.4	16.8	-35.2	-37.9
18	-34.9	15.6	-36.5	-36.9
19	-34.7	13.0	-42.5	-37.6
Average	-34.4	15.2	-37.8	-37.4
Standard Deviation (dB)	0.5	2.9	5.7	1.2

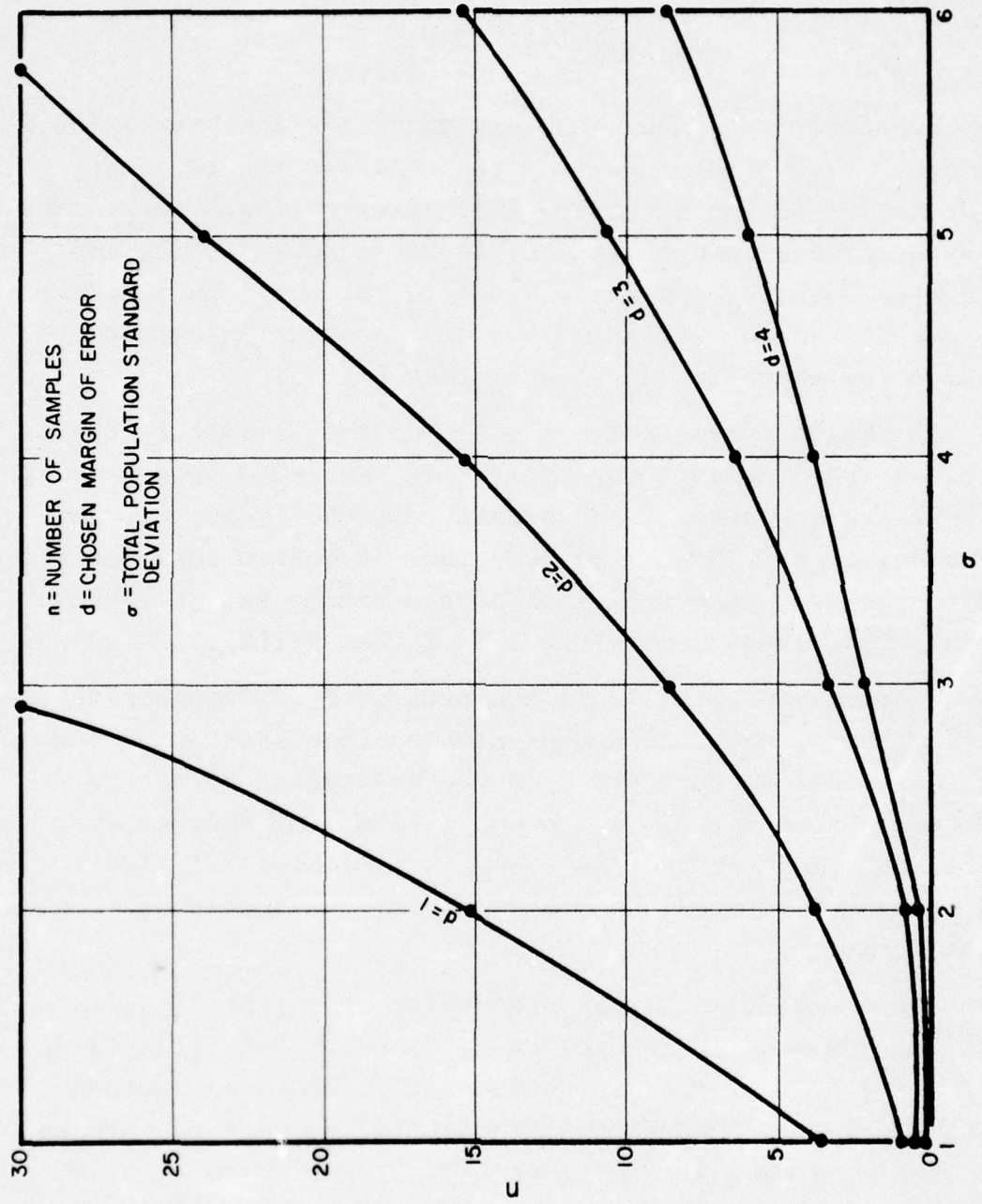

FIG. 33—SAMPLE SIZE AS A FUNCTION OF STANDARD DEVIATION AND MARGIN OF ERROR AT THE 95% CONFIDENCE LEVEL

TRACOR, INC. DWG. A6-55-45
AUSTIN, TEXAS 3-8-67 ARASTABI/SL

It should be noted from Tables I-III that the estimated volume-plus-surface scattering strength,

$$\mu_{SL} = \mu_S(\theta_S) + \mu_L ,$$

is highly dependent upon the value estimated for the bottom loss. A deviation of the bottom loss from its mean creates twice as great a deviation in the estimated scattering strength, μ_{SL}. The extreme right-hand column of each table was computed using the average bottom loss, $\overline{B}_n$, over all pings in the set. Thus, these columns demonstrate the variations which are actually related to the measured reverberation at time t_3 (see Fig. 5).

To obtain consistent estimates of the parameter, the bottom losses from Tables I through III are averaged over n samples. Tables IV-VI are composed of the average bottom losses, $\overline{B}_n$, for several values of n. These average values of bottom loss are then compared to the average bottom loss of the entire set of consecutive pings (obtained from column 3 of Tables I-III).

Similar tables (VII-IX) are presented to demonstrate the effect of averaging upon the volume-plus-surface scattering strength, μ_{SL}. In these tables, the values of the scattering strengths averaged over n samples, $\overline{\mu}_{SLn}$, are compared to the average over the entire set. Each scattering strength in Tables VII-IX was computed using the bottom loss averaged over the number of samples under consideration.

For example, the first scattering strength, $\overline{\mu}_{SL3}$, in Table VII was computed in the following manner. Using the first three values of bottom loss from Column 3, Table I, an average was computed (entered in Column 2, Table IV) and used to compute three scattering strengths for pings 1-3. These three scattering strengths were averaged to obtain the first value in Column 2, Table VII. Dropping ping 1 and including ping 4, the process was repeated to obtain the second average value for surface scattering strength in Column 2, Table VII.

TRACOR, INC. 6500 TRACOR LANE, AUSTIN, TEXAS 78721

Table IV
AVERAGES OF BOTTOM LOSS
Set 1

Ping i	$\overline{B}_3$ [a]	$\overline{B}_{20}-\overline{B}_3$	$\overline{B}_4$ [b]	$\overline{B}_{20}-\overline{B}_4$	$\overline{B}_5$ [c]	$\overline{B}_{20}-\overline{B}_5$	$\overline{B}_6$ [d]	$\overline{B}_{20}-\overline{B}_6$
1	14.9	-0.3	15.1	-0.5	14.6	0.0	14.5	0.1
2	14.9	-0.3	14.3	0.3	14.2	0.4	14.5	0.1
3	13.6	1.0	13.6	1.0	14.0	-0.6	14.3	0.3
4	14.1	0.5	14.5	0.1	14.7	-0.1	14.9	-0.3
5	14.0	0.6	14.5	0.1	14.7	-0.1	15.0	-0.4
6	15.1	-0.5	15.2	-0.6	15.4	-0.8	15.2	-0.6
7	15.6	-1.0	15.9	-1.3	15.4	-0.8	15.3	-0.7
8	15.9	-1.3	15.4	-0.8	15.3	-0.7	15.1	-0.5
9	15.2	-0.6	15.2	-0.6	15.0	-0.4	14.7	-0.1
10	15.0	-0.4	14.9	-0.3	14.5	0.1	14.5	0.1
11	14.3	0.3	14.0	0.6	14.1	0.5	14.5	0.1
12	14.1	0.5	14.2	0.4	14.6	0.0	14.7	-0.1
13	13.9	0.7	14.6	0.0	14.7	-0.1	14.1	0.5
14	14.6	0.0	14.8	-0.2	14.1	0.5	13.7	0.9
15	15.4	-0.8	14.4	0.2	13.8	0.8	14.2	0.4
16	14.3	0.3	13.7	0.9	14.1	0.5		
17	12.7	1.9	13.5	1.1				
18	12.9	1.7						
19								
20								

[a] bottom loss averaged over pings i to i+2
[b] bottom loss averaged over pings i to i+3
[c] bottom loss averaged over pings i to i+4
[d] bottom loss averaged over pings i to i+5

TRACOR, INC. 6500 TRACOR LANE, AUSTIN, TEXAS 78721

Table V
AVERAGES OF BOTTOM LOSS
Set 2

Ping i	$\overline{B}_3$ [a]	$\overline{B}_{20}-\overline{B}_3$	$\overline{B}_4$ [b]	$\overline{B}_{20}-\overline{B}_4$	$\overline{B}_5$ [c]	$\overline{B}_{20}-\overline{B}_5$	$\overline{B}_6$ [d]	$\overline{B}_{20}-\overline{B}_6$
1	18.2	1.7	18.3	1.8	18.3	1.8	17.8	1.3
2	18.3	1.8	18.3	1.8	17.7	1.2	17.3	0.8
3	18.6	0.9	17.8	1.3	17.3	0.8	16.4	-0.1
4	17.4	0.9	16.9	0.4	15.8	-0.7	16.4	-0.1
5	16.3	-0.2	15.1	-1.4	15.9	-0.6	16.2	-0.3
6	14.1	-2.4	15.4	-1.1	15.8	-0.7	15.6	-0.9
7	15.4	-1.1	15.9	-0.6	15.6	-0.9	15.9	-0.6
8	16.3	-0.2	15.7	-0.8	16.1	-0.4	16.2	-0.3
9	17.1	0.6	17.2	0.7	17.1	0.6	17.0	0.5
10	16.6	0.1	16.6	0.1	16.6	0.1	16.4	-0.1
11	16.3	0.2	16.4	-0.1	16.2	-0.3	16.3	-0.3
12	17.0	0.5	16.6	.1	16.6	0.1	16.4	-0.1
13	16.7	-0.3	16.4	-0.1	16.1	-0.4	15.9	-0.6
14	16.3	-0.2	16.0	-0.6	15.8	-0.7	15.9	-0.6
15	15.8	-0.7	15.6	-0.9	15.7	-0.8	15.8	-0.7
16	15.6	-0.9	15.8	-0.7	15.8	-0.7		
17	15.5	-0.1	15.6	-0.9				
18	15.7	0.8						

[a][b][c][d] same as Table IV

TRACOR, INC. 6500 TRACOR LANE, AUSTIN, TEXAS 78721

Table VI
AVERAGES OF BOTTOM LOSS
Set 3

Ping i	$\overline{B}_3$ [a]	$\overline{B}_{20}-\overline{B}_3$	$\overline{B}_4$ [b]	$\overline{B}_{20}-\overline{B}_4$	$\overline{B}_5$ [c]	$\overline{B}_{20}-\overline{B}_5$	$\overline{B}_6$ [d]	$\overline{B}_{20}-\overline{B}_6$
1	16.1	-0.9	16.8	-1.6	16.4	-1.2	16.5	-1.3
2	18.7	-3.5	17.7	-2.5	17.6	-2.4	17.3	-2.1
3	18.1	-2.9	17.9	-2.7	17.5	-2.3	17.7	-2.5
4	17.0	-1.8	16.8	-1.6	17.1	-1.9	17.0	-1.8
5	16.0	-0.8	16.7	-1.5	16.6	-1.4	15.4	-0.2
6	17.3	-2.1	17.0	-1.8	15.5	-0.3	15.6	-0.4
7	17.0	-1.8	15.1	0.1	15.3	-0.1	15.0	0.2
8	14.7	0.5	15.1	0.1	14.7	0.5	15.0	0.2
9	14.0	1.2	13.8	1.4	14.2	1.0	14.5	0.7
10	13.0	2.2	13.8	1.4	14.2	1.0	13.7	1.5
11	15.2	0.0	15.4	-0.2	14.6	0.6	14.0	1.2
12	15.1	0.1	14.1	1.1	13.5	1.7	14.1	1.1
13	14.4	0.8	13.6	1.6	14.3	0.9	14.5	0.7
14	12.8	2.4	13.8	1.4	14.2	1.0	14.0	1.2
15	13.1	2.1	13.7	1.5	13.6	1.6		
16	14.6	0.6	14.2	1.0				
17	15.1	0.1						

[abcd] same as Table IV

TRACOR, INC. 6500 TRACOR LANE, AUSTIN, TEXAS 78721

Table VII
AVERAGE SURFACE +
VOLUME SCATTERING STRENGTHS

Set 1

Ping i	$\bar{\mu}^{a}_{SL3}$	$\bar{\mu}_{SL20} - \bar{\mu}_{SL3}$	$\bar{\mu}^{b}_{SL4}$	$\bar{\mu}_{SL20} - \bar{\mu}_{SL4}$	$\bar{\mu}^{c}_{SL5}$	$\bar{\mu}_{SL20} - \bar{\mu}_{SL5}$	$\bar{\mu}^{d}_{SL6}$	$\bar{\mu}_{SL20} - \bar{\mu}_{SL6}$
1	-32.7	-0.8	-31.7	-1.8	-32.3	-1.2	-32.6	-0.9
2	-31.7	-1.8	-32.5	-1.0	-32.8	-0.7	-32.4	-1.1
3	-33.7	0.2	-33.8	0.3	-33.1	-0 4	-32.6	-0.9
4	-32.5	-1.0	-32.0	-1.5	-31.6	-1.9	-31.5	-2.0
5	-33.1	-0.4	-32.4	-1.1	-32.1	-1.4	-31.8	-1.7
6	-31.5	-2.0	-31.4	-2.1	-31.1	-2.4	-31.6	-1.9
7	-30.5	-3.0	-30.4	-3.1	-31.2	-2.3	-31.2	-2.3
8	-30.4	-3.1	-31.4	-2.1	-31.4	-2.1	-31.5	-2.0
9	-31.7	-1.8	-31.7	-1.8	-31.7	-1.8	-32.4	-1.1
10	-31.9	-1.6	-31.9	-1.6	-32.7	-0.8	-32.9	-0.6
11	-32.5	-1.0	-33.4	-0.1	-33.5	0.0	-32.9	-0.6
12	-33.1	-0.4	-33.3	-0.2	-32.6	-0.9	-32.7	-0.8
13	-33.9	0.5	-32.9	-0.6	-32.9	-0.6	-34.2	0.7
14	-33.2	-0.3	-33.2	-0.3	-34.7	1.2	-35.3	1.8
15	-32.3	-1.2	-34.4	0.9	-35.1	1.6	-34.6	1.1
16	-34.5	1.0	-35.4	1.9	-34.6	1.1		
17	-37.3	3.8	-35.4	1.9				
18	-36.8	3.3						
19								
20								

[a] averaged over pings i to i+2
[b] averaged over pings i to i+3
[c] averaged over pings i to i+4
[d] averaged over pings i to i+5

TRACOR, INC. 6500 TRACOR LANE, AUSTIN, TEXAS 78721

Table VIII

AVERAGE SURFACE +

VOLUME SCATTERING STRENGTHS

Set 2

Ping i	$\bar{\mu}^{a}_{SL3}$	$\bar{\mu}_{SL20} - \mu_{SL3}$	$\bar{\mu}^{b}_{SL4}$	$\bar{\mu}_{SL20} - \mu_{SL4}$	$\bar{\mu}^{c}_{SL5}$	$\bar{\mu}_{SL20} - \mu_{SL5}$	$\bar{\mu}^{d}_{SL6}$	$\bar{\mu}_{SL20} - \mu_{SL6}$
1	-32.0	-4.3	-32.1	-4.2	-32.5	-3.8	-33.3	-3.0
2	-32.5	-3.8	-32.9	-3.4	-33.7	-2.6	-34.5	-1.8
3	-22.6	-1.7	-33.8	-2.5	-34.7	-1.6	-37.1	-0.8
4	-33.5	-2.8	-35.5	-0.8	-38.2	1.9	36.8	0.5
5	-36.5	0.2	-39.7	3.4	-37.7	1.4	-37.4	1.1
6	-41.6	5.2	-38.7	2.4	-38.2	1.9	-38.7	2.4
7	-39.1	2.8	-38.4	2.1	-39.9	3.6	-38.0	1.7
8	-40.4	4.1	-39.1	2.8	-37.9	1.6	-37.6	1.3
9	-35.7	-0.6	-35.1	1.2	-35.2	-1.1	-34.9	-1.4
10	-24.9	-1.4	-36.6	0.3	-36.0	-0.3	-36.8	0.5
11	-36.7	0.4	-35.9	-0.4	-35.8	-0.5	-35.4	-0.9
12	-33.2	-3.1	-33.4	-2.9	-33.3	-3.0	-35.0	-1.3
13	-33.8	-2.5	-33.5	-2.8	-35.3	-1.0	-35.5	-0.8
14	-33.1	-3.2	-35.2	-1.1	-35.4	-0.9	-35.5	-0.8
15	-35.8	-0.5	-35.9	-0.4	-35.8	-0.5	-35.6	-0.7
16	-36.2	-0.1	-36.0	-0.3	-35.6	-0.7		
17	-36.8	0.5	-36.1	-0.2				
18	-35.3	-1.0						
19								
20								

[a][b][c][d] same as Table VII

TRACOR, INC. 6500 TRACOR LANE, AUSTIN, TEXAS 78721

Table IX
AVERAGE SURFACE +
VOLUME SCATTERING STRENGTHS

Set 3

Ping i	$\bar{\mu}^{a}_{SL3}$	$\bar{\mu}_{SL20} - \bar{\mu}_{SL3}$	$\bar{\mu}^{b}_{SL4}$	$\bar{\mu}_{SL20} - \bar{\mu}_{SL4}$	$\bar{\mu}^{c}_{SL5}$	$\bar{\mu}_{SL20} - \bar{\mu}_{SL5}$	$\bar{\mu}^{d}_{SL6}$	$\bar{\mu}_{SL20} - \bar{\mu}_{SL6}$
1	-35.3	-2.1	-34.6	-2.8	-35.4	-2.0	-35.1	-2.3
2	-30.1	-7.3	-33.3	-4.1	-33.3	-4.1	-34.0	-3.4
3	-33.0	-4.4	-33.1	-4.3	-34.0	-3.4	-33.5	-3.9
4	-34.8	-2.6	-35.5	-3.9	-34.6	-2.8	-34.9	-2.5
5	-36.6	-0.8	-35.1	-2.3	-35.4	-2.0	-37.8	-0.4
6	-33.9	-3.5	-34.6	-2.8	-37.6	0.2	-36.8	-0.6
7	-34.9	-2.5	-41.1	3.7	-37.5	0.1	-38.0	0.6
8	-38.9	1.5	-37.5	0.1	-38.1	0.7	-37.6	0.2
9	-39.7	2.3	-40.0	2.6	-39.0	1.6	-39.1	1.7
10	-41.2	3.8	-39.7	2.3	-39.0	1.6	-40.7	3.3
11	-36.3	-1.1	-37.1	-0.3	-38.9	1.5	-40.1	2.7
12	-38.4	1.0	-40.4	3.0	-41.3	3.9	-39.3	1.9
13	-40.2	2.8	-41.5	4.1	-39.0	1.6	-38.6	1.2
14	-43.6	6.2	-40.0	2.6	-39.3	1.9	-39.8	2.4
15	-40.2	2.8	-39.3	1.9	-39.9	2.5		
16	-36.9	-0.5	-38.3	0.9				
17	-36.1	-1.3						
18								
19								

[a][b][c][d] same as Table VII

It is evident that averaging the results of several pings provides a considerable improvement over the single ping estimates.

Since it is expected that reverberation data may be sampled continuously during normal ship operation, this type of analysis will be necessary in determining, ultimately, the number of parameter samples to be included in obtaining an average value for a parameter if the average (and final in situ prediction) is to be statistically significant, and trends in the data, i.e., actual changes in the average parameter values, are not to be obscured. This investigation will be continued when a sufficient quantity of documented data becomes available.

TRACOR, INC. 6500 TRACOR LANE, AUSTIN, TEXAS 78721

6. SAMPLE SIGNAL-TO-NOISE COMPUTATIONS

Figure 34 shows graphs, for several bottom bounce beam depression angles, of the predicted signal-to-noise ratio (dB) at the output of the AN/SQS-26 receiving beamformer when the system is surface reverberation limited. The surface scattering strength for these curves was obtained from the Chapman-Harris equation of Section 3.3.2 for a wind speed of 12 knots. The target was assumed to be just below the thermocline with a 15 dB target strength. Since the two-way transmission loss is about the same for both echo and surface reverberation for a given depression angle, any change in the peak signal-to-noise ratio should be the result of a change in the amount of energy scattered back from the surface. As the depression angle increases, the size of the surface scattering area decreases. In this example, however, the decrease in size is more than offset by the increase in scattering strength associated with the larger surface grazing angles, and the peak signal-to-noise ratio decreases.

Signal-to-noise curves are shown again in Fig. 35, but in this case the system is volume reverberation limited by sound energy returned from the deep scattering layer. The effective scattering area once again decreases in size as the depression angle increases, but since there is no associated grazing angle dependence, there is a relative decrease in the volume reverberation. The peak signal-to-noise ratio in this case increases with increasing grazing angle.

Recapitulating, when the system is volume reverberation limited (i.e., when the volume scattering strength is large relative to the surface scattering strength) the expected peak signal-to-noise ratio increases with increasing grazing angle. The opposite is true when surface reverberation is the predominant background. In this case, the peak signal-to-noise ratio decreases as the depression angle becomes steeper.

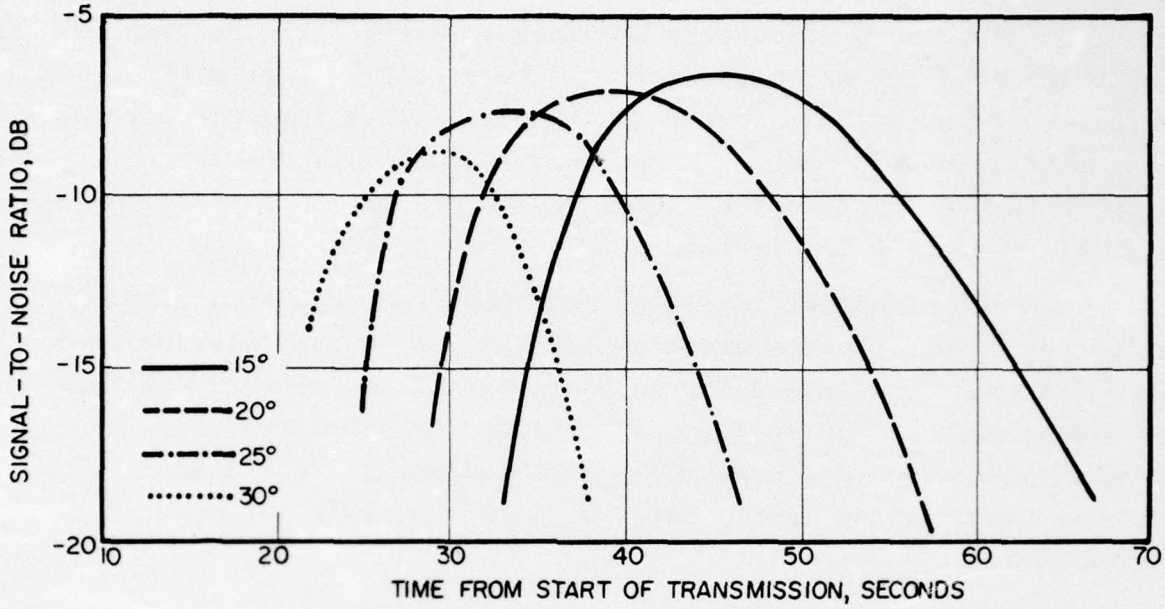

FIG. 34 - SIGNAL-TO-NOISE RATIO FOR BOTTOM BOUNCE TRACK WITH VARYING DEPRESSION ANGLES FOR SURFACE REVERBERATION LIMITED CASE WITH 12 KNOT WIND SPEED

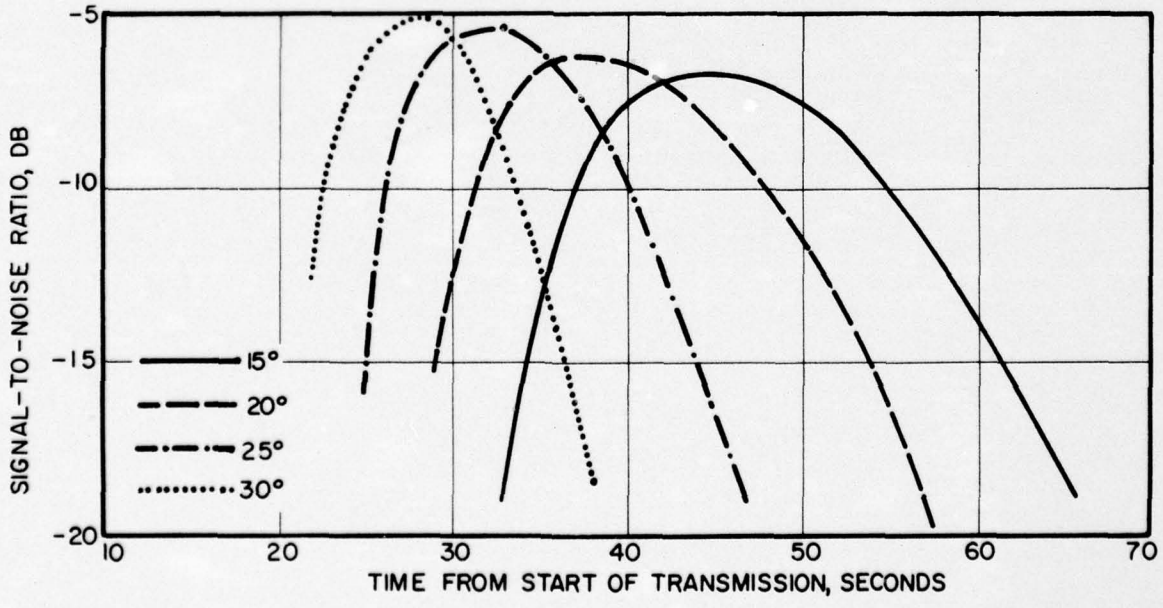

FIG. 35 - SIGNAL-TO-NOISE RATIO FOR BOTTOM BOUNCE TRACK WITH VARYING DEPRESSION ANGLES FOR VOLUME REVERBERATION LIMITED CASE

TRACOR, INC. DWG. A6-55-47
AUSTIN, TEXAS 3-13-67 ANASTASI/SL

The above discussion provides an example of the need for reliable parameter estimates for in situ performance prediction. Although the relative change in sonar performance (measured by peak signal-to-noise ratio in the above example) is not large between any two consecutive bottom bounce depression angles, the over-all variation is significant.

The parameter estimates determined through an analysis of bottom bounce reverberation cycles may, of course, also be used in performance prediction for surface channel and convergence zone operating modes. Models for prediction of echo and reverberation levels for these modes have been developed but are not discussed in this report since little data has been available for model validation.

7. SUMMARY AND CONCLUSIONS

In situ performance prediction is based on a number of parameters describing the target, the sonar, and the environment. Reasonable target parameters must be assumed; the sonar parameters are known; and some of the environmental parameters (such as wind speed and water depth) may be obtained using existing in situ measurements. Information concerning the remaining environmental parameters may be obtained from an analysis of a local sonar reverberation history.

In this report, a method for obtaining these parameters from a recorded series of AN/SQS-26 bottom bounce reverberation cycles has been considered. The parameter estimation program, which has been discussed, relates the sound intensity measurement at a specific time during a reverberation cycle to the types of reverberation (or bottom reflected sound energy) reaching the receiver at that time over known propagation paths. The equations resulting from this association may be solved to yield values for volume (biological layer) scattering strength, bottom scattering strength, and bottom loss. This method requires an independent estimate of the surface scattering strength. The parameter estimates determined from data recorded in one bottom bounce mode may be used for performance prediction in other sonar operating modes. A performance prediction model which compares favorably with available sea data has been developed for the bottom bounce modes. Also, models describing sonar performance for the surface channel and convergence zone modes have been programmed; however, no sea data has been available yet for validation.

An initial analysis of the ping-to-ping stability (repeatability) of AN/SQS-26 reverberation cycles and the corresponding parameter estimates indicates that meaningful average values for the parameters can be obtained over relatively few pings; however, additional analyses of this type are required.

It has thus been shown in this report that the proposed system for determining in situ environmental parameters is feasible and worthy of further pursuit. Further work on this task depends heavily upon acquiring AN/SQS-26 reverberation data under various environmental conditions and sonar operating modes. It is expected that an analysis of this data will yield the required relationship between wind speed and surface scattering strength for the AN/SQS-26 frequency and bandwidth (or validate existing relationships). The data will also permit the refinement and validation of the parameter estimation program and the surface channel and convergence zone performance prediction models.

TRACOR, INC. 6500 TRACOR LANE, AUSTIN, TEXAS 78721

APPENDIX A

BOTTOM BOUNCE REVERBERATION

A.1 REVERBERATION MODEL[1]

In deriving the equations used in this model, an effort was made to account for all applicable parameters whose values are known (such as those pertaining to the sonar) or may be reasonably estimated (oceanographic parameters). Full three-dimensional beam patterns for both source and receiver are considered, and the refractive effects of the medium are taken into account. For a given set of parameter values, the model predicts the reverberation intensity as a function of time after transmission.

For convenience, the initial discussion of the model assumes a near-surface sonar and a constant sound velocity. In the actual programmed model, the sonar depth is variable and the refractive effects of the medium, due to variations in the sound velocity, are accounted for with the aid of classical ray theory. This application of ray theory is discussed in Section A.2.

The total reverberation received at any particular time t is, of course, the sum of the intensity contributions from each of the individual reverberation paths at that time. The total number of paths which must be considered in a given situation depends upon the actual values of the sonar and oceanographic parameters involved. Some of the principal paths are discussed below.

A.1.1 Biological Scattering Layer Reverberation

Investigations during the past several years into the characteristics of μ_V, the scattering strength per unit volume of the ocean, have yielded the following results:

---

[1] Fowler, S. G. "Bottom Bounce Reverberation Modeling and Bottom Loss (U)," TRACOR Document No. 66-355-C, Contract NObsr-93140, November 16, 1966, Confidential.

- At certain depths in the ocean there are regions of relatively high backscattering strength. These regions are layers, parallel to the sea surface, containing a high concentration of biological scatterers.
- The depth and thickness of a layer and the average value of μ_V within a layer are dependent upon ocean area, season of the year, and time of day.
- For a given set of conditions, μ_V within a layer is frequency dependent.
- Layer reverberation can be a primary contributor to the masking background in the operation of a bottom bounce sonar.

Computations of scattering layer reverberation are based on the physical model shown in Fig. A-1. Within the layer μ_V may vary with depth. That is,

$$\mu_V = \mu_V(z), \qquad d_L - \frac{S_L}{2} \le z \le d_L + \frac{S_L}{2} ,$$

where d_L is the average depth of the layer and S_L is the layer thickness.

Consider the volume reverberation from a scattering layer when source and receiver are omnidirectional and at a distance d_L from the layer. The reverberation received from the layer at a time t, measured from the beginning of a τ-second transmission, is the result of scattering within an insonified volume V(t) whose dimensions are determined by the layer thickness and the requirement,

$$t-\tau \le t_s \le t ,$$

where t_s is the round trip travel time from the source-receiver to an elemental scattering volume. If the sound velocity is constant (=c) throughout the medium, the ray paths are straight lines,

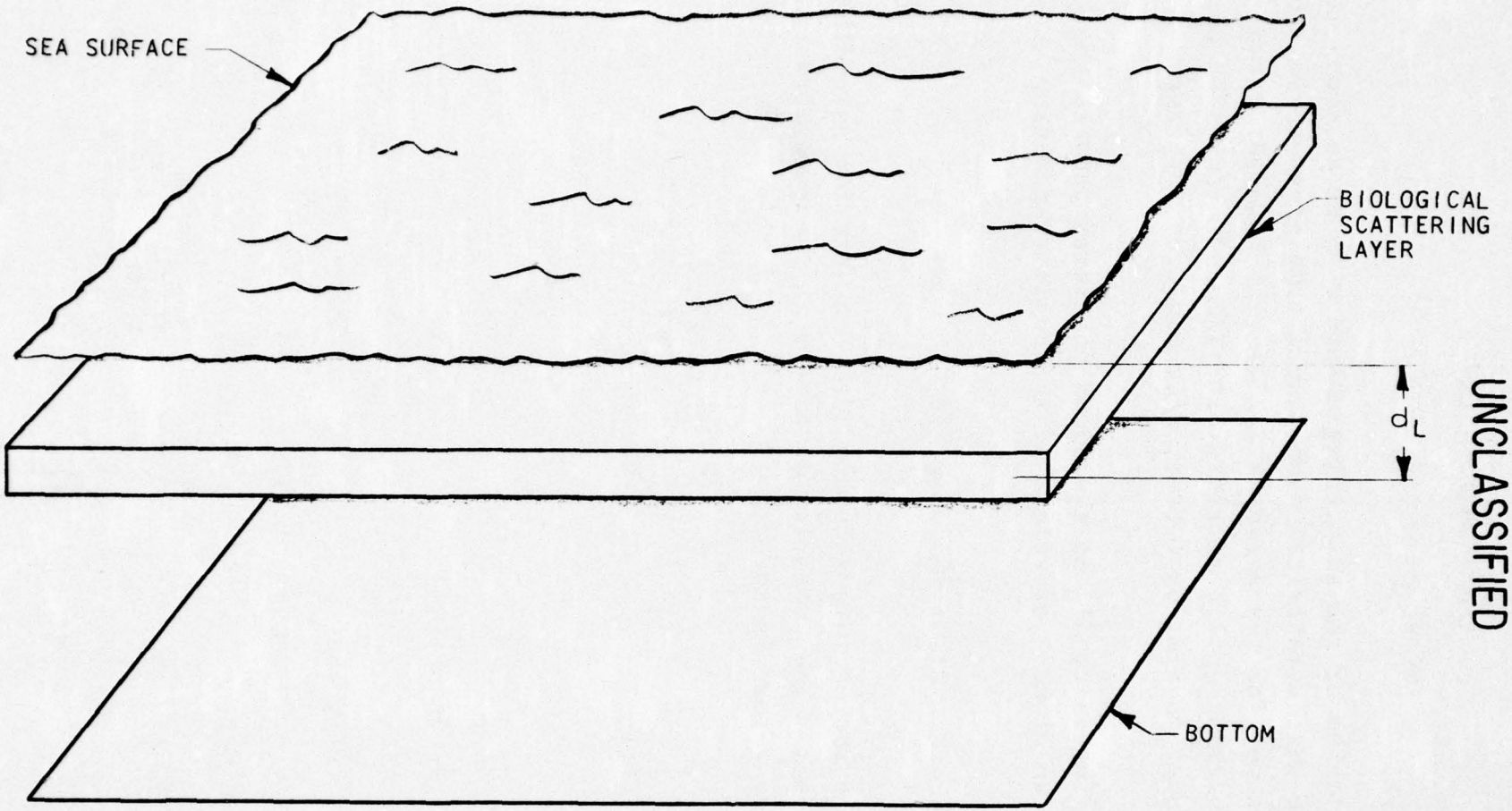

FIG. A-5 - BIOLOGICAL SCATTERING LAYER

and a cross section of the scattering volume will be as shown in Fig. A-2. Due to the restriction on travel time given above, the scattering volume (for $t-\tau \geq 2(d_L + S_L/2)/c$) is bounded by two concentric spherical shells of radii $c(t-\tau)/2$ and $ct/2$. The upper and lower boundaries are, of course, determined by the layer thickness.

The intensity dI_L of the sound scattered back to the receiver from an element of volume dV is (neglecting medium attenuation)

$$dI_L = \frac{I_o}{r^4} \mu_V(z)\, dV,$$

where I_o is the source intensity and $1/r^4$ accounts for spreading loss out and back. The intensity at time t of the reverberation from the entire volume is then

$$I_L(t) = \int_{V(t)} dI_L = I_o \int_{z=d_1}^{d_2} \int_{\alpha=0}^{2\pi} \int_{r=r_1}^{r_2} \frac{\mu_V(z)}{r^3}\, dr\, d\alpha\, dz\ ,$$

where

$d_1 = d_L - S_L/2,$

$d_2 = d_L + S_L/2,$

$r_1 = c(t-\tau)/2,$

$r_2 = ct/2,$ and

α = bearing angle of dV.

The integration may be carried out to give

$$I_L = \pi I_o \int_{d_1}^{d_2} \mu_V(z)dz \left[\frac{1}{r_1^2} - \frac{1}{r_2^2}\right] = \frac{4\pi\, I_o\, \mu_L}{c^2} \frac{2\tau t - \tau^2}{t^2(t-\tau)^2}\ , \qquad \text{(A1)}$$

FIG. A-2 - CROSS SECTION OF SCATTERING LAYER GEOMETRY

TRACOR, INC. | DWG. 6-55-2
AUSTIN, TEXAS 8-10-66 FOWLER

where

$$\mu_L = \int_{d_1}^{d_2} \mu_V(z)\, dz.$$

In taking data on layer scattering strength, the quantity actually measured is μ_L. From this measured quantity, a scattering strength per unit volume may be derived if $\mu_V(z)$ is assumed constant throughout the layer and if some estimate of layer thickness can be obtained. The uncertainties involved in deriving μ_V from μ_L are apparent. In many cases of practical interest this step need not be taken, and layer reverberation may be computed from a knowledge of μ_L alone.

Notice in Eq. (A1) that, for a fixed layer depth, the relative time variation of layer reverberation is independent of layer thickness. For example, a layer one yard thick would give rise to a reverberation envelope identical, except for the initial build up, to that observed from a layer 100 yards thick if $\mu_V(z)$ changed between the two layers such that

$$\mu_L = \int_{d_1}^{d_2} \mu_V(z)\, dz$$

were the same for each. Extending this line of reasoning, we may finally replace the layer by a surface, at a depth d_L, whose scattering strength per unit area is independent of grazing angle and given by a measured value of μ_L. This approach is followed in the TRACOR computation of layer reverberation. Bottom bounce reverberation from a scattering layer at a depth d_L below the surface is calculated in the same manner as a surface reverberation (Section A.1.2), but the surface considered in this case is of course displaced downward to a depth d_L.

Due to the presence of the sea surface, a given scatterer within a layer may contribute to the total layer reverberation by four propagation paths, one path involving no surface reflections, one path involving two surface reflections, and two paths involving one surface reflection. On the scale of bottom bounce propagation geometry, the scattering layers are close to the sea surface and the propagation loss and travel times associated with the four paths mentioned above differ little. The net effect of surface multipaths (assuming no surface reflection loss) is to increase the intensity computed for a single path by a factor of 4, or an increase in the computed reverberation level of 6 dB.

A.1.2 Boundary Reverberation

The geometry for the simplest case of bottom reverberation is illustrated in Fig. A-3. The reverberation received at time t is the result of scattering from the bottom in an area A(t) whose dimensions are determined by the requirement,

$$t-\tau \leq t_s \leq t \ ,$$

where t_s is the time required for sound to travel to an elemental scattering area on the bottom and return. The intensity of the reverberation received from an element of area dA is

$$dI_B = \frac{\mu_B(\gamma)\ B_T(\alpha,\theta)\ B_R(\alpha,\theta).10^{-2kr/10}}{r^4}\ dA \ , \qquad \text{(A2)}$$

and the reverberation from the entire area is given by

$$I_B(t) = \int_{A(t)} dI_B, \qquad \text{(A3)}$$

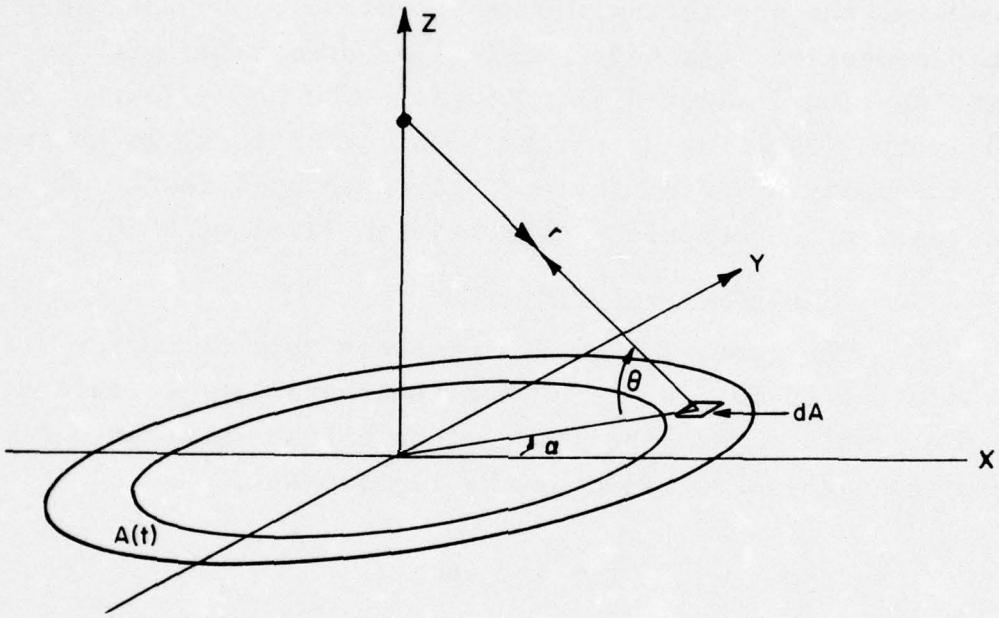

Fig. A-3 –SCATTERING AREA FOR BOTTOM REVERBERATION RECEIVED AT TIME t

TRACOR, INC. | DWG 769-274
AUSTIN, TEXAS 6/11/65 BE/SL

where

r = distance from source to dA,

$B_T(\alpha,\theta)$ = source intensity of transmitted sound in the direction of a line from the source through dA. (This line is defined by a bearing angle α and a depression angle θ.),

$B_R(\alpha,\theta)$ = receiving beam pattern attenuation in the direction of the line defined by α and θ,

k = medium attenuation (dB/yd) for the frequency used,

$\mu_B(\gamma)$ = scattering strength per unit area of the bottom,

θ = depression angle of ray at the transducer, and

γ = grazing angle of the ray at the bottom.

Associated with the first order bottom reverberation path just discussed are three additional paths. In Fig. A-4, the basic path is indicated in the left-most diagram, and the additional paths provided by surface reflections are indicated to the right. The relative importance of these additional paths depends primarily upon the directional characteristics of the source and receiver. Other important paths for bottom reverberation are shown in Fig. A-5 in two dimensions. The equations for the intensity of the reverberation propagating along these (and any additional paths due to surface reflections), are derived in a manner similar to that discussed for first order bottom reverberation. Bottom and surface reflectivity losses are taken into account when applicable.

The equations for surface reverberation are essentially the same as those for the bottom, differing mainly in the subscripts on the parameters and the value used for scattering strength. Figure A-6 indicates the scattering area and propagation path for surface reverberation involving two specular reflections at the ocean bottom. The intensity of the reverberation received along this path is

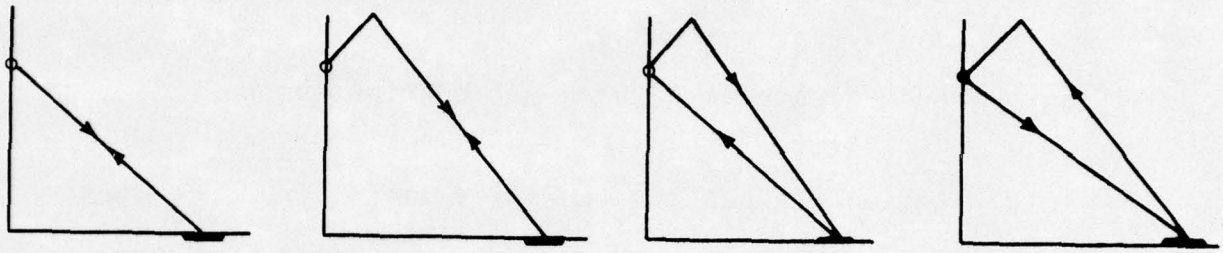

FIG. A-4 – MULTIPATHS DUE TO SURFACE REFLECTIONS

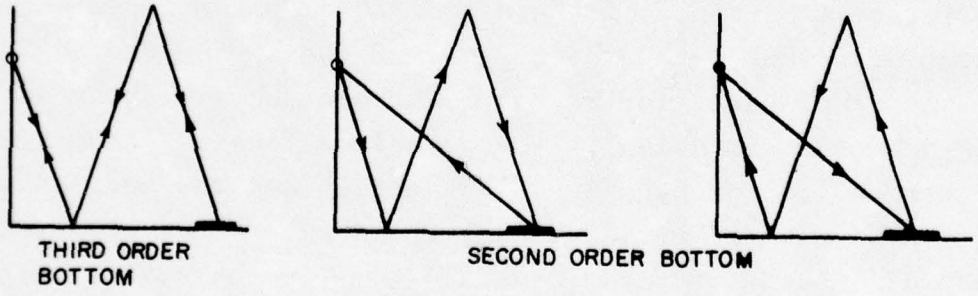

FIG. A-5 – PROPAGATION PATHS FOR BOTTOM REVERBERATION

TRACOR, INC. AUSTIN, TEXAS | DWG. 6-13-230 | 2-16-66 FOWLER/SL

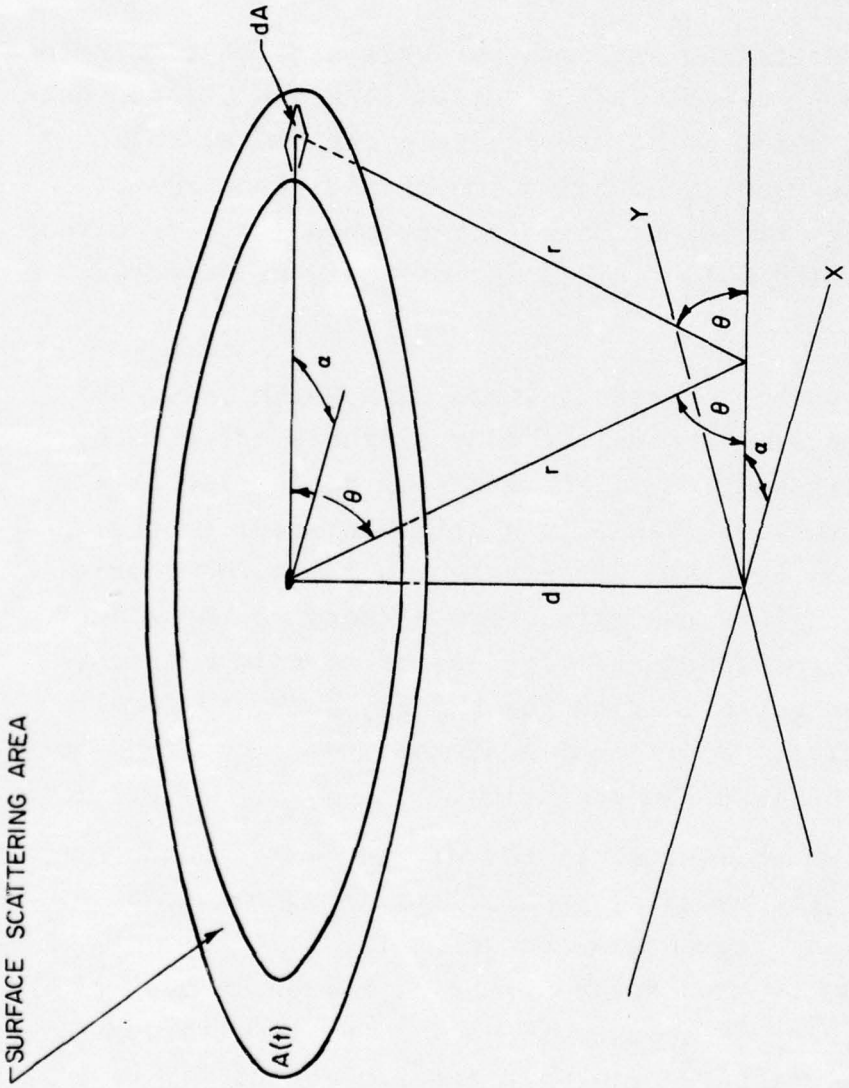

FIG. A-6 – PROPAGATION PATH FOR SURFACE REVERBERATION VIA THE BOTTOM

TRACOR, INC. AUSTIN, TEXAS | DWG. 6-13-231 | 6-8-66 FOWLER/SH

$$I_S(t) = \int_{A(t)} \frac{\mu_S(\theta)\ B_T(\alpha,\theta)\ B_R(\alpha,\theta)\ 10^{-\frac{4kr}{10}}\ 10^{-\frac{2BL}{10}}}{(2r)^4}\ dA\ , \qquad (A4)$$

where $\mu_S(\theta)$ is the scattering strength per unit area of the surface at the grazing angle θ, and BL is the bottom loss (in dB) per bottom reflection. For a bottom bounce sonar in deep water this reverberation path is usually of prime importance since the scattered sound energy traveling this path reaches its peak within the time interval during which target echoes would be expected.

A.2 REFRACTION

In most cases of interest, sound rays which leave the source at large depression angles are only slightly affected by refraction, and the assumption in the previous discussion of a straight line ray path will result in negligible error in the computed reverberation levels. For rays which leave the source at small depression angles, the refractive effects of the medium due to variations in the sound velocity are of more importance, and the straight line approximation for the ray path may result in an appreciable error. Modification of the model equations to account for refraction is discussed below.

The curve which represents the variation of sound velocity with depth (the velocity profile) is approximated by a series of straight line segments as shown in the left half of Fig. A-7. The medium is thus divided into n layers, in each of which the sound velocity is assumed to vary linearly with depth. The following ray equations, derived in the literature[2,3], give the relationships between the variables and parameters shown in Fig. A-7.

[2] Officer, C.B., Introduction to the Theory of Sound Transmission, McGraw-Hill, New York, 1958.

[3] Physics of Sound in the Sea, Part I, PB 11202, Summary Tech. Report, NDRC, U. S. Department of Commerce, OTS.

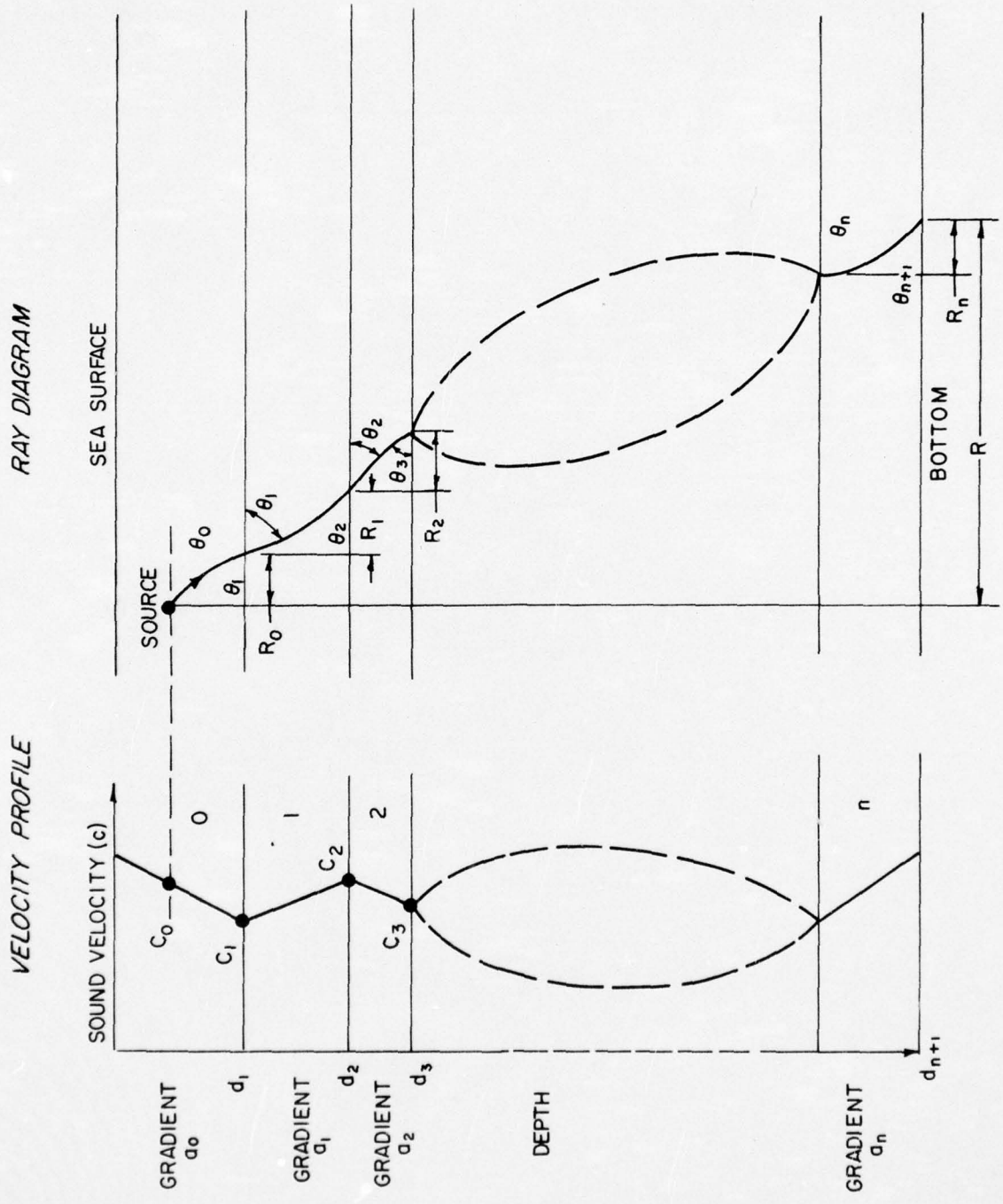

FIG. A-7 -RAY PATH IN LAYERED MEDIUM

TRACOR, INC. | DWG. 713-101
AUSTIN, TEXAS | 6-7-66 FOWLER/SL

$$\frac{\cos\theta_i}{c_i} = \frac{\cos\theta_o}{c_o} \tag{A5}$$

$$R_i = \frac{c_o}{\cos\theta_o} \frac{\sin\theta_i - \sin\theta_{i+1}}{a_i} , \tag{A6}$$

$$R(\theta_o) = \sum_{i=0}^{n} R_i , \tag{A7}$$

$$\frac{\partial R_i}{\partial \theta_o} = - \frac{R_i}{\sin\theta_i} \frac{\tan\theta_o}{\sin\theta_{i+1}} \tag{A8}$$

$$\frac{\partial R(\theta_o)}{\partial \theta_o} = \sum_{i=0}^{n} \frac{\partial R_i}{\partial \theta_o} , \tag{A9}$$

$$I[R(\theta_o),\theta] = - \frac{B_T(\alpha,\theta_o) \cos\theta_o}{R(\theta_o) \frac{\partial R(\theta_o)}{\partial \theta_o} \sin\theta} \tag{A10}$$

$$t_i = \frac{1}{a_i} \ln \frac{c_{i+1}}{c_i} \frac{1 + \sin\theta_i}{1 + \sin\theta_{i+1}} , \tag{A11}$$

$$t(\theta_o) = \sum_{i=0}^{n} t_i , \tag{A12}$$

$$a_i = \frac{c_{i+1} - c_i}{d_{i+1} - d_i} , \tag{A13}$$

$$PL_i = \frac{c_o}{a_i \cos\theta_o} (\theta_i - \theta_{i+1}) , \tag{A14}$$

$$PL(\theta_o) = \sum_{i=0}^{n} PL_i , \tag{A15}$$

where

$I[R(\theta_o),\theta]$ = intensity of a ray at a horizontal distance $R(\theta_o)$ from the source at a point where the ray makes an angle θ with a horizontal plane (the ray is inclined at an angle θ_o at the source),

t_i = travel time through the i^{th} layer,

a_i = gradient in the i^{th} layer,

PL_i = path length (along ray) in the i^{th} layer, and

$PL(\theta_o)$ = path length (along ray) for a ray through n layers.

The use of the above equations in calculating the reverberation intensity in a variable velocity medium will be illustrated by consideration of a special case shown in Fig. A-8. In this case, as argued before in the discussion of the iso-velocity model, the scattering area associated with the reverberation received at time t is determined by the requirement that the time, t_s, required for the sound energy to travel from the source to an element of the scattering area and return must satisfy

$$t - \tau \leq t_s \leq t \ .$$

From Eqs. (A11) and (A12) and Fig. A-8, we have

$$t_s = t_s(\theta_o,\Phi_o) = \sum_{i=0}^{n} \frac{1}{a_i} \ln \left[\frac{c_{i+1}}{c_i} \frac{1 + \sin\theta_i}{1 + \sin\theta_{i+1}} \right]$$

$$+ 3 \sum_{i=0}^{n} \frac{1}{a_i} \ln \left[\frac{c_{i+1}}{c_i} \frac{1 + \sin\Phi_i}{1 + \sin\Phi_{i+1}} \right], \quad \text{(A16)}$$

where, from Eq. (A5),

$$\theta_i = \cos^{-1} \left[\frac{c_i}{c_o} \cos\theta_o \right] \ , \text{ and} \quad \text{(A17)}$$

$$\Phi_i = \cos^{-1} \left[\frac{c_i}{c_o} \cos\Phi_o \right] \ . \quad \text{(A18)}$$

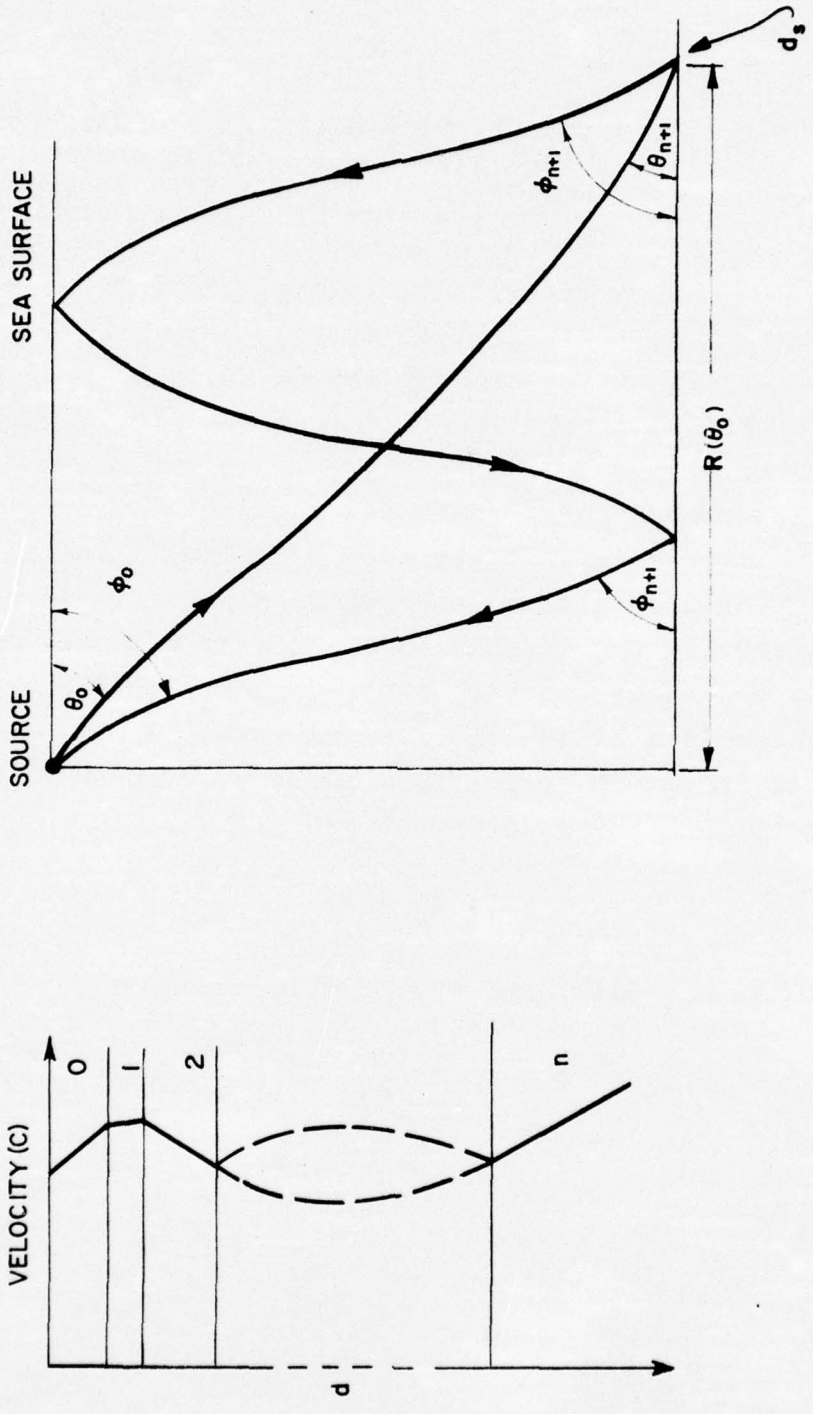

FIG A-8-SECOND ORDER REVERBERATION PATH

TRACOR, INC 1 DWG. 713-100
AUSTIN, TEXAS 10/12/65 BBE/LBH

The horizontal distance, $R(\theta_o)$, traveled by the ray from the source to dS is the same as that traveled by the ray from dS back to the source, which is $3R(\Phi_o)$. Thus, from Eqs. (A6) and (A7),

$$\sum_{i=0}^{n} \frac{c_o}{\cos\theta_o} \cdot \frac{\sin\theta_i - \sin\theta_{i+1}}{a_i} = 3 \sum_{i=0}^{n} \frac{c_o}{\cos\Phi_o} \cdot \frac{\sin\Phi_i - \sin\Phi_{i+1}}{a_i}, \quad \text{(A19)}$$

where θ_i and Φ_i are related to θ_o and Φ_o by Eqs. (A17) and (A18). Equations (A16) and (A19) are solved simultaneously for values of θ_o and Φ_o by standard numerical iterative techniques.

The intensity of the sound incident on dS is, by Eq. (A10),

$$I_i = - \frac{B_T(\alpha,\theta_o) \cos\theta_o \cdot 10^{-kPL(\theta_o)/10}}{R(\theta_o) \frac{\partial R(\theta_o)}{\partial \theta_o} \sin\theta_{n+1}},$$

where k is the medium attenuation (dB per yard), and the path length is given by Eq. (A15). The intensity of the sound received due to scattering from dS is

$$dI = I_i \cdot 10^{-\frac{BL}{10}} \cdot 10^{-\frac{SL}{10}} \left[\frac{B_R(\alpha,\Phi_o) \cos\Phi_o}{3R(\Phi_o) \frac{3\partial R(\Phi_o)}{\partial \Phi_o} \sin\Phi_{n+1} \left(\frac{c_o}{c_{n+1}}\right)^2} \right]$$

$$\cdot 10^{-\frac{k}{10}[3PL(\Phi_o)]} \cdot \mu(\theta_{n+1},\Phi_{n+1}) dS , \quad \text{(A21)}$$

where BL and SL are, respectively, the bottom and surface reflection losses in dB. The reverberation received at time t, due to scattering from the entire area, is

$$I(t) = \int_S dI . \quad \text{(A22)}$$

The equations used in calculating the reverberation levels for paths other than the one shown are derived by an extension of the above technique.

A.3 BEAM PATTERN COMPUTATIONS FOR A CYLINDRICAL ARRAY

A.3.1 Introduction

As may be judged from the reverberation equations of the previous section, the transmitting and receiving beam patterns govern, to a large extent, the level and time variation of the received reverberation. The best accuracy in reverberation prediction is, of course, obtained when these functions are most accurately represented. In this section a method of computing the beam pattern functions for a cylindrical transducer is discussed. The equations presented here have been used in computing patterns for both the AN/SQS-26 and AN/SQS-23 sonar systems. Similar techniques were used in developing a program for the computation of patterns for a spherical array, particular emphasis being placed on the AN/BQS-6 parameters.

Although the equations presented here can be used with reasonable accuracy in computing reverberation for a ship-mounted transducer, they are of course, still only approximations to the actual transmitter and receiver responses. No account has been taken of the effects of radiation impedance or the surrounding dome and hull structure. When more quantitative information describing these effects becomes available, it will be incorporated in the program. These factors are expected to have the most pronounced effect on the patterns at the steeper depression angles.

A.3.2 Geometry and Derivations

Figure A-9(a) shows a cylindrical transducer of radius R and height h consisting of N staves (vertical rows) and K rows (horizontal rows). A particular element n,k may be specified by giving the number of the stave, n, and the number of the row, k, in which the element is found.

The pressure response of an individual element in a given direction, relative to its maximum response in a direction normal to its surface, will be described by the function $p(\varphi,\beta)$. For a square element

$$p(\varphi,\beta) = \frac{\sin(qa\cos\beta\sin\varphi)}{qa\cos\beta\sin\varphi} \cdot \frac{\sin(qa\sin\beta)}{qa\sin\beta},$$

$$|\beta| \leq \frac{\pi}{2} \text{ and } |\varphi| \leq \frac{\pi}{2}$$

$$p(\varphi,\beta) = 0, \text{ otherwise,}$$

where

$q = 2\pi/\lambda$,

a = element half width, and

λ = wavelength of the transmitted sound.

The angular coordinates φ and β are indicated in Fig. A-9(b).

In transmitting, the contribution of the element n,k to the pressure field at a distant point z is, from the standard solution to the wave equation,

$$p_{n,k} = \frac{HST_n VST_k p(\varphi,\beta) e^{i[2\pi(ft - \frac{s_{n,k}}{\lambda}) + \gamma_{n,k}]}}{s_{n,k}},$$

where

HST_n = horizontal shading factor for the n^{th} stave,

VST_n = vertical shading factor for the k^{th} row,

$\gamma_{n,k} = HPT_n - VPT_k$,

HPT_n = horizontal phasing for the n^{th} stave,

VPT_k = vertical phasing for the k^{th} row,

f = frequency of the transmitted sound,

t = time measured from start of transmission,

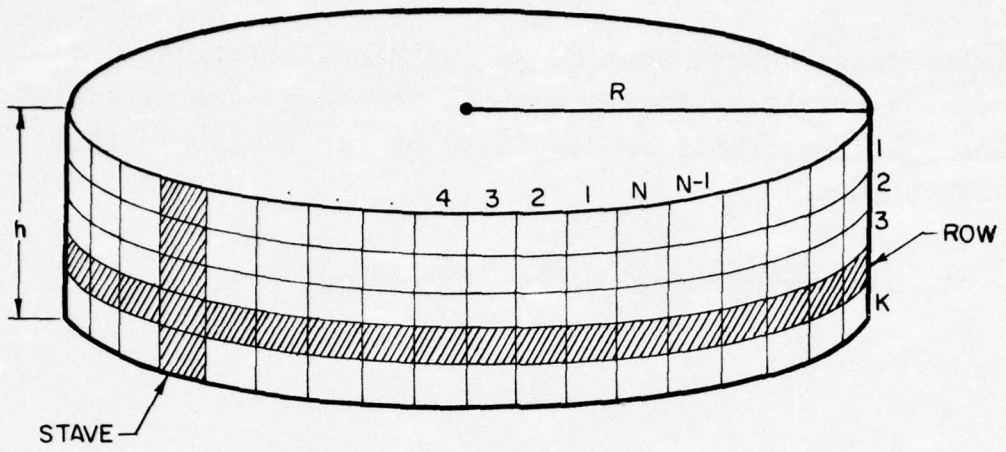

FIG. A-9(a) – CYLINDRICAL TRANSDUCER

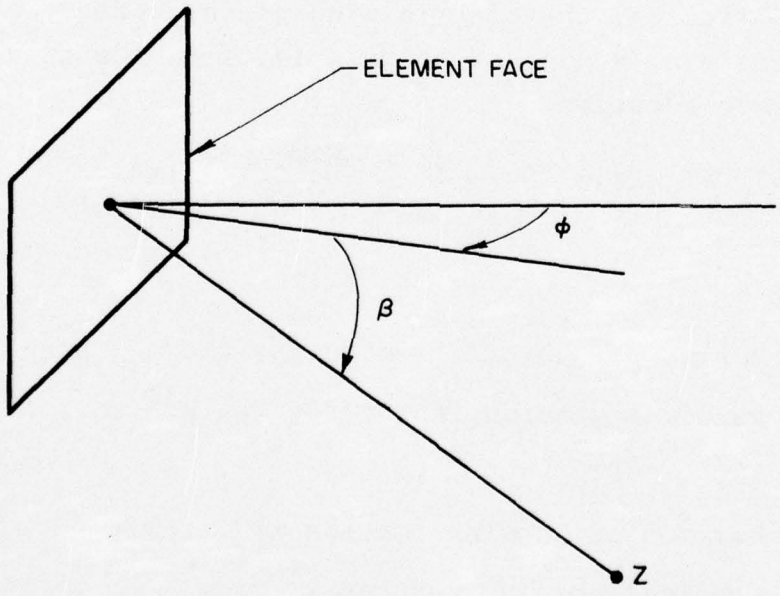

FIG. A-9(b) – ELEMENT FACE AND ANGULAR COORDINATES

TRACOR, INC. DWG. A769-271
AUSTIN, TEXAS 6/11/65

$s_{n,k}$ = distance from the element n,k to the point z, and

φ and β define a line from the element n,k to the point z as shown in Fig. A-9(b).

The total pressure P at the point is the sum of all such contributions, or

$$P = \sum_n \sum_k \frac{HST_n VST_k \; p(\varphi,\beta) e^{i[2\pi(ft - \frac{s_{n,k}}{\lambda} + \gamma_{n,k}]}}{s_{n,k}} ,$$

where the sums are over all staves and rows involved in the transmission.

To obtain a range normalized expression for P, desirable for computational economy, a reference plane is constructed normal to a line from the transducer center to the point z as shown in Fig. A-10. The distance, $s_{n,k}$, from the element n,k to the point z will be approximated by the sum of the distances from the element to the plane, along a normal to the plane, and from the plane to the point. That is,

$$s_{n,k} \approx r_{n,k} + r .$$

We may determine the accuracy of this approximation by writing

$$s_{n,k} = r_{n,k} + r + \epsilon(r) . \qquad (A23)$$

From Fig. A-10 we have

$$s_{n,k} = \left[(r + r_{n,k})^2 + u^2\right]^{\frac{1}{2}} .$$

Thus,

$$\epsilon(r) = s_{n,k} - (r_{n,k} + r), \text{ or}$$

$$\epsilon(r) = \left[(r + r_{n,k})^2 + u^2\right]^{\frac{1}{2}} - (r + r_{n,k}).$$

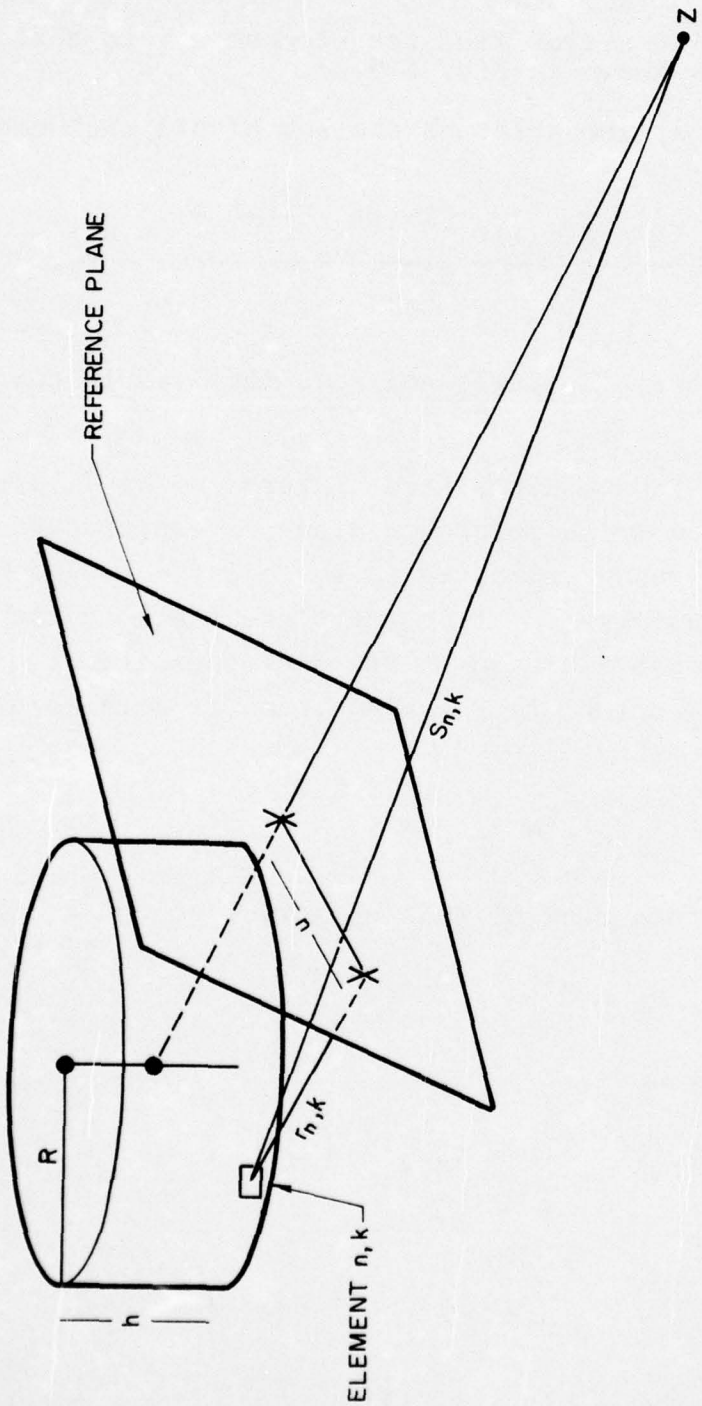

FIG. A-10 — REFERENCE PLANE AND RANGE APPROXIMATION GEOMETRY

TRACOR, INC. AUSTIN, TEXAS DWG. A769-270 6/11/65 BE/SL

Since u is never greater than $[R^2 + (h/2)^2]^{\frac{1}{2}}$, we have finally

$$\epsilon(r) \leq \left[(r + r_{n,k})^2 + R^2 + (h/2)^2\right]^{\frac{1}{2}} - (r + r_{n,k}).$$

If we require the error of approximation never to exceed some preassigned value, ϵ_o, then we must have

$$\epsilon(r) \leq \epsilon_o, \text{ or}$$

$$\left[(r + r_{n,k})^2 + R^2 + (h/2)^2\right]^{\frac{1}{2}} - (r + r_{n,k}) \leq \epsilon_o .$$

The above expression may be rewritten as

$$r \geq \frac{R^2 + (h/2)^2 - \epsilon_o^2}{2\epsilon_o} - r_{n,k} , \tag{A24}$$

which implies that, for a specified maximum error ϵ_o in the approximation for $s_{n,k}$, there is a minimum range such that, for all ranges greater than this minimum, the incurred error, $\epsilon(r)$, is less than ϵ_o.

One additional approximation is needed. We have

$$\frac{1}{s_{n,k}} = \frac{1}{r + r_{n,k} + \epsilon(r)} = \frac{1}{r}(E) ,$$

where

$$E = \frac{1}{1 + \dfrac{r_{n,k} + \epsilon(r)}{r}} . \tag{A25}$$

If $r >> r_{n,k} + \epsilon(r)$, then E is very nearly unity and little error is incurred if $1/s_{n,k}$ is replaced by $1/r$. With this approximation, the expression for P may now be written as

$$P \approx \sum_n \sum_k \frac{HST_n VST_k \; p(\varphi,\beta) e^{i[2\pi(ft - \frac{r + r_{n,k}}{\lambda}) + \gamma_{n,k}]}}{r},$$

or

$$P \approx \frac{e^{i2\pi(ft - \frac{r}{\lambda})}}{r} \sum_n \sum_k HST_n VST_k \; p(\varphi,\beta) e^{-i(\frac{2\pi r_{n,k}}{\lambda} - \gamma_{n,k})},$$

where φ and β define the line from the element n,k normal to the plane. The square of the absolute value of the pressure is

$$|P|^2 = \frac{1}{r^2}\left[\sum_n \sum_k HST_n VST_k \; p(\varphi,\beta) \cos(2\pi r_{n,k}/\lambda - \gamma_{n,k})\right]^2$$

$$+ \frac{1}{r^2}\left[\sum_n \sum_k HST_n VST_k \; p(\varphi,\beta) \sin(2\pi r_{n,k}/\lambda - \gamma_{n,k})\right]^2 .$$

In Fig. A-11(a) is shown the top row of elements and the line CD formed by the intersection of the plane of the row and the reference plane. The staves are numbered clockwise. Figure A-11(b) shows a side view of the n^{th} stave and the edge of the reference plane. From Fig. A-11(a) we have

$$r_n = AB - R\cos(\psi_n - \alpha) ,$$

and from Fig. A-11(b),

$$r_{n,k} = r_n \cos\theta - (k-1)\, S \sin\theta ,$$

where S is the center-to-center spacing of the elements in a stave. Each element subtends, in the plane of the row, an angle ψ at the transducer center, and thus

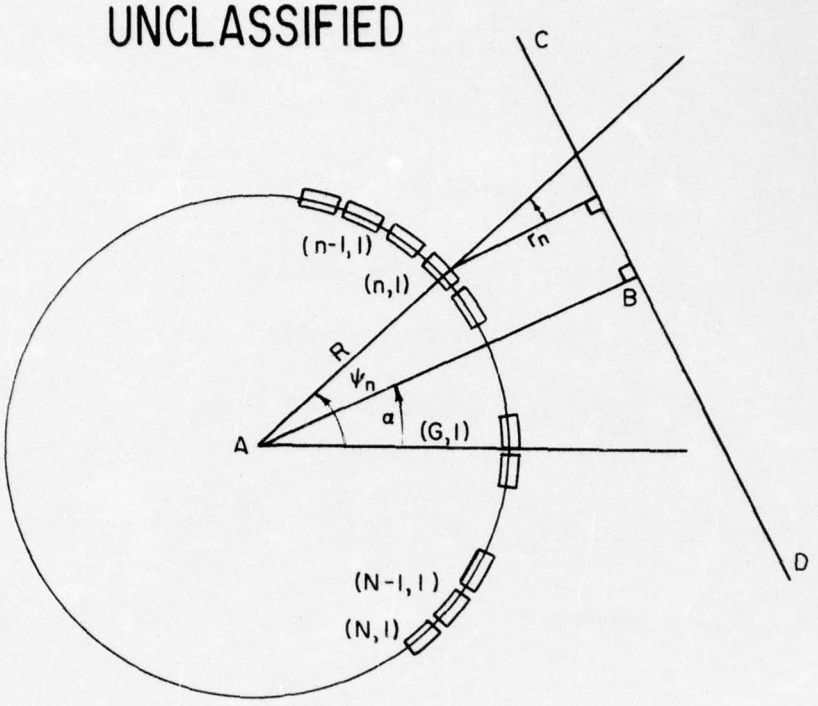

FIG. A-11(a)- TOP VIEW OF TRANSDUCER

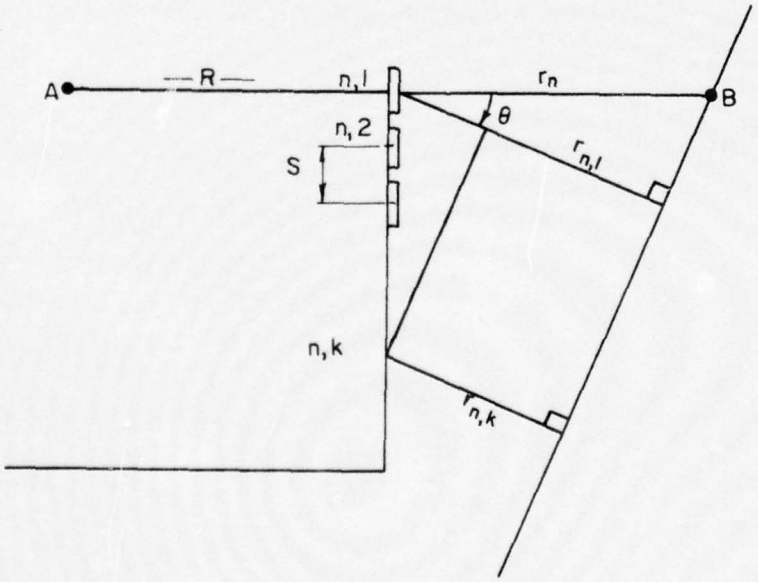

FIG. A-11(b)-EDGE VIEW OF REFERENCE PLANE AND STAVES

TRACOR, INC. DWG. A769-273
AUSTIN, TEXAS 6/11/65 BE/SL

AD-A033 125 TRACOR INC AUSTIN TEX F/G 17/1
IN SITU PERFORMANCE PREDICTION.(U)
MAR 67 M N ANASTASI, S F FOWLER NOBSR-95149
UNCLASSIFIED TRACOR-67-262-C NL

2 OF 2
AD
A033125

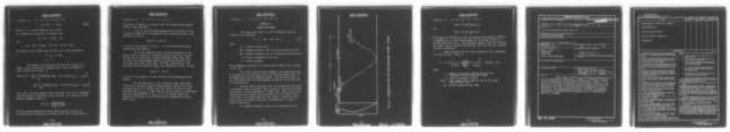

END
DATE
FILMED
2-77

$$\psi_n = (G - n + \tfrac{1}{2})\ \psi\ , \qquad \text{(A26)}$$

where G is the stave shown in Fig. A-11(a).

For simplicity we take AB = R and have then

$$r_n = R[1 - \cos(\psi_n - \alpha)]\ ,$$

and

$$r_{n,k} = R[1 - \cos(\psi_n - \alpha)]\cos\theta - (k-1)\ S\ \sin\theta\ .$$

The angles at the element face, φ and β, are, from the figure,

$$\varphi = \psi_n - \alpha, \text{ and}$$

$$\beta = \theta\ .$$

The square of the absolute value of the pressure at a range r and in a direction determined by α and θ, as shown in Figs. A-11(a) and A-11(b), is

$$|P(\alpha,\theta,r)|^2 = \frac{1}{r^2}\left[\sum_n\sum_k HST_n VST_k\ p(\psi_n - \alpha,\theta)\cos(2\pi r_{n,k}/\lambda - \gamma_{n,k})\right]^2$$

$$+ \frac{1}{r^2}\left[\sum_n\sum_k HST_n VST_k\ p(\psi_n - \alpha,\theta)\sin(2\pi r_{n,k}/\lambda - \gamma_{n,k})\right]^2 .$$

If α_o and θ_o are the angular values for which $P(\alpha,\theta,1)$ is a maximum, then the relative intensity at unit distance, as a function of the angular arguments alone, is

$$I(\alpha,\theta) = \frac{|P(\alpha,\theta,1)|^2}{|P(\alpha_o,\theta_o,1)|^2}\ ,$$

with the understanding that $I(\alpha,\theta)$ may be used as a factor in calculating the intensity at a distant point only if the range to

that point is equal to or greater than the minimum range implied by Eqs. (A23) and (A24).

If I_o is the specified maximum source intensity at unit distance we have for the transmitted sound intensity along a line defined by α and θ,

$$B_T(\alpha,\theta) = I_o I(\alpha,\theta) \ .$$

A plot of 10 log $B_T(\alpha,\theta)$ with $I_o = 1$ is the transmitting three-dimensional beam pattern.

All of the equations which have been discussed so far may be used to compute the receiving pattern function if we substitute for the previously defined parameters HST_n, VST_k, HPT_n, and VPT_k, the corresponding shading and phasing values for the receiving mode, HSR_n, VSR_k, HPR_n, and VPR_k, respectively. The relative receiver response along a line defined by α and θ is then

$$B_R(\alpha,\theta) = I(\alpha,\theta) \ .$$

A plot of 10 log $B_R(\alpha,\theta)$ is the receiving three-dimensional beam pattern.

For the dimensions of the transducer, Eqs. (A24) and (A25) imply a minimum range for computational accuracy of 63 yds. At ranges equal to or greater than this value, the error in the approximation for $s_{n,k}$ is less than $\lambda/8$ and the factor E, associated with the approximation of $1/s_{n,k}$ by $1/r$ is greater than 0.96, implying a resulting error in the intensity computation of less than 0.3 dB.

TRACOR, INC. 6500 TRACOR LANE, AUSTIN, TEXAS 78721

APPENDIX B

TARGET ECHO MODEL

The target echo level, S, may be computed using the standard sonar equation,

$$S = I_o - \Delta BR - \Delta BT - 2H + T \ , \qquad (B1)$$

where

I_o = on-axis source level,

ΔBR = angular deviation loss of receiving beam pattern,

ΔBT = angular deviation loss of transmitting beam pattern,

H = one-way propagation loss, and

T = target strength.

The propagation geometry for a bottom bounce target echo is shown in Fig. B-1.

The source level, target strength, and target depth must be assigned values according to the type of sonar being used, its operating mode, and the expected target. The remaining terms in Eq. (B1) depend upon the environmental parameters, as in the case of reverberation.

The ray theory equations (Eqs. A3 through A15) discussed in Appendix A (Sec. A.2) must, then, be used to account for refractive effects in the computation of target echo. Thus, target echo computations also require the specification of the angular deviation losses of the beam patterns, water depth, velocity profile, bottom loss, and target range, R_T, corresponding to a time, t, after transmission.

The angular deviation losses of the beam patterns are

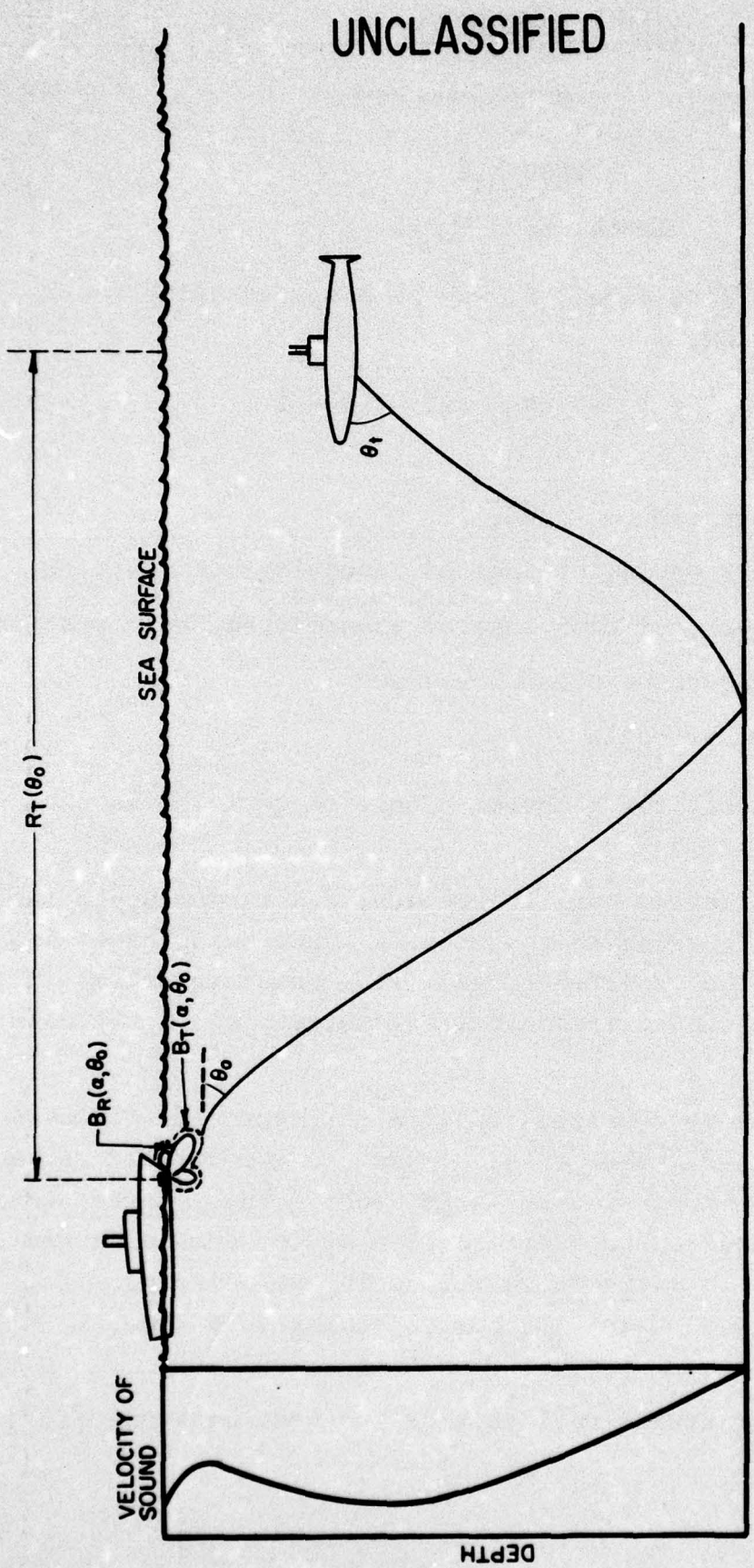

FIG. B-1 — PROPAGATION PATH FOR BOTTOM BOUNCE TARGET ECHOES

TRACOR, INC. DWG. A6-55-46
AUSTIN, TEXAS 3-9-67 ANASTASI/SL

$$\Delta BR = 10 \log \left[B_R(\alpha, \theta_o) \right]$$

and

$$\Delta BT = 10 \log \left[B_T(\alpha, \theta_o) \right] ,$$

where $B_R(\alpha,\theta_o)$ and $B_T(\alpha,\theta_o)$ are the beam pattern responses defined in Appendix A, α is the bearing angle of the target relative to the main beam axis and θ_o (the depression angle of the ray reaching the target) may be found by solving Eqs. (A7) and (A12) by standard iterative techniques.

Again employing the ray theory equations, the propagation loss may be found. This is,

$$H = 10 \log \left[\frac{\cos\theta_o}{R(\theta_o) \cdot \frac{\partial R(\theta_o)}{\partial \theta_o} \cdot \sin\theta_t} \right] - kPL(\theta_o) - BL ,$$

where

θ_t = angle at the target between the ray and a horizontal plane through the target

k = medium attenuation (dB/yd)

$PL(\theta_o)$ = path length (yds) along the ray to the target (see Eq. A15), and

BL = bottom reflection loss (dB).

UNCLASSIFIED

DOCUMENT CONTROL DATA - R&D

(Security classification of title, body of abstract and indexing annotation must be entered when the overall report is classified)

1. ORIGINATING ACTIVITY *(Corporate author)*

TRACOR, Inc., 6500 Tracor Lane, Austin, Texas 78721

2a. REPORT SECURITY CLASSIFICATION

[redacted]

2b. GROUP

IV

3. REPORT TITLE

In Situ Performance Prediction (U)

4. DESCRIPTIVE NOTES *(Type of report and inclusive dates)*

Technical Memorandum

5. AUTHOR(S) *(Last name, first name, initial)*

Anantasi, M. N. and Fowler, S. F.

6. REPORT DATE	7a. TOTAL NO. OF PAGES	7b. NO. OF REFS
20 March 1967	102	10

8a. CONTRACT OR GRANT NO.

NObsr-95149

b. PROJECT NO.

SS041-001

c. Tasks 8100, 10906, 8224

d.

9a. ORIGINATOR'S REPORT NUMBER(S)

TRACOR 67-262-C

9b. OTHER REPORT NO(S) *(Any other numbers that may be assigned this report)*

10. AVAILABILITY/LIMITATION NOTICES

11. SUPPLEMENTARY NOTES

12. SPONSORING MILITARY ACTIVITY

Naval Ship Systems Command
Department of the Navy, Code 1631
Washington, D. C. 20360

13. ABSTRACT

This report discusses the parameters required for an in situ performance prediction, a method of obtaining estimates of these parameters from received reverberation levels, and a means of performance prediction based on these estimates. The problem is discussed in general and the solution is pursued for the particular case of the active bottom bounce modes of the AN/SQS-26. The ping-to-ping stability of AN/SQS-26 reverberation cycles is investigated and several sets of environmental parameters determined from an analysis of the reverberation data are included.

DD FORM 1 JAN 64 1473

Unclassified

Security Classification

Unclassified

Security Classification

14. KEY WORDS	LINK A		LINK B		LINK C	
	ROLE	WT	ROLE	WT	ROLE	WT
Performance Prediction (Sonar)						
Reverberation						
Bottom Bounce Sonar						
Reverberation Stability						
AN/SQS-26						

INSTRUCTIONS

1. ORIGINATING ACTIVITY: Enter the name and address of the contractor, subcontractor, grantee, Department of Defense activity or other organization *(corporate author)* issuing the report.

2a. REPORT SECURITY CLASSIFICATION: Enter the overall security classification of the report. Indicate whether "Restricted Data" is included. Marking is to be in accordance with appropriate security regulations.

2b. GROUP: Automatic downgrading is specified in DoD Directive 5200.10 and Armed Forces Industrial Manual. Enter the group number. Also, when applicable, show that optional markings have been used for Group 3 and Group 4 as authorized.

3. REPORT TITLE: Enter the complete report title in all capital letters. Titles in all cases should be unclassified. If a meaningful title cannot be selected without classification, show title classification in all capitals in parenthesis immediately following the title.

4. DESCRIPTIVE NOTES: If appropriate, enter the type of report, e.g., interim, progress, summary, annual, or final. Give the inclusive dates when a specific reporting period is covered.

5. AUTHOR(S): Enter the name(s) of author(s) as shown on or in the report. Enter last name, first name, middle initial. If military, show rank and branch of service. The name of the principal author is an absolute minimum requirement.

6. REPORT DATE: Enter the date of the report as day, month, year; or month, year. If more than one date appears on the report, use date of publication.

7a. TOTAL NUMBER OF PAGES: The total page count should follow normal pagination procedures, i.e., enter the number of pages containing information.

7b. NUMBER OF REFERENCES: Enter the total number of references cited in the report.

8a. CONTRACT OR GRANT NUMBER: If appropriate, enter the applicable number of the contract or grant under which the report was written.

8b, 8c, & 8d. PROJECT NUMBER: Enter the appropriate military department identification, such as project number, subproject number, system numbers, task number, etc.

9a. ORIGINATOR'S REPORT NUMBER(S): Enter the official report number by which the document will be identified and controlled by the originating activity. This number must be unique to this report.

9b. OTHER REPORT NUMBER(S): If the report has been assigned any other report numbers *(either by the originator or by the sponsor)*, also enter this number(s).

10. AVAILABILITY/LIMITATION NOTICES: Enter any limitations on further dissemination of the report, other than those imposed by security classification, using standard statements such as:

(1) "Qualified requesters may obtain copies of this report from DDC."

(2) "Foreign announcement and dissemination of this report by DDC is not authorized."

(3) "U. S. Government agencies may obtain copies of this report directly from DDC. Other qualified DDC users shall request through

_____."

(4) "U. S. military agencies may obtain copies of this report directly from DDC. Other qualified users shall request through

_____."

(5) "All distribution of this report is controlled. Qualified DDC users shall request through

_____."

If the report has been furnished to the Office of Technical Services, Department of Commerce, for sale to the public, indicate this fact and enter the price, if known.

11. SUPPLEMENTARY NOTES: Use for additional explanatory notes.

12. SPONSORING MILITARY ACTIVITY: Enter the name of the departmental project office or laboratory sponsoring *(paying for)* the research and development. Include address.

13. ABSTRACT: Enter an abstract giving a brief and factual summary of the document indicative of the report, even though it may also appear elsewhere in the body of the technical report. If additional space is required, a continuation sheet shall be attached.

It is highly desirable that the abstract of classified reports be unclassified. Each paragraph of the abstract shall end with an indication of the military security classification of the information in the paragraph, represented as *(TS), (S), (C), or (U)*.

There is no limitation on the length of the abstract. However, the suggested length is from 150 to 225 words.

14. KEY WORDS: Key words are technically meaningful terms or short phrases that characterize a report and may be used as index entries for cataloging the report. Key words must be selected so that no security classification is required. Identifiers, such as equipment model designation, trade name, military project code name, geographic location, may be used as key words but will be followed by an indication of technical context. The assignment of links, rules, and weights is optional.

Unclassified

Security Classification